UNIVERSITY OF CALIFORNIA

Los Angeles

The Critical Casimir Effect
in Model Physical Systems

A dissertation submitted in partial satisfaction

of the requirements for the degree

Doctor of Philosophy in Physics

by

Jonathan Ariel Bergknoff

2012

ABSTRACT OF THE DISSERTATION

The Critical Casimir Effect
in Model Physical Systems

by

Jonathan Ariel Bergknoff

Doctor of Philosophy in Physics

University of California, Los Angeles, 2012

Professor Joseph Rudnick, Chair

The Casimir effect is an interaction between the boundaries of a finite system when fluctuations in that system correlate on length scales comparable to the system size. In particular, the critical Casimir effect is that which arises from the long-ranged thermal fluctuation of the order parameter in a system near criticality. Recent experiments on the Casimir force in binary liquids near critical points and ^{4}He near the superfluid transition have redoubled theoretical interest in the topic. It is an unfortunate fact that exact models of the experimental systems are mathematically intractable in general. However, there is often insight to be gained by studying approximations and toy models, or doing numerical computations. In this work, we present a brief motivation and overview of the field, followed by explications of the $O(2)$ model with twisted boundary conditions and the $O(n \to \infty)$ model with free boundary conditions. New results, both analytical and numerical, are presented.

The dissertation of Jonathan Ariel Bergknoff is approved.

Giovanni Zocchi

Alex Levine

Lincoln Chayes

Joseph Rudnick, Committee Chair

University of California, Los Angeles

2012

To my parents, Hugh and Esther Bergknoff

Table of Contents

LIST OF FIGURES

VITA

2006	B.A. (Physics) and B.A. (Mathematics), Cornell University.
2008	M.S. (Physics), UCLA.

CHAPTER 1

Introduction

1.1   The Casimir Effect

In 1948, Casimir and Polder published an article[1] considering the effect of quantum elec-
trodynamics on the van der Waals force between a neutral atom and an infinite, perfectly
conducting plane. The classical result is that the interaction energy of this system goes as
L^{-3}, with L the distance between the atom and the plane. Casimir and Polder recovered
this result for small L, but found the energy to go as L^{-4} at large L. They argued that the
decrease was the result of retardation effects (i.e. of the finite speed of light).

Just months later, Casimir revisited the problem on his own. He showed that, by con-
sidering the zero point energy of the quantized electromagnetic field under simple boundary
conditions, the same sort of result could be obtained with less computational difficulty. More-
over, this formulation of the problem is relevant in a far broader class of physical systems.
It is common in even the simplest quantum field theories to find an infinite ground state
energy of the form

$$E_0 \propto \sum_n \hbar\omega_n$$

which is considered an unobservable constant that shifts the energy scale, and is therefore
discarded. However, under boundary conditions, the ω_n will depend on the system's param-
eters, e.g. its size. Then, changes in those parameters can cause observable changes in the
ground state energy, which is a surprising and exciting result.

Casimir predicted just that. Suppose two infinite, perfectly conducting parallel plates
are in a vacuum, separated by a distance L. By considering the ground state energy as a

function of L, Casimir predicted that they would attract eachother with a force per unit area[2]

$$\frac{F}{A} = -\hbar c \; \frac{\pi^2}{240} \cdot \frac{1}{L^4}.$$

(1.1)

By employing a physically motivated cutoff scheme, he was able to extract this sensical, finite result from the divergent ground state energy. We will demonstrate this calculation in detail in section 1.2.

In 1953, Casimir proposed a model for the electron[3], with the Casimir effect holding a ball of charge together in opposition to the Coulomb repulsion. An interesting twist came in 1968, when Boyer performed the non-trivial computation suggested by Casimir and found that the Casimir force in this system was *repulsive*, i.e. contributed to expanding the ball[4]. The Casimir force is therefore, in general, something distinct from the van der Waals force which must always be attractive (and is, besides, peculiar to the EM field). The Casimir effect is profoundly affected by geometry and, as we will see in section 1.3, by boundary conditions.

The most generic description of the Casimir effect is a pressure on a system caused by the fluctuations of a quantity subjected to boundary conditions. This broad characterization opens the door to a study of a Casimir effect in condensed matter systems, where we consider the large thermal fluctuations of the order parameter in a confined system near a critical point. Because the critical Casimir effect is the main topic of interest in this work, it will be discussed in depth in a later introductory section.

In the remainder of this introductory chapter, we will continue to detail the development of the Casimir force. Relatively simple calculations in quantum field theory will illustrate the origin of the Casimir force and its dependence on boundary conditions. The connection of the Casimir effect to systems with critical thermal fluctuations will be made clear, and an overview of the results in the field will provide motivation and context to the original work presented later in this document. Then, we will discuss the experimental verification of Casimir forces which has seen great progress, particularly since the late 1990s.

In chapter 2, we will consider the XY model in a three-dimensional film geometry with "twisted" boundary conditions. The continuously tunable boundary conditions enable us to manipulate the strength and direction of the critical Casimir force on the system.

In chapter 3, we will consider the $O(n \to \infty)$ model in a three-dimensional film geometry with free boundary conditions. This model is closely related to the spherical model, which is famous for its elegance and mathematical simplicity. We will carefully discuss the model and present new results, both analytic and numeric, in chapter 3.

The models and boundary conditions mentioned above will be defined in section 1.7.

1.2   Casimir's Seminal Computation

We begin with a computation that closely follows Casimir's impressively short and clever original work[2] concerning the vacuum energy of the quantized electromagnetic field. Consider two perfectly conducting plates in a vacuum, one at $z = 0$ and one at $z = L$. The plates each have cross-sectional area A, large enough that we may neglect edge effects.

The Hamiltonian of the quantized electromagnetic field may be expressed as[5]

$$H = \sum_{\mathbf{k}, \lambda} \hbar \omega(\mathbf{k}, \lambda) \left[\frac{1}{2} + a^\dagger(\mathbf{k}, \lambda) a(\mathbf{k}, \lambda) \right] \tag{1.2}$$

with operator $a^\dagger(\mathbf{k}, \lambda)$ creating a photon with momentum $\mathbf{k}$ and polarization λ and its conjugate a destroying that state. We have a dispersion relation

$$\omega(\mathbf{k}, \lambda) = \omega(\mathbf{k}) = c|\mathbf{k}|, \tag{1.3}$$

independent of the photon's polarization λ which may take either of two values. The vacuum energy is therefore found to be

$$E_0 = \langle 0|H|0 \rangle = \frac{1}{2} \cdot 2 \cdot \sum_{\mathbf{k}} \hbar c|\mathbf{k}| = \hbar c \sum_{\mathbf{k}} |\mathbf{k}|. \tag{1.4}$$

The boundary conditions at the plates quantize the component $k_z = n\pi/L$, $n \in \{0, 1, 2, \ldots\}$, while k_x and k_y may take any real values. We ignore the fact that $k_z = 0$ has only one, not

two, polarizations (it doesn't affect the final result), and find

$$E_0(L) = \hbar c \sum_{n=0}^{\infty} \frac{A}{(2\pi)^2} \int_{-\infty}^{\infty} dk_x \, dk_y \, \sqrt{k_x^2 + k_y^2 + \left(\frac{n\pi}{L}\right)^2}$$

$$= \frac{\hbar c A}{2\pi} \sum_{n=0}^{\infty} \int_0^{\infty} dr \, r \sqrt{r^2 + \left(\frac{n\pi}{L}\right)^2}. \quad (1.5)$$

where we now explicitly write the L dependence of the vacuum energy. Our quantity of interest is the difference between the energy $E_0(L)$ in the present configuration, and the energy in the absence of the plates (which is formally the same as $E_0(L \to \infty)$). One may think of this as isolating the finite-size component of the interaction energy — subtracting off whatever would have been in that same amount of space if the plates weren't there. In the limit of large L, the sum over n may be approximated as an integral, and our interaction energy is

$$U = E_0(L) - E_0(L \to \infty)$$

$$= \frac{\hbar c A}{2\pi} \left[\sum_{n=0}^{\infty} \int_0^{\infty} dr \, r \sqrt{r^2 + \left(\frac{n\pi}{L}\right)^2} - \int_0^{\infty} dr \, dn \, r \sqrt{r^2 + \left(\frac{n\pi}{L}\right)^2} \right]. \quad (1.6)$$

We now regulate the divergences by a factor $f(u)$ that is 1 for u below some cutoff, but dies off at large u so that everything converges. This is motivated by the fact that the high frequency/short wavelength modes (such as X-rays), which will correspond to large u, are not actually confined between the plates. They simply pass through the plates, so we expect their (divergent) contributions to the two terms to exactly cancel. One such $f(u)$ could be a step function $f(u < u^*) = 1$, $f(u > u^*) = 0$, with u^* some physically chosen cutoff. However, we won't find it necessary to refer to a specific regulator, we just require that $f(0) = 1$ and that all derivatives of $f(u)$ exist and vanish at $u = 0$. Now we insert the regulator,

$$U = \frac{\hbar c A}{2\pi} \left[\sum_{n=0}^{\infty} \int_0^{\infty} dr \, r \sqrt{r^2 + \left(\frac{n\pi}{L}\right)^2} f\left(\sqrt{r^2 + \left(\frac{n\pi}{L}\right)^2}\right) \right.$$

$$\left. - \int_0^{\infty} dr \, dn \, r \sqrt{r^2 + \left(\frac{n\pi}{L}\right)^2} f\left(\sqrt{r^2 + \left(\frac{n\pi}{L}\right)^2}\right) \right] \quad (1.7)$$

4

and apply the Euler-Maclaurin formula[6]

$$\sum_{n=0}^{\infty} g(n) - \int_0^{\infty} dn \ g(n) = -B_1 g(0) - \frac{1}{2} B_2 g'(0) - \frac{1}{4!} B_4 g'''(0) - \dots, \qquad (1.8)$$

with B_i the Bernoulli numbers and

$$g(n) = \int_0^{\infty} dr \ r \sqrt{r^2 + \left(\frac{n\pi}{L}\right)^2} f\left(\sqrt{r^2 + \left(\frac{n\pi}{L}\right)^2}\right) = \frac{1}{2} \int_{(n\pi/L)^2}^{\infty} du \ u^{1/2} f(u^{1/2})$$

after a change of variable $u = r^2 + (n\pi/L)^2$. By the fundamental theorem of calculus,

$$g'(n) = -\frac{\pi^3}{L^3} n^2 f(n\pi/L), \qquad (1.9)$$

and further derivatives are simple to compute. We find that the only non-vanishing derivative at $n = 0$ is $g'''(0) = -2\pi^3/L^3$ so our result is

$$U = \frac{\hbar c A}{2\pi} \left[\frac{g(0)}{2} - \frac{1}{4!} \cdot \frac{-1}{30} \left(-\frac{2\pi^3}{L^3} \right) \right] = \frac{\hbar c A}{2\pi} \left[\frac{g(0)}{2} - \frac{\pi^3}{360 L^3} \right] \qquad (1.10)$$

with $g(0)$ independent of L. The force per unit area is then

$$\frac{F}{A} = -\frac{1}{A} \frac{\partial U}{\partial L} = -\hbar c \frac{\pi^2}{240} \cdot \frac{1}{L^4}. \qquad (1.11)$$

This was Casimir's original result: the two conducting plates attract eachother as a result of the fluctuations in the vacuum.

1.3   An Even Simpler System Exhibiting The Casimir Effect

Although Casimir originally applied this approach to the electromagnetic field, we can quickly see that it is a more general effect. Take the simplest quantum field theory, a real scalar field in one dimension. We will now show that this field theory also exhibits a Casimir force when subjected to boundary conditions.

Proceeding from first principles, suppose a set of N identical masses m are evenly spaced along the x-axis between $x = 0$ and $x = L$, with springs of force constant k and equilibrium length $b = L/(N-1)$ between each. Let $\xi_i(t)$ be the displacement of mass m_i from

equilibrium. The Lagrangian of this system is

$$\mathcal{L} = \frac{1}{2} \sum_i \left(m\dot{\xi}_i^2 - k\left(\xi_{i+1} - \xi_i\right)^2 \right) = \frac{b}{2} \sum_i \left(\frac{m}{b}\dot{\xi}_i^2 - kb \left(\frac{\xi_{i+1} - \xi_i}{b} \right)^2 \right) \tag{1.12}$$

where the summation runs $i = 1 \ldots N$ on the kinetic terms and $i = 1 \ldots N - 1$ on the potential terms. The factors of b are introduced to facilitate taking the continuum limit of very closely spaced masses $(N \to \infty)$. In that limit, $b \to 0$ while $m/b \approx Nm/L = \mu$ is the mass density of the system and kb may be interpreted[7] as the Young's modulus Y. The quotient $(\xi_{i+1} - \xi_i)/b$ becomes a spatial derivative and $\sum_i b \to \int dx$. Therefore, elevating $\xi_i(t)$ to a continuously valued classical field $\xi(x,t)$, we have

$$\mathcal{L} = \frac{1}{2} \int_0^L dx \left[\mu \left(\frac{\partial \xi}{\partial t} \right)^2 - Y \left(\frac{\partial \xi}{\partial x} \right)^2 \right] = \int_0^L dx \, \ell(x,t), \tag{1.13}$$

defining the Lagrangian density ℓ. The conjugate momentum of the field ξ is $\pi = \partial\ell/\partial\dot{\xi} = \mu\dot{\xi}$, so that the Hamiltonian is

$$\mathcal{H} = \int_0^L dx \left[\frac{\pi^2}{2\mu} + \frac{Y}{2} \left(\frac{\partial \xi}{\partial x} \right)^2 \right]. \tag{1.14}$$

Before applying second quantization to the fields ξ and π, we will expand them in Fourier series in order to simplify the spatial derivative:

$$\xi(x,t) = L^{-1/2} \sum_k \hat{\xi}(k,t) \, e^{ikx} \quad \text{and} \quad \pi(x,t) = L^{-1/2} \sum_k \hat{\pi}(k,t) \, e^{ikx} \tag{1.15}$$

with $k = 2\pi n/L$, $n \in \mathbb{Z}$. This quantization of k corresponds to periodic boundary conditions (at the end of this section we will consider Dirichlet boundary conditions and find that they lead to a different Casimir force). Making use of orthogonality, the Hamiltonian becomes

$$\mathcal{H} = \frac{1}{2\mu} \sum_k \left[\hat{\pi}(k,t)\hat{\pi}(-k,t) + \mu k^2 Y \, \hat{\xi}(k,t)\hat{\xi}(-k,t) \right] \tag{1.16}$$

which is reminiscent of a harmonic oscillator's $p^2 + \omega^2 x^2$. Note that, taking the complex conjugate of Eqn. (1.15), one finds that $\hat{\xi}(-k,t) = \hat{\xi}(k,t)^\dagger$ and $\hat{\pi}(-k,t) = \hat{\pi}(k,t)^\dagger$ in order for the fields to be real.

6

Now we canonically quantize the fields, considering ξ and π, and their respective Fourier coefficients, as operators, and imposing the equal-time commutation relations

$$[\xi(x_1,t),\pi(x_2,t)] = i\hbar\delta(x_1 - x_2), \quad [\xi(x_1,t),\xi(x_2,t)] = 0, \quad [\pi(x_1,t),\pi(x_2,t)] = 0. \quad (1.17)$$

The first of these relations implies a similar result for the Fourier coefficients, namely

$$i\hbar\delta(x_1 - x_2) = \frac{i\hbar}{L}\sum_k e^{ik(x_1 - x_2)} = [\xi(x_1,t),\pi(x_2,t)]$$

$$= \frac{1}{L}\sum_{k_1,k_2} e^{ik_1 x_1}e^{ik_2 x_2}\left(\hat{\xi}(k_1,t)\hat{\pi}(k_2,t) - \hat{\pi}(k_2,t)\hat{\xi}(k_1,t)\right) \quad (1.18)$$

which forces

$$[\hat{\xi}(k_1,t),\hat{\pi}(k_2,t)] = i\hbar\delta_{k_1,-k_2}. \quad (1.19)$$

In the spirit of a harmonic oscillator calculation, we define ladder operators (suppressing arguments)

$$a = \frac{1}{\sqrt{2\mu|k|}}\left(|k|\sqrt{\mu Y}\hat{\xi} + i\hat{\pi}\right) \qquad \text{and} \qquad a^\dagger = \frac{1}{\sqrt{2\mu|k|}}\left(|k|\sqrt{\mu Y}\hat{\xi}^\dagger - i\hat{\pi}^\dagger\right) \quad (1.20)$$

and compute

$$\sum_k |k|a^\dagger a = \mathcal{H} + \frac{i}{2}\sqrt{\frac{Y}{\mu}}\sum_k |k|\left(\hat{\xi}(-k)\hat{\pi}(k) - \hat{\pi}(-k)\hat{\xi}(k)\right). \quad (1.21)$$

If the final term is split up into two sums, and one of the sums has its index reversed, $k \to -k$ (recall $k = 2\pi n/L$ with n running over all integers), then we get the commutator $[\hat{\xi}^\dagger, \hat{\pi}] = i\hbar$, and the result is

$$\mathcal{H} = \sum_k |k|\left(a^\dagger a + \frac{\hbar}{2}\sqrt{\frac{Y}{\mu}}\right) = \sum_k |k|a^\dagger a + \frac{2\pi\hbar c}{L}\sum_{n=1}^{\infty} n \quad (1.22)$$

where we have identified the propagation speed of waves in the medium as $c = \sqrt{Y/\mu}$. Because the ladder operator a annihilates the normalized ground state $|0\rangle$, we have ground state energy

$$E_0(L) = \langle 0|\mathcal{H}|0\rangle = \frac{2\pi\hbar c}{L}\sum_{n=1}^{\infty} n. \quad (1.23)$$

7

We will proceed, as in the previous section, by subtracting off the ground state energy in the case of $L \to \infty$. Instead of using the Euler-Maclaurin formula, we will illustrate a method of regularizing the sum. Write

$$E_0(L, r) = \frac{2\pi\hbar c}{L} \sum_{n=1}^{\infty} n e^{-rn} = -\frac{2\pi\hbar c}{L} \frac{\partial}{\partial r} \sum_{n=1}^{\infty} e^{-rn} = \frac{2\pi\hbar c}{4L} \frac{1}{\sinh^2(r/2)}. \quad (1.24)$$

Now expand this expression about $r = 0$,

$$E_0(L, r \sim 0) = \frac{\pi\hbar c}{2L} \left[\frac{4}{r^2} - \frac{1}{3} + O(r^2) \right]. \quad (1.25)$$

In the $L \to \infty$ regime, we integrate over k instead of summing. Revisiting Eqn. (1.22), we have

$$E_0(L \sim \infty, r) = \frac{\hbar c}{2} \int_{-\infty}^{\infty} \frac{L}{2\pi} dk \; |k| \, e^{-r|k|L/2\pi} = \frac{\hbar c L}{2\pi} \int_{0}^{\infty} dk \, k \, e^{-rkL/2\pi} = \frac{2\pi\hbar c}{Lr^2} \quad (1.26)$$

which exactly cancels the divergence in the energy of the constrained system. Therefore the Casimir force in this system is

$$F = -\frac{d\left(E_0 - E_{0,L\to\infty}\right)}{dL} = -\frac{\pi\hbar c}{6L^2}. \quad (1.27)$$

The force is attractive, as before, but the L dependence is now L^{-2} instead of L^{-4} because the dimension of the system is two smaller.

   Let us now change the boundary conditions. Enforcing a Dirichlet condition $\xi(x = 0, t) = \xi(x = L, t) = 0$, we find the appropriate Fourier expansion is now

$$\xi(x, t) = \left(\frac{2}{L}\right)^{1/2} \sum_k \hat{\xi}(k, t) \sin(kx) \quad \text{and} \quad \pi(x, t) = \left(\frac{2}{L}\right)^{1/2} \sum_k \hat{\pi}(k, t) \sin(kx) \quad (1.28)$$

with $k = n\pi/L$ and n a positive integer. The resulting Hamiltonian, from Eqn. (1.14), is

$$\mathcal{H} = \frac{1}{2\mu} \sum_k \left[\hat{\pi}(k)^2 + \mu k^2 Y \hat{\xi}(k, t)^2 \right]. \quad (1.29)$$

The remainder of the computation goes through with few changes. In the end, we find

$$\mathcal{H} = \sum_k |k| a^\dagger a + \frac{\pi\hbar c}{2L} \sum_{n=1}^{\infty} n \quad (1.30)$$

8

and the Casimir force is

$$F_{\text{Dirichlet}} = -\frac{\pi \hbar c}{24L^2}.$$
(1.31)

This demonstrates the dependence of the Casimir force on boundary conditions. The dependence can be dramatic, with one sort of boundary conditions giving rise to a much stronger Casimir force than another. In section 1.7 we will go into more detail about the effect of boundary conditions, and in chapter 2 we will explore a system where a continuously variable boundary condition can tune the Casimir force in both strength and direction.

1.4   The Critical Casimir Effect

In 1978, Fisher and de Gennes studied a binary mixture near its critical "demixing" point. We will now briefly describe the argument that they made[8]. Let the system be composed of two fluids called A and B with mean concentrations $\bar{\Phi}$ and $1 - \bar{\Phi}$ respectively. The system has a critical point $(\bar{\Phi}_c, T_c)$ as indicated in the rough phase diagram, fig. 1.1. For[1] $T > T_c$, the fluids mix perfectly into one phase, but for $T < T_c$, there will be, depending on $\bar{\Phi}$, a separated solution (such as oil and water, for which T_c is well above room temperature), an A-rich solution (small amount of B dissolved in a lot of A) or a B-rich solution.

If a wall is inserted into such a mixture, it will locally perturb the concentration Φ from its mean value $\bar{\Phi}$ because we expect the wall to preferentially interact with one of the two fluids. That perturbation will penetrate about a correlation length ξ from the wall into the mixture. Now suppose this system is just above its critical point, fixing $\bar{\Phi} = \Phi_c$ for simplicity but taking T just larger than T_c. In that case, the correlation length would, in bulk[2], diverge as $\xi \sim t^{-\nu}$ with reduced temperature $t = (T - T_c)/T_c$ and ν a universal critical exponent for the Ising model[9].

Next, place a second wall at a distance L from the first wall. When the correlation length gets large, on the order of L, the perturbation from each wall is felt by the other. Invoking

---

[1]This is an *upper* critical point. There also exist binary mixtures with *lower* critical points such that demixing occurs when $T > T_c$.

[2]i.e., when the system size is taken to infinity.
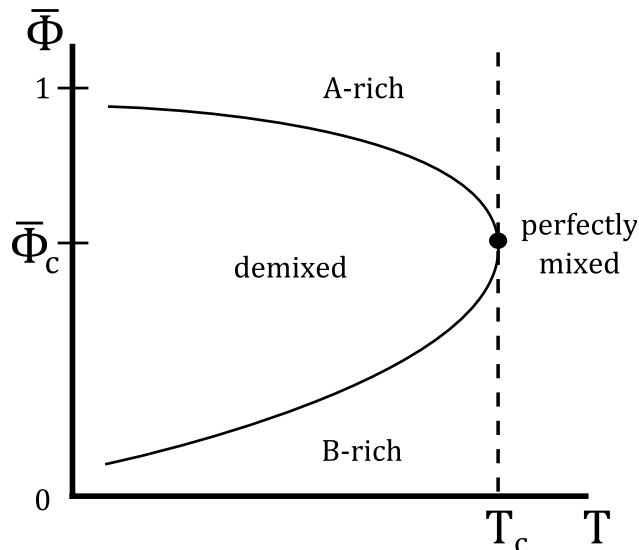
Figure 1.1: Schematic phase diagram of a binary mixture.

finite-size scaling theory, which will be discussed in section 1.5, the interaction energy (per unit area) due to finite-size effects is shown to be

$$U \approx -\frac{k_B T}{L^2},$$ (1.32)

so that the plates attract eachother as a result of the confinement. This is reminiscent of the Casimir effect. It was quickly understood that this line of reasoning could be applied to any critical system, because it relies only on long-ranged correlations and the finite-size scaling hypothesis.

Now, we broadly define a Casimir effect as any pressure induced by imposing boundary conditions on a fluctuating field[10, 11]. When the fluctuations are long-ranged (comparable to the smallest dimension of the system), there will be a Casimir force between the confining surfaces. As discussed above, this will happen for any system near a critical point because the order parameter has critical fluctuations on a scale ξ which becomes large, diverging in the bulk/thermodynamic limit. For that reason, we often call the Casimir effect generated by thermal fluctuations the "critical" Casimir effect. It is worth noting that Kardar and Li showed in 1992 that thermal fluctuations of Goldstone modes can also give rise to Casimir

10

forces away from critical points[12], e.g. for superfluid helium below the lambda transition. However, the present work will be focused on Casimir effects in neighborhoods of critical points.

1.5 Finite-Size Scaling Theory

Any real system, being composed of a finite number of particles and having a partition function given by a finite sum of exponentials, will not exhibit true thermodynamic singularities but may instead approximate them. When the correlation length of the system is small compared to the size of the system, the approximation is very good. Close to a critical point, the correlation length becomes large and the finiteness of the system must be treated carefully. The result, seen experimentally, is that the singularities are replaced by rounded extrema at temperatures shifted from the bulk values[13].

In a bulk system, one can make the *ad hoc* hypothesis that the free energy and, consequently, other thermodynamic functions should satisfy scaling relations of the form[14, 9]

$$F(\lambda^p t, \lambda^q m) = \lambda F(t, m) \tag{1.33}$$

for appropriately chosen exponents p and q, where F is the free energy (of an Ising ferromagnet, for illustration), t is the reduced temperature, m is the magnetization and λ is an arbitrary scaling parameter. We call the function F homogeneous if it satisfies a condition like this one.

By taking derivatives of Eqn. (1.33), we can relate the exponents p and q to the critical exponents α, β, ν, etc. of the system. Furthermore, doing so shows that the scaling assumption on F yields exact relations (as opposed to inequalities) between critical exponents[9, 15]. It is very common, finally, to set the arbitrary parameter λ to a value such as $t^{-1/p}$ and thus find

$$F(t, m) = \lambda^{-1} F(\lambda^p t, \lambda^q m) = t^{1/p} F(1, t^{-q/p} m) = t^{1/p} W(t^{-q/p} m), \tag{1.34}$$

where we define a scaling function $W(x)$ of the variable $x = t^{-q/p} m$. Thus, the function F

has been reduced from a function of two variables to a function of just one; this is sometimes called "data collapse". The scaling hypothesis has many compelling features, and it may in fact be justified by renormalization group arguments[15], but it was entirely *ad hoc* at the time it was proposed by Widom in the 1960s.

In a finite system, it is natural to make the same sort of scaling hypothesis. This was first done by Fisher and his colleagues in the 1970s[16, 17]. The simplest case to consider is a thin film geometry, which is particularly accessible to both experiment (see section 1.8) and theory. Working in d dimensions, let the film have a thickness L along its axis, and a uniform cross-sectional "area" A in its $d-1$ other dimensions so its total volume is LA.

Near a critical point, when ξ becomes as large as L, let us consider an intensive property P (e.g. the specific heat) of the system. Suppose that the singular part[3] of P goes as $t^{-\rho}$ in the bulk, defining some critical exponent ρ. In the finite system, P will not have a singularity, but we can still talk about a "singular" part of P which will reproduce the $t^{-\rho}$ singularity in the thermodynamic limit. The finite-size scaling hypothesis is the statement that this singular part of P should scale as[16, 15]

$$P_{\text{sing}}(L, t) \approx L^{\rho/\nu} X(atL^{1/\nu}) \tag{1.35}$$

with system-specific scaling factor a and $X(x)$ a "finite-size scaling function", not determined by this analysis, which depends only on the system's bulk universality class, spatial dimension, and the boundary conditions. This scaling form is expected to apply when $T \approx T_c$, the correlation length is comparable to L, and the dimension d is lower than the system's upper critical dimension d_c[11]. Note that $\xi \approx \xi_0 t^{-\nu}$ so the argument of X could also be taken to be L/ξ and ξ_0, which is a system-specific correlation length scale, takes the place of the factor a.

---

[3]For instance, we ignore the constant if $P = \text{const} - t^{-\rho}$.

1.6 The Casimir Force in Critical Films

We continue the analysis of the $A \times L$ film geometry described in the previous section. The free energy $\mathcal{F}$ of this system, in the vicinity of a bulk critical point and with A large enough that edge effects are negligible, decomposes as[11, 18]

$$\frac{\mathcal{F}(T, L)}{k_B T_c A} = L f_{\text{bulk}}(T) + f_{s,1}(T) + f_{s,2}(T) + \delta f(T, L) \tag{1.36}$$

where f_{bulk} is the bulk free energy density, $f_{s,i}$ are free energies per unit area due to the presence of each boundary of the film, and $\delta f(T, L)$ is the free energy per unit area from finite-size effects, all measured in units of $k_B T_c$. Per the comments on finiteness in section 1.5, it is customary to break each contribution into singular and non-singular parts[19]. The singularity in the bulk term (and, generally, the surface terms as well) must be canceled by the singular part of the finite-size term[4]. What remains of $\delta f(T, L)$ after that cancellation we will call the excess, $\delta f_{\text{ex}}(T, L)$, and it is this quantity which is responsible for the Casimir force.

The finite-size scaling hypothesis now states that this excess free energy density scales as[5]

$$\delta f_{\text{ex}}(T, L) = L^{-(d-1)} \Theta(L/\xi) \tag{1.37}$$

where Θ is a universal scaling function, depending only on dimensionality and the universality classes of the bulk system and the surfaces. Some systems have strictly infinite correlation length below T_c in which case this scaling form is meaningless for those temperatures. In general, temperatures above and below T_c should be treated separately and will have different scaling functions $\Theta_{\pm}(y)$. The resulting Casimir force per unit area is

$$\frac{F_{\text{Cas}}(T, L)}{k_B T_c A} = -\frac{\partial(\delta f_{\text{ex}})}{\partial L} = L^{-d} \vartheta(L/\xi) \tag{1.38}$$

with

$$\vartheta(y) = (d-1)\Theta(y) - y\Theta'(y) \tag{1.39}$$

---

[4]However, the singular part of the finite-size contribution may introduce singularities of its own, because $A \to \infty$ is the thermodynamic limit for the $(d-1)$-dimensional cross section (film layer).

[5]in relation to the discussion above, $\rho = -(d-1)\nu$.

also universal. This scaling behavior means that if $L^d F_{\text{Cas}}$ is plotted versus aLt^ν, with a a non-universal scaling factor, then all data points should fall on the graph of $\vartheta(y)$. This is a particular instance of "data collapse"[11]. Finally, note that the scale of the critical Casimir force is set by $k_B T_c$ as opposed to $\hbar c$ as it was in the context of quantum fields.

While finite-size scaling is a very strong statement which aids in the study of finite-size effects, analytic results are still hard to come by. In particular, the scaling functions are very rarely calculable in closed form (although they may be computed numerically). There has been considerable success, however, in analytically computing "Casimir amplitudes", defined as $\Delta = \Theta(0)$, i.e. at $t = 0$, for each given bulk universality class, set of boundary conditions and dimensionality. These amplitudes are universal quantities (in the same sense as for the scaling functions) and often help to illustrate how the strength and direction of the Casimir force depend on boundary conditions within a particular universality class.

1.7   Results on Critical Casimir Forces

As it will be of general import throughout this work, we now define the $O(n)$ model. The model consists of a lattice whose sites are occupied by n-component vector spins. The spins participate in nearest neighbor interactions, with the Hamiltonian

$$H^{(n)} = -J \sum_{\langle \mathbf{s}, \mathbf{s}' \rangle} \mathbf{s} \cdot \mathbf{s}' \tag{1.40}$$

where the sum runs over nearest neighbors and the coupling J will be taken here to be positive (ferromagnetic, i.e. spins tend to align in order to lower the energy). By the nature of the scalar product, the Hamiltonian is invariant under a simultaneous orthogonal transformation of all the spins in the system (i.e. its symmetry group is $O(n)$).

The model finds many physical applications, exhibiting varied behavior as spin dimensionality n and spatial dimensionality d change[20]. The $n = 1$ (Ising) universality class models uniaxial ferromagnets, vapor-liquid critical phenomena, and binary mixtures, among other things. The $n = 2$ (XY) universality class models anisotropic ("easy plane") ferro-

magnets and ^{4}He superfluid[21]. The $n = 3$ (Heisenberg) universality class corresponds to a classical ferromagnet. The $n \rightarrow \infty$ case is also significant, though perhaps not physical. It was found by Stanley in 1968 to be formally equivalent[22] to the exactly solvable Berlin-Kac spherical model[23] which will be discussed in chapter 3.

Theoretical study of the critical Casimir effect has been primarily focused on the $O(n)$ model because of its relative simplicity and its application to experimentally accessible systems. Critical Casimir forces have been measured in both binary mixtures and superfluid Helium (see section 1.8), while theoretical and numerical results abound for Ising, XY and spherical universality classes. Within each universality class, behavior depends strongly on boundary conditions, giving rise to several different scaling functions of interest for each n. The boundary conditions most often studied are periodic ($\phi(z + L) = \phi(z)$), anti-periodic ($\phi(z + L) = -\phi(z)$) and Dirichlet or "fixed" ($\phi(z = 0)$ and $\phi(z = L)$ specified). One also often sees "free" boundary conditions, which set the field to zero immediately outside the bounds of the system. Free boundary conditions are a special case of Dirichlet boundary conditions.

Fixed boundary conditions in the Ising model amount to specifying up or down for the spins on each surface of the system. The symbols $(+, +)$, $(+, -) = (-, +)$ and $(-, -)$ are commonly used to describe those boundary conditions for a film geometry. However, the notation is sometimes also used in a more general way to refer to "like" or "unlike" boundary conditions in other systems. For instance, two plates placed in a binary mixture which both preferentially attract (or repel) the same species would be termed $(+, +)$ boundary conditions. If they preferred opposite species, that would be $(+, -)$ boundary conditions. It is generally believed[11] that symmetric boundary conditions, such as $(+, +)$, always give rise to attractive Casimir forces while anti-symmetric boundary conditions always give rise to repulsion.

Scaling functions for $(+, +)$ and $(+, -)$ boundary conditions on the three-dimensional Ising model were approximated by mean field theory[24] in 1997. More recently, Monte Carlo simulation[25] showed rough, but qualitative, agreement with the mean field result

15

(e.g. extrema on the correct side of T_c). The $(+,+)$ scaling function was computed by local functional methods in 2008, agreeing very well with the Monte Carlo results[26]. This system is arguably the most relevant to critical Casimir experiments, and scaling functions have recently been measured for it (see section 1.8). Lower dimensional Ising models are, of course, more amenable to solution. There are exact results for the scaling functions of the one- and two-dimensional Ising model[27, 28, 29] under all boundary conditions of interest. In $d \geq 4$, mean-field theory is exact for the Ising model[15] and the relevant scaling functions have been computed[24].

There are fewer results for the XY model, almost all of them in three dimensions. The earliest computations for the system were by Krech and Dietrich[18, 30] who in fact derived a broad class of results for general symmetry order n, with periodic, anti-periodic and Dirichlet boundary conditions, using perturbation theory. However, those results were not applicable for T just below T_c and were thus of limited interest. Measurements on superfluid ^{4}He films[31] around the lambda point inspired further work on the system, both purely theoretical[32, 33, 34] as well as numerical[35, 25, 36]. Among other things, it was eventually understood that the experimental system had to be modeled using free boundary conditions; predictions using other boundary conditions were substantially off.

In chapter 2, we will consider the XY model in $d = 3$ under "twisted" Dirichlet boundary conditions: the spins in one boundary orient in one direction while the spins in the other boundary orient in another. These boundary conditions bridge the gap between $(+, +)$ and $(+, -)$ which are no twist and 180° twist, respectively. We will see how the system crosses over from the purely attractive Casimir force, in the former case, to the purely repulsive Casimir force, in the latter case, in a continuous way.

The spherical model is of great interest because it is especially tractable. The model may be exactly solved[37, 15] in the bulk in any dimension d, and quite a bit of computation may be done by hand even in the finite-size case. Results have been obtained for the mean spherical model (the spherical and mean spherical models are defined and discussed in more detail in chapter 3) in arbitrary dimension with periodic boundary conditions[38, 39]. Study

has also been made of the model with Dirichlet and Neumann boundary conditions in a three-dimensional film geometry[40, 41]. In chapter 3 we will discuss a closely related model.

1.8 Experimental Verification of the Casimir Effect

With some coarse estimates of laboratory conditions, $A = 1\,\mathrm{cm}^2$ and $L = 1\,\mu\mathrm{m}$, we find a Casimir force of $\sim 1.3 \times 10^{-7}\,\mathrm{N}$ from Eqn. (1.1). For perspective, the gravitational force between two $1\,\mathrm{g}$ point masses a distance $1\,\mu\mathrm{m}$ apart is $\sim 6.7 \times 10^{-5}\,\mathrm{N}$. Although the Casimir force is extremely weak at laboratory-accessible separations, it has nevertheless been experimentally observed. After fifty years of incremental improvements but ultimately unsatisfactory experiments[42, 43, 44, 45], the first experiment providing conclusive evidence of the Casimir effect came in 1997 by Lamoreaux. That experiment[46] involved a flat plate and a large-radius sphere (physically similar to two flat plates but far easier to arrange parallel to eachother) with a torsion pendulum for measurement of the force, and it achieved agreement with theory (a modified form of Eqn. (1.1)) to about $\sim 5\%$.

In the years following Lamoreaux's experiment, there have been dramatic improvements in techniques for measuring Casimir forces. In 1998, Mohideen, et al. used an atomic force microscope to make extremely accurate measurements[47] of the Casimir force between a plane and a sphere. In 2002, Bressi, et al. tried to directly measure the parallel-plate Casimir force and achieved 15% agreement with theory (the experiment had previously only been attempted by Sparnaay in 1958 but his results could only be said to "not contradict Casimir's theoretical prediction"[43]).

Measurement of the critical Casimir effect also faced difficulties[48]. A common experimental setting is a thin film of critical fluid, which occurs naturally for fluid systems in the wetting transition[11], where a gas is in contact with a flat substrate and partially condenses into liquid on the subtrate. The resulting liquid has a film geometry, i.e. wide and thin. The thickness of the film is determined by a balance of gravitational, van der Waals and Casimir forces. It turns out that critical film thicknesses are on the order of $10^{-8}\,\mathrm{m}$ and

critical Casimir forces are on the other of 10^{-15} N, both prohibitively small and difficult to measure[10]. However, owing to some clever experiments, the critical Casimir effect has been observed very accurately in recent years.

In 1999, Garcia and Chan measured the thickness of a ^{4}He film adsorbed between copper substrates[31], near the critical endpoint of the λ-transition[6], by measuring the capacitance of the arrangement (the Helium film and vapor act as dielectrics of variable width). They obtained results for the Casimir force which show a big dip near T_c and a less extreme but non-zero depression for $T \ll T_c$. The system may be modeled by the three-dimensional XY model with Dirichlet boundary conditions (order parameter vanishing at both boundaries). The big dip, due to the critical Casimir force, has been reproduced very well in Monte Carlo simulations[35, 25]. The low temperature depression, larger than expected from just the presence of Goldstone modes[12], was shown in 2004 to be a Casimir force resulting from surface fluctuations[32].

The first attempt at measuring the critical Casimir effect in a binary liquid (the original prediction of Fisher and de Gennes) was made by Mukhopadhyay and Law[49] in 1999, using ellipsometry on a wetting film, and gave qualitatively encouraging but inconclusive results. In 2005, Fukuto et al. performed an X-ray scattering experiment[50] on another binary mixture film, obtaining cleaner results over a wider temperature range. The model corresponding to these experiments is the three-dimensional Ising model with $(+, -)$ boundary conditions, because the experiments had one substrate preferentially attracting one component and the second subtrate preferentially attracting the other component. The experimental data have moderate agreement with Monte Carlo results[25] obtained two years later, showing a strictly positive scaling function and hence a repulsive force. Another experiment by Rafai et al in 2007 found an attractive Casimir force, as expected, for a similar system with symmetric $(+, +)$ boundary conditions[51].

Finally, the critical Casimir effect was recently measured using colloids suspended in a critical mixture. The method, called "total internal reflection microscopy", gives direct

---

[6]$T_c = 2.17$ K, $p_c = 0.05$ bar

access to the net force on the colloid. The experiment performed by Hertlein et al. in 2008 shows fantastic agreement with theory for the Casimir force in a water-lutidine mixture at temperatures beneath the lower critical demixing point[52], but the data doesn't extend to temperatures close to T_c. This technique promises to yield excellent experimental data in the years to come.

CHAPTER 2

The Casimir Force in the XY Model with Twisted Boundary Conditions

2.1 Introduction

Recall from section 1.6 that a d-dimensional system with a temperature T and film geometry $A \times L$ has a thermodynamic Casimir force defined by [53, 15]

$$\frac{F_{\text{Cas}}^{(\tau)}(T, L)}{k_B T_c A} = -\frac{\partial(\delta f_{\text{ex}}^{(\tau)})}{\partial L}, \tag{2.1}$$

where $\delta f_{\text{ex}}^{(\tau)}(T, L)$ is the excess free energy density and the superscript τ now denotes the boundary conditions.

Accumulated evidence supports the conclusion that if the boundary conditions are identical – or sufficiently similar – at both surfaces bounding the system, then $F_{\text{Cas}}^{(\tau)}$ will be negative[30, 54, 55, 56]. For concreteness, consider a fluid in the vicinity of its liquid-vapor critical point, which is modeled by the Ising universality class. If the fluid is confined between identical walls, the Casimir force between those walls will be *attractive* for large separations. On the other hand, if the fluid wets one of the walls while the other wall prefers the vapor phase, then the Casimir force will be repulsive. This implies that if the boundary conditions differ sufficiently then the Casimir force can be expected to be positive, or *repulsive*, for the entire range of thermodynamic parameters.

In the intermediate case in which one of the surfaces has a weak preference for one of the phases of the fluid while the other one exhibits a strong preference, or for a given ratio of the surface fields and/or of surface enhancements on both surfaces, it has been recently

demonstrated[57, 56, 58] that one can observe much richer behavior, with the Casimir force changing its sign once, or even twice[56], as the temperature is adjusted. In addition, it has been shown[59] via Monte Carlo simulations that, in a system with a three-dimensional film geometry $L_\parallel^2 \times L$ and subject to periodic boundary conditions, both the magnitude and the sign of the Casimir force depend on the aspect ratio $a_r = L/L_\parallel$. In this case general arguments have been advanced to suggest that, at the bulk critical point, the Casimir force vanishes for $a_r = 1$ and becomes repulsive for $a_r > 1$. These results are supported by exact calculations for the two-dimensional Ising model.

According to the work of Lifshitz[60] and the subsequent generalizations, the force is attractive in any system with a slab- or film-like structure in which a material B separates two identical half-spaces $A \equiv C$. When B is a vacuum, this remains true even when the half-spaces A and C are not identical. This prediction, up to now, has been verified for all materials for which the Casimir force has been measured. Theoretical predictions exist, however, suggesting that in the latter case a repulsive Casimir force can be generated by special selection of the material properties of A and C[61]. However, such a situation has not been experimentally realized. The omnipresence of attractive quantum Casimir electromagnetic forces for objects in vacuum or air affects the work of micro- and nano-machines[62, 63, 64, 65] and can cause sticking of their working surfaces. The possibility of realizing and controlling a repulsive critical Casimir force might be one of the ways of overcoming such a difficulty.

In an attempt to shed additional light on the influence of differing boundary conditions on the critical Casimir force, we now consider a d-dimensional film system with $\infty^{d-1} \times L$ geometry[1] and consisting of local dynamical variables, such as magnetic moments, possessing $O(2)$ symmetry. The moments in each boundary surface are all constrained to point in the same direction. However, the directions fixed on each surface may be different, and we denote by α the relative angle between them. Furthermore, in the case in which the moments have variable amplitudes, those amplitudes are fixed at a non-zero value. Alternatively, one might think of the studied system as a lattice gas of elongated rod-like molecules embedded on a

---

[1]i.e., infinite in $d-1$ dimensions and of length L in the last dimension.

lattice.

We investigate both the equilibrium behavior of those moments (or molecules)—and the Casimir force that arises as a result of that behavior—as a function of T and α. As we will see, among the results of our calculation are a Casimir force that depends in a continuous way on both the parameter α and the temperature, and that can be made attractive or repulsive. In particular, by varying α and/or T, one can control both the sign and the magnitude of the Casimir force in a reversible way.

We will refer to the boundary conditions described above as "twisted" boundary conditions. Subject to them, the moments within the system settle into a state in which they rotate with respect to each other as the region between the boundaries is traversed, creating a diffuse interface within it. Finite-size scaling theory dictates that, in the vicinity of the bulk critical point T_c,

$$\delta f_{\text{ex}}^{(\alpha)}(T, L) = L^{-(d-1)} X_{\text{ex}}^{(\alpha)}(x_t) \tag{2.2}$$

where $\delta f_{\text{ex}}^{(\alpha)}$ is the excess free energy density (see section 1.5), $X_{\text{ex}}^{(\alpha)}$ is a universal scaling function, $x_t = a_t t L^{1/\nu}$ is the appropriate scaling variable, $t = (T - T_c)/T_c$ is the reduced temperature, and a_t is a non-universal scaling factor. ν is the (universal) critical exponent that characterizes the temperature divergence of the bulk two-point correlation length ξ when approaching the bulk critical temperature from above. The Casimir force is

$$F_{\text{Cas}}^{(\alpha)}(T, L) = L^{-d} X_{\text{Cas}}^{(\alpha)}(x_t). \tag{2.3}$$

The scaling functions $X_{\text{ex}}^{(\alpha)}$ and $X_{\text{Cas}}^{(\alpha)}$ are universal (for the XY class, in this case), given a particular set of boundary conditions and spatial dimensionality.

The structure of this chapter is as follows. In section 2.2, we define a lattice three-dimensional mean-field XY model and present numerical results for the behavior of the Casimir force within it. Section 2.3 presents analytical results for the scaling function of the Casimir force within the Ginzburg-Landau mean-field theory of the three-dimensional XY model. In section 2.4, we detail the numerical computations used to obtain the results presented for the lattice and continuum models. In both section 2.2 and section 2.3, we find

interesting behavior of the system when $\alpha = \pi$. We study this special case in section 2.5. We deduce the existence of an additional second-order phase transition that is specific to this finite system. The chapter closes with a discussion presented in section 2.6. Technical details of several derivations and computations are relegated to appendices.

2.2 The Casimir Force in the Three-Dimensional Mean-Field XY Model on a Lattice

Consider a square lattice of dimensions $\infty^{d-1} \times L$, with each site populated by an $O(2)$ fixed-length magnetic moment of magnitude m. We split up the lattice into $(d-1)$-dimensional planes labeled $0, \ldots, N+1$, where $L = (N+1)a$, with a being the lattice spacing taken in the remainder to be equal to one. Neglecting the fluctuation within the planes, all moments in plane i must take the same value (i.e. point in the same dirction), equal to their mean value. However, due to the anisotropy along the finite dimension, the moments will vary between planes. Let the moment in plane i be $\mathbf{m}_i$. We take a nearest-neighbor coupling with strength J both in the plane and out of it, and so the energy of a moment in plane i will be

$$U_i = -J\mathbf{m}_i \cdot (2(d-1)\mathbf{m}_i + \mathbf{m}_{i-1} + \mathbf{m}_{i+1}) \tag{2.4}$$

or, defining an effective magnetic field $\mathbf{H}_i = J(2(d-1)\mathbf{m}_i + \mathbf{m}_{i-1} + \mathbf{m}_{i+1})$ at that site, $U_i = -\mathbf{m}_i \cdot \mathbf{H}_i$.

Approximating the moment $\mathbf{m}_i$ as being isolated, in an external magnetic field $\mathbf{H}_i$, we can assign it the local partition function

$$Z_i = \int_0^{2\pi} d\theta \; e^{\beta m H_i \cos\theta} = 2\pi I_0(\beta m H_i) \tag{2.5}$$

with $\beta = (k_B T)^{-1}$ and θ the angle between $\mathbf{H}_i$ and $\mathbf{m}_i$. On average, the component of $\mathbf{m}_i$ along $\mathbf{H}_i$ is

$$\langle m \cos\theta \rangle = \frac{1}{\beta} \frac{d \ln Z}{dH_i} = m \frac{I_1(\beta m H_i)}{I_0(\beta m H_i)}, \tag{2.6}$$

where I_0 and I_1 are the modified Bessel functions of the first kind, while the component
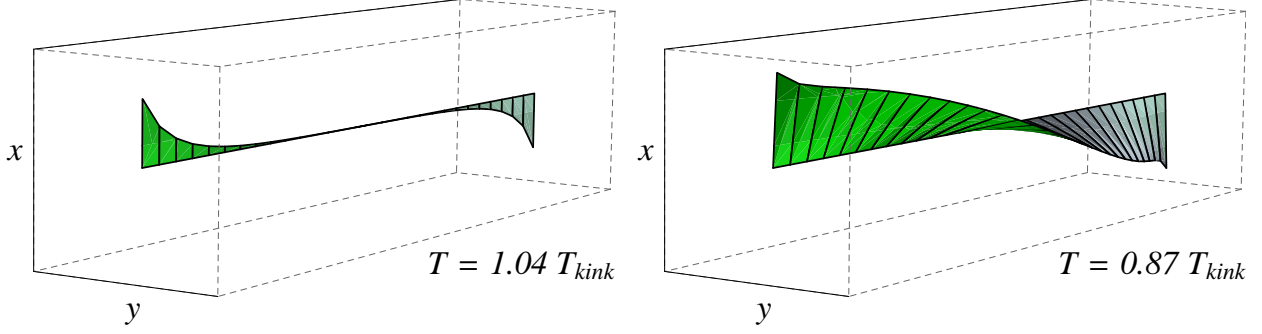
Figure 2.1: Renderings of the moments ($d = 3$, $N = 30$, $\alpha = \pi$) for temperatures above (left) and below (right) the temperature where a kink occurs in the Casimir force.

normal to $\mathbf{H}_i$ is

$$\langle m \sin \theta \rangle = \frac{1}{Z} \int_0^{2\pi} d\theta \; m \sin \theta \; e^{\beta m H_i \cos \theta} = 0 \tag{2.7}$$

so that the averaged moment is entirely along $\mathbf{H}_i$. Inserting the definition of $\mathbf{H}_i$ in terms of neighboring moments, we see that $\mathbf{m}_i$ must satisfy the equation

$$\mathbf{m}_i = m \cdot \frac{2(d-1)\mathbf{m}_i + \mathbf{m}_{i-1} + \mathbf{m}_{i+1}}{|2(d-1)\mathbf{m}_i + \mathbf{m}_{i-1} + \mathbf{m}_{i+1}|} \cdot R\left(\beta m J \left|2(d-1)\mathbf{m}_i + \mathbf{m}_{i-1} + \mathbf{m}_{i+1}\right|\right) \tag{2.8}$$

in the mean-field approximation (all quantities now implicitly averaged), with $R(u) = I_1(u)/I_0(u)$.

We will fix the boundary values $\mathbf{m}_0$ and $\mathbf{m}_{N+1}$ while $\mathbf{m}_i$, with $i = 1, \ldots, N$, are free to vary. We also define $\mathbf{m}_{-1} = \mathbf{m}_{N+2} = 0$ for notational convenience (so that $\mathbf{H}_0$ and $\mathbf{H}_{N+1}$ are defined). The function

$$f(\{\mathbf{m}_i\}, N) = \sum_{i=0}^{N+1} \left[\frac{1}{2}\mathbf{m}_i \cdot \mathbf{H}_i - \frac{1}{\beta} \ln \left(I_0\left(\beta m H_i\right)\right)\right] \tag{2.9}$$

may be regarded as the total free energy functional of the system, because minimizing with respect to $\{\mathbf{m}_i\}$ yields the self-consistency conditions (2.8) (See appendix A).

In order to compute the Casimir force on the system, we must also find the free energy per site in the bulk, i.e. when the system is very large. In that case, the moments $\{\mathbf{m}_i\}$ will all be identical (at least near the center) and Eqn. (2.8) tells us that the equation $m_{i,\text{bulk}} =$

$mR(2dm\beta Jm_{i,\text{bulk}})$ determines their common magnitude $m_{i,\text{bulk}}$. For $T > dJm^2/k_B$, the only solution is $m_{i,\text{bulk}} = 0$ while for $T < dJm^2/k_B$, there is a non-zero solution. Thus, the bulk system exhibits a transition at $T_{c,\text{bulk}} = dJm^2/k_B$ between an ordered $(T < T_{c,\text{bulk}})$ and a disordered phase.

Re-inserting the lattice spacing a, the bulk free energy density is

$$f_b = \frac{1}{a}\left[dJm^2_{i,\text{bulk}} - \frac{1}{\beta}\ln\left(I_0\left(2dm\beta Jm_{i,\text{bulk}}\right)\right)\right] \tag{2.10}$$

and the Casimir force will be computed as
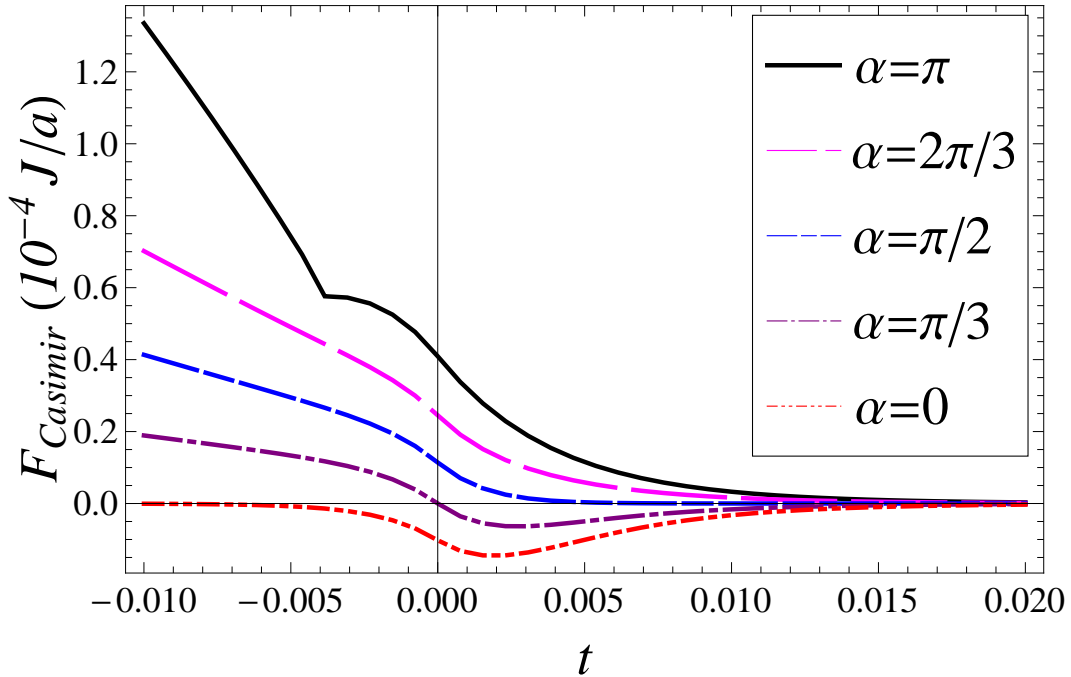
Figure 2.2: The Casimir force in the lattice model $(d = 3, N = 30)$ as a function of reduced temperature t for various values of the twist angle, α.

$$F_{\text{Cas}} = -\frac{\partial}{\partial L}\left(f - Lf_b\right) \approx f_b - \frac{f(N+1) - f(N)}{a}. \tag{2.11}$$

Until this point, the model has been somewhat general. We now restrict our attention to the case of twisted boundary conditions and $d = 3$, and investigate the system numerically.

This amounts to solving the simultaneous Eqns. (2.8) with particular values of $\mathbf{m}_0$ and $\mathbf{m}_{N+1}$. Specifically, we are interested in how the behavior of the system depends on the relative angle α between $\mathbf{m}_0$ and $\mathbf{m}_{N+1}$. Details of the numerical calculation are found in section 2.4.

When the twist angle is zero, we find that the Casimir force is purely attractive (i.e, negative), as expected for matching boundary conditions. These features are illustrated in the plot of Casimir force versus reduced temperature (Fig. 2). As the twist is increased, a low temperature region of repulsive Casimir force emerges. At a twist angle of $\pi/2$, the Casimir force becomes purely repulsive. When the system nears anti-symmetric boundary conditions, $\alpha = \pi$, the Casimir force develops a kink at a temperature $T_{\mathrm{kink}} < T_{c,\mathrm{bulk}}$.

The nature of the kink will be discussed at greater length in a subsequent section, but we begin to understand it from the renderings (fig. 2.1). Below the kink temperature, the moments achieve the twist of π by rotating about the axis while maintaining almost their full length m. Above the kink temperature, the moments all reside in a plane, and the twist is localized to the center of the system, where the magnetization has shrunk to zero. The nearest-neighbor interaction between moments imposes a free energy penalty for both rotating with respect to neighbors and varying in length. The transition indicates the point at which these penalties trade off in dominance.

2.3 The Casimir Force in the Ginzburg-Landau Mean-Field Theory of the Three-Dimensional XY Model

We now consider the continuous analogue of this system in the Ginzburg-Landau mean-field theory. The order parameter of the system is the magnetization profile $\mathbf{m}(z)$, where z is the finite dimension of the system. The behavior of the system is found by minimizing the free energy functional (per unit area),

$$\mathcal{F}\left[\mathbf{m}; t, L\right] = \int_{-L/2}^{L/2} dz \left[\frac{b}{2}\left|\frac{d\mathbf{m}}{dz}\right|^2 + \frac{1}{2}at\left|\mathbf{m}\right|^2 + \frac{1}{4}g\left|\mathbf{m}\right|^4\right], \tag{2.12}$$

with respect to $\mathbf{m}$ and subject to certain boundary conditions. This functional is the simplest non-trivial energy (expanding in a power series in the order parameter which is small in the vicinity of a critical point) which respects the $O(n)$ symmetry of the system[66, 15]. The derivative term, proportional to $(\mathbf{m}(z + \delta) - \mathbf{m}(z))^2$, is necessary to give the ferromagnetic interaction between layers which took the form $\mathbf{m}_i \cdot \mathbf{m}_{i+1}$ on the lattice, Eqn. (2.4). The quantity t represents the reduced temperature while b, a and g are all positive constants, whose microscopic nature is left unspecified.

Switching to polar coordinates,

$$\mathbf{m}(z) = (\Phi(z) \cos \varphi(z), \Phi(z) \sin \varphi(z)), \tag{2.13}$$

the free energy functional is rewritten as

$$\mathcal{F}[\Phi, \varphi; t, L] = \int_{-L/2}^{L/2} dz \left[\frac{b}{2} \left(\frac{d\Phi}{dz} \right)^2 + \frac{b}{2} \Phi^2 \left(\frac{d\varphi}{dz} \right)^2 + \frac{1}{2} at\Phi^2 + \frac{1}{4} g\Phi^4 \right]. \tag{2.14}$$

Minimization with respect to $\varphi(z)$ gives

$$\frac{d}{dz} \left(\Phi^2 \frac{d\varphi}{dz} \right) = 0 \tag{2.15}$$

which leads to

$$\Phi(z)^2 \left(\frac{d\varphi}{dz} \right) = P_\varphi \tag{2.16}$$

with an integration constant P_φ, independent of z, which roughly indicates the degree of twisting in the system. The condition from minimizing with respect to Φ is similarly computed as

$$b \frac{d^2\Phi}{dz^2} = b\Phi \left(\frac{d\varphi}{dz} \right)^2 + at\Phi + g\Phi^3 \tag{2.17}$$

or, with the identification (2.16),

$$b \frac{d^2\Phi}{dz^2} = b \frac{P_\varphi^2}{\Phi^3} + at\Phi + g\Phi^3. \tag{2.18}$$

The details of computing the functional derivatives above are laid out in appendix B. The problem is now that of solving Eqn. (2.18) subject to twisted boundary conditions:

$$\varphi(\pm L/2) = \pm\alpha/2,$$

$$\Phi(\pm L/2) = \infty, \tag{2.19}$$

27

i.e. where the moments at the boundaries are twisted by an angle α relative to one another. The fact that we may take the order parameter to be infinite at the boundaries was argued by Fisher and Nakanishi[67]: in the vicinity of critical phenomena, we have $\Phi \sim t^\beta$ and correlation length $\xi \sim t^{-\nu}$, with the standard critical exponents β and ν. This gives $\xi \sim \Phi^{-\nu/\beta}$ and therefore the effect of a large value Φ is felt in a very small local region. The critical phenomena occurring in the bulk of the system will be unaffected by a large order parameter at the boundary, so we are free to set it to infinity (i.e. it does not give substantially different results from any other large value) and we do so in order to simplify some of the subsequent mathematics.

Note that, because of reflection symmetry in Eqn. (2.18) and the boundary conditions imposed on Φ, we have that $\Phi(z) = \Phi(-z)$ and, thus, $\Phi'(z) = -\Phi'(-z)$, whence $\Phi'(0) = 0$. From the symmetry of Eqn. (2.16) one concludes $\varphi(z) = -\varphi(-z)$ which leads to $\varphi(0) = 0$.

Multiplying (2.18) by $d\Phi/dz$ and integrating with respect to z, we find a first integral

$$P_\Phi = -\frac{1}{2}b\left[\frac{P_\varphi^2}{\Phi^2} + \left(\frac{d\Phi}{dz}\right)^2\right] + \frac{1}{2}a\,t\,\Phi^2 + \frac{1}{4}g\,\Phi^4, \tag{2.20}$$

with P_Φ being another integration constant independent of z. Let $\Phi_0 \equiv \Phi(z = 0)$ be the amplitude of the order parameter at the center of the interval. Then, taking into account that $\Phi'(0) = 0$ one can conveniently express P_Φ as

$$P_\Phi = -\frac{1}{2}b\frac{P_\varphi^2}{\Phi_0^2} + \frac{1}{2}a\,t\,\Phi_0^2 + \frac{1}{4}g\,\Phi_0^4, \tag{2.21}$$

from which it follows that

$$\left(\frac{d\Phi}{dz}\right)^2 = P_\varphi^2\left(\frac{1}{\Phi_0^2} - \frac{1}{\Phi^2}\right) + \hat{a}t\left(\Phi^2 - \Phi_0^2\right) + \frac{\hat{g}}{2}\left(\Phi^4 - \Phi_0^4\right), \tag{2.22}$$

where

$$\hat{a} = \frac{a}{b}, \qquad \hat{g} = \frac{g}{b}. \tag{2.23}$$

28

The last result allows us to express the boundary conditions as

$$
\frac{L}{2} = \int_0^{L/2} dz = \int_{\Phi_0}^{\infty} d\Phi \frac{dz}{d\Phi}
$$

$$
= \int_{\Phi_0}^{\infty} d\Phi \frac{1}{\sqrt{P_\varphi^2 \left(\Phi_0^{-2} - \Phi^{-2}\right) + \hat{a}t \left(\Phi^2 - \Phi_0^2\right) + \frac{\hat{g}}{2} \left(\Phi^4 - \Phi_0^4\right)}} \quad (2.24)
$$

and

$$
\frac{\alpha}{2} = \int_0^{L/2} dz \frac{d\varphi}{dz} = \int_{\Phi_0}^{\infty} d\Phi \frac{d\varphi}{dz} \cdot \frac{dz}{d\Phi}
$$

$$
= P_\varphi \int_{\Phi_0}^{\infty} \frac{d\Phi}{\Phi^2} \frac{1}{\sqrt{P_\varphi^2 \left(\Phi_0^{-2} - \Phi^{-2}\right) + \hat{a}t \left(\Phi^2 - \Phi_0^2\right) + \frac{\hat{g}}{2} \left(\Phi^4 - \Phi_0^4\right)}}. \quad (2.25)
$$

These equations relate the integration constants, P_φ and Φ_0, to the system's external parameters, L and α.

The stress tensor operator for a system with the free energy functional (2.12) is [68]

$$
T_{k,l} = b \frac{\partial \mathbf{m}}{\partial x_k} \frac{\partial \mathbf{m}}{\partial x_l} - \delta_{k,l} \left\{ \frac{1}{2} b \left[\Phi'^2 + \Phi^2 \varphi'^2 \right] + \frac{1}{2} at\Phi^2 + \frac{1}{4} g\Phi^4 \right\}
$$

$$
- b \left[\frac{d-2}{4(d-1)} + O\left(g^3\right) \right] \left[\frac{\partial^2}{\partial x_k \partial x_l} - \delta_{k,l} \nabla^2 \right] \Phi^2. \quad (2.26)
$$

Calculating the $\langle T_{z,z} \rangle$ component, we obtain

$$
\langle T_{z,z} \rangle = \frac{1}{2} b \left[\left(\frac{d\Phi}{dz} \right)^2 + \frac{P_\varphi^2}{\Phi^2} \right] - \frac{1}{2} at\Phi^2 - \frac{1}{4} g\Phi^4 \quad (2.27)
$$

which we expect to be a z-independent quantity equal to the pressure $-\partial f/\partial L$ between plates confining a fluctuating medium[24, 68]. In our case, we see that

$$
\langle T_{z,z} \rangle \equiv -P_\Phi, \quad (2.28)
$$

by (2.20). From Eqns. (2.21) and (2.27) one observes that the Casimir force (the excess pressure over the bulk one) in this system is

$$
F_{\text{Cas}}(t, L) = - \left[-\frac{1}{2} b \frac{P_\varphi^2}{\Phi_0^2} + \frac{1}{2} a t \, \Phi_0^2 + \frac{1}{4} g \, \Phi_0^4 + \frac{1}{4g} (at)^2 \theta(-t) \right] \quad (2.29)
$$

where $\theta(x)$ is the Heaviside step function. Here, we have taken into account that the bulk free energy density f_b for the system is $f_b(t < 0) = -(at)^2/4g$ while $f_b(t > 0) = 0$. This

follows easily from Eqns. (2.18) and (2.14), because the spatial derivatives are vanishingly small in the bulk. As expected, the Casimir force is sensitive to the boundary conditions, through the quantities P_φ and Φ_0. An alternate, more verbose, computation of the Casimir force in this system is found in appendix B.

It is easy to show that $F_{\text{Cas}}(t, L)$ obeys the expected scaling. Indeed, in terms of the variables

$$z = L\zeta, \quad \Phi = \sqrt{\frac{2}{\hat{g}}} X_\Phi L^{-1}, \quad \Phi_0 = \sqrt{\frac{2}{\hat{g}}} X_0 L^{-1}, \quad P_\varphi = \frac{2}{\hat{g}} X_\varphi L^{-3}, \quad \hat{a}t = x_t L^{-2} \tag{2.30}$$

the Casimir force reads (note that ζ, X_Φ, X_0, X_φ and x_t are all dimensionless)

$$F_{\text{Cas}}(t, L) = \frac{b}{\hat{g}} L^{-4} X_{\text{Cas}}^{(\alpha)}(x_t), \tag{2.31}$$

where

$$X_{\text{Cas}}^{(\alpha)}(x_t) = \begin{cases} X_\varphi^2 / X_0^2 - \left(\frac{1}{2}x_t + X_0^2\right)^2, & x_t \leq 0 \\ X_\varphi^2 / X_0^2 - X_0^2 \left(x_t + X_0^2\right), & x_t \geq 0 \end{cases} . \tag{2.32}$$

Taking into account that mean-field theories for short-ranged systems are effective $d = 4$ theories[15], one concludes that Eqn. (2.31) is in full agreement with the expected scaling behavior (2.3) of the Casimir force. In appendix E we will derive the low temperature asymptotic behavior of the scaling function, finding

$$X_{\text{Cas}}^{(\alpha)}(x_t) \sim \frac{1}{2}\alpha^2 \left[|x_t| + 4\sqrt{2|x_t|} + \frac{1}{2}\left(48 - 3\alpha^2\right) \right], \tag{2.33}$$

when $x_t \to -\infty$.

One can further simplify (2.32) by introducing the convenient combinations of scaling variables

$$\tau = x_t / X_0^2, \quad \text{and} \quad p = X_\varphi / X_0^3. \tag{2.34}$$

Then the scaling function of the Casimir force reads

$$X_{\text{Cas}}^{(\alpha)}(\tau) = \begin{cases} X_0^4[p^2 - (1 + \tau)], & \tau \geq 0 \\ X_0^4[p^2 - (1 + \tau/2)^2], & \tau \leq 0 \end{cases} . \tag{2.35}$$

30

Eqns. (2.24) and (2.25) then become

$$X_0 = \int_1^\infty \frac{dx}{\sqrt{(x-1)[x^2 + x(1+\tau) + p^2]}},$$

(2.36)

and

$$\alpha = 2pX_0^3 \int_0^{1/2} \frac{d\zeta}{X_\Phi^2(\zeta)}.$$

(2.37)
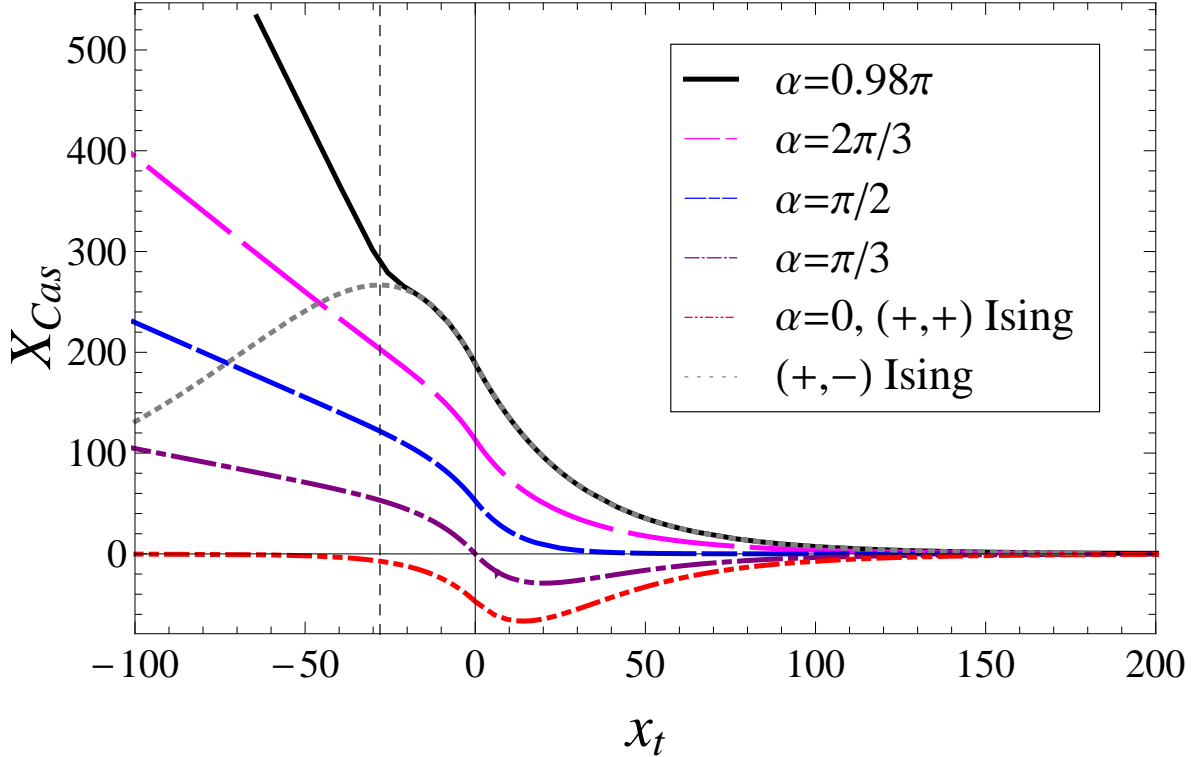
Figure 2.3: A plot of the dimensionless scaling function for the Casimir force, X_{Cas}, versus x_t (also dimensionless) for several values of α. The dotted curve is the Casimir scaling function in the Ising-like case of a critical fluid under $(+,-)$ boundary conditions. For x_t above a certain value, this curve coincides with the one for the model studied here when twisted by an angle $\alpha \approx \pi$.

In order to determine the Casimir force scaling function $X_{\text{Cas}}^{(\alpha)}(x_t)$, all one needs to know is the behavior of $X_0 = X_0(x_t|\alpha)$ and $X_\varphi(x_t|\alpha) = pX_0^3$ as functions of $x_t = \tau X_0^2$ at a given fixed value of the angle α. For that, one has to solve Eqns. (2.36) and (2.37) after determining

the function $X_\Phi(\zeta)$ from

$$\frac{1}{2} - \zeta = \frac{1}{2X_0} \int_{[X_\Phi(\zeta)/X_0]^2}^{\infty} \frac{dx}{\sqrt{(x-1)[x^2 + x(1+\tau) + p^2]}} \qquad (2.38)$$

with $0 \leq \zeta < 1/2$, which is derived in the same way as Eqn. (2.24) but integrating from ζ instead of from 0.

The analytical treatment of Eqns. (2.36)-(2.38) is performed in appendix D. The numerical evaluation of the expressions derived there is described in section 2.4 and leads to the results for the Casimir force presented in fig. 2.3. A comparison between the continuum results of this section and the lattice results of the previous section show excellent agreement – see fig. 2.4. In order to demonstrate it, we scale the lattice results (t, F_{Cas}) to $(a_t N^2 t, a_F N^4 F_{\text{Cas}})$, where the scaling factors a_t and a_F are determined by forcing the Casimir force with $\alpha = 0$ and $t = 0$ to agree between the two models. This was done numerically for $N = 50$, where we find $a_t \approx 2.977$ and $a_F \approx 7.480 \times 10^{-5}$. fig. 2.5 shows a comparison between the low temperature behavior of the Casimir force with the analytically derived asymptotic behavior reported in Eqn. (2.33). We find that, for all α, the asymptotic behavior is achieved for $x_t \lesssim -150$.

From Eqn. (2.35) one can also infer some general properties of the Casimir force. Taking into account that, at any fixed x_t and α, p is a definite function of x_t and α, i.e. that $p = p(\tau|\alpha)$ one can, e.g., determine the coordinates $x_{t,0}^\alpha$ of the zeros for the Casimir force for a given angle α. According to Eqn. (2.35) one has that $X_{\text{Cas}}^{(\alpha)} = 0$ for $p(\tau|\alpha) = \sqrt{1+\tau}$, with $\tau \geq 0$ and for $p(\tau|\alpha) = 1 + \tau/2$ when $-2 \leq \tau \leq 0$. A plot of the positions of these zeros in the (x_t, α)-plane is presented in fig. 2.6.

The figure demonstrates how, by changing, e.g., the twist angle α, we can, at a given temperature t, make the Casimir force either repulsive or attractive. For $0 < \alpha < \pi/2$, this can also be achieved by changing the temperature, i.e. the scaling variable x_t, at a given fixed value of α. We also conclude that, when $\alpha \to 0$, the position of the zero value of the Casimir force approaches $-\infty$. This implies that when $\alpha = 0$, the Casimir force will be attractive for all temperatures. Actually, for $\alpha = 0$, $X_{\text{Cas}}^{(\alpha)}(x_t)$ coincides with the known
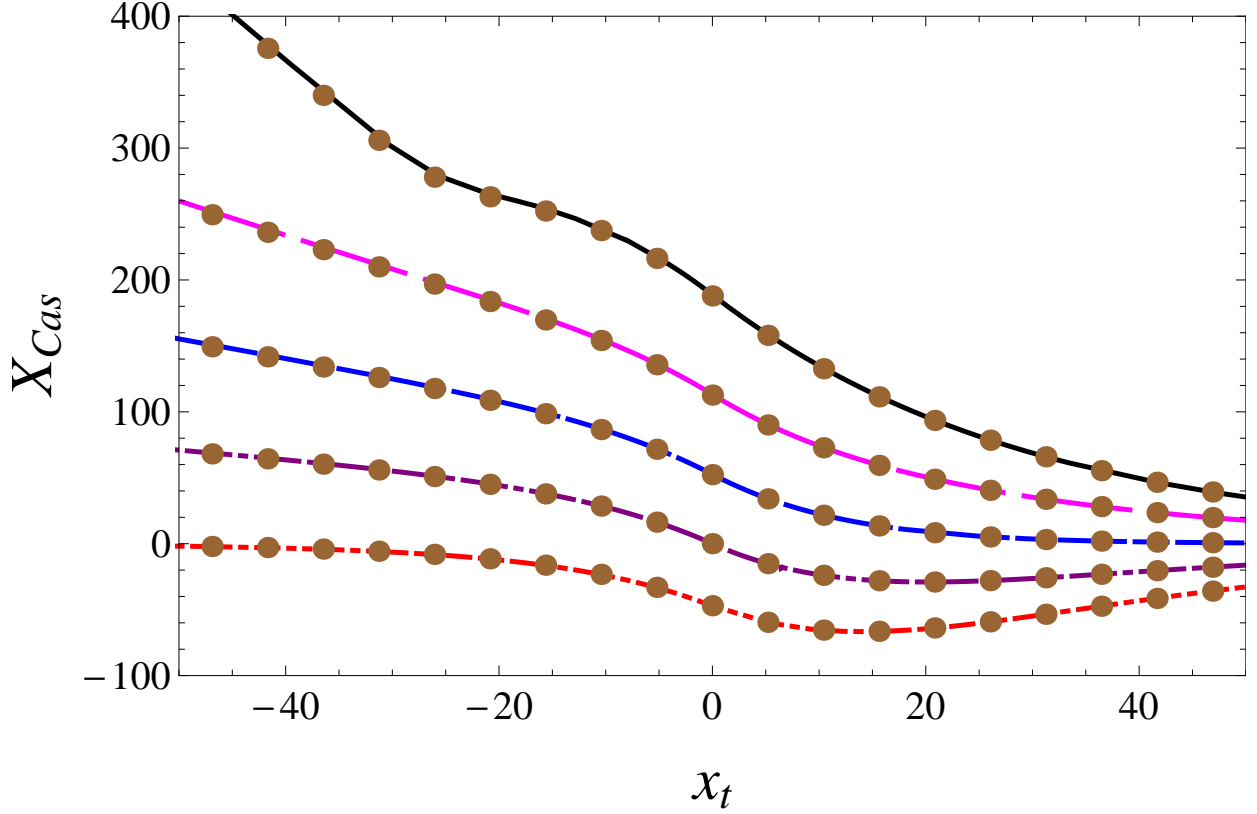
Figure 2.4: The scaling functions for the Casimir force in the Ginzburg-Landau model (solid curves), overlaid with those from the lattice model with $N = 50$ (brown points), for several values of α (from top to bottom: $\alpha = 0.98\pi$, $\alpha = 2\pi/3$, $\alpha = \pi/2$, $\alpha = \pi/3$, $\alpha = 0$).

result for the Ising model system[24]. The behavior of $X_{\text{Cas}}^{(+,+)}(x)$ is shown as a thick black line in fig. 2.3. These results are briefly re-derived in appendix D for the convenience of the reader.

When $\alpha \to \pi/2$, we observe in fig. 2.6 that $x_{t,0}^{(\alpha)} \to \infty$. Thus $\alpha > \pi/2$ implies that the Casimir force will be repulsive for all values of x_t. As α increases, the repulsive force becomes stronger. We see from fig. 2.3 that, when $\alpha = \pi/2$, the force is practically zero for all temperatures above the critical temperature of the finite system, while, for $\alpha > \pi/2$, it is repulsive in the whole temperature region. The cases $\alpha = 2\pi/3$ and $\alpha = 0.98\pi$ illustrate these features in the figure. It is also seen numerically that, for $x_t > -10$, the $\alpha = 0.98\pi$ curve

agrees with that of the mean-field Ising model with $(+, -)$ boundary conditions. At lower temperatures, there is an abrupt departure from the Ising model which will be discussed in section 2.5. The analytical expressions for the Ising model are known from [24]. For completeness, these results are recalled in Eqn. (D.22) of appendix D.
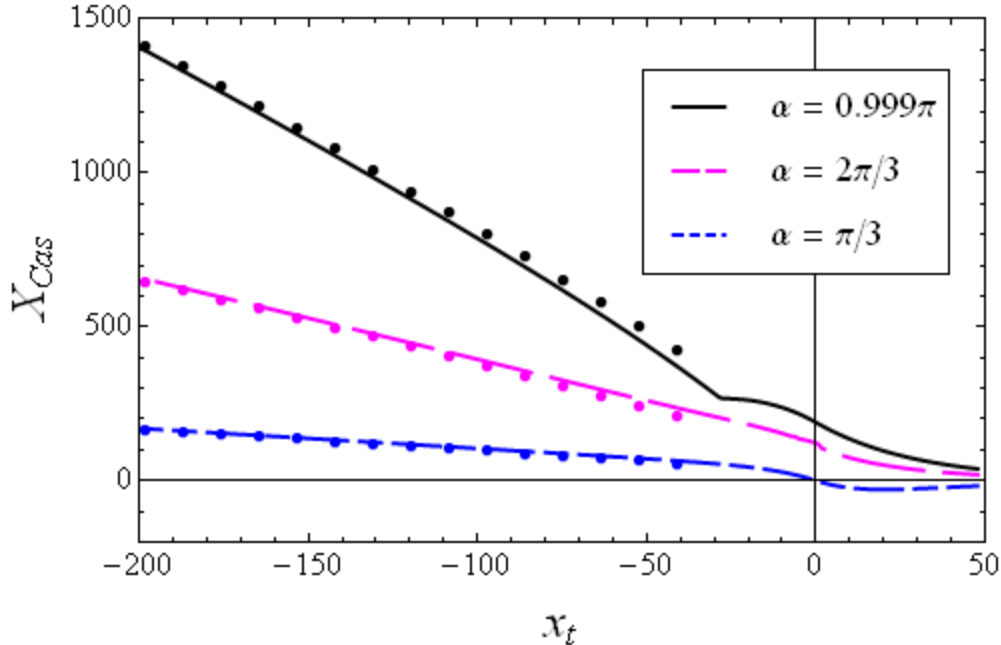
Figure 2.5: Casimir force curves in the Ginzburg-Landau model for several values of α, overlaid with their respective asymptotic expressions (dotted) given by Eqn. (2.33) as proven in appendix C.

The behavior of the critical Casimir force, $\Delta_{\text{Cas}}^{(\alpha)} = X_{\text{Cas}}^{(\alpha)}(x_t = 0)/3$, as a function of α, is illustrated in fig. 2.6. Note that the Casimir amplitude becomes zero at $\alpha = \pi/3$, so that the Casimir force for $\alpha = \pi/3$ changes its sign at $x_t = 0$. This was initially reported in [24] and may also be seen in fig. 2.6. Note that, in [24], a different type of parametrization of the amplitude and phase profiles is used – they are parametrized via the Casimir amplitudes. This led to a restriction of the results presented to the critical temperature only. For example, for the determination of the Casimir amplitudes in [24] one has to solve, in our notations, the following system of equations (see Eqn. (3.16) in [24]):
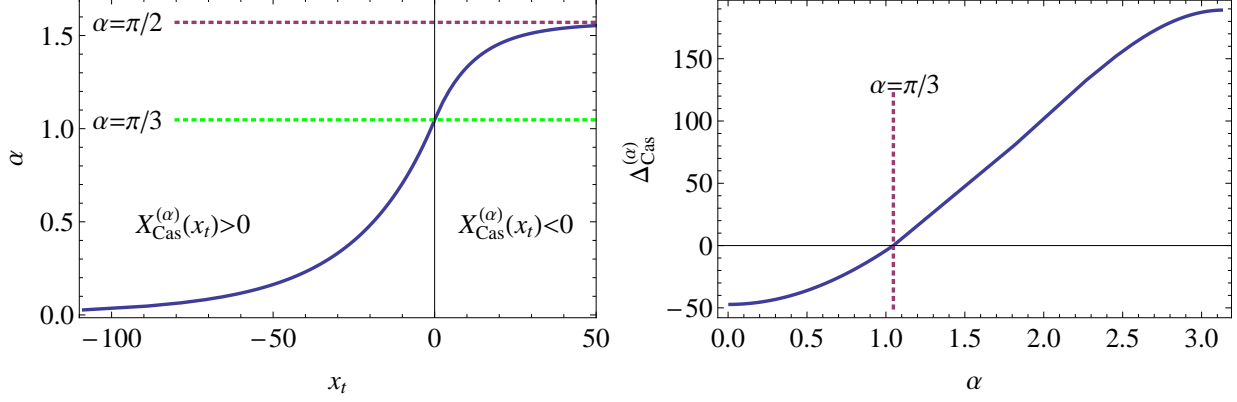
Figure 2.6: Left: The positions $x_{t,0}^{(\alpha)}$ of the zeros of the Casimir force in the (x_t, α)-plane. Right: The Casimir amplitude $\Delta_{\mathrm{Cas}}^{(\alpha)}$ as a function of the twist angle α. This curve was initially reported by Krech[24], and follows from the results of appendix D. The Casimir amplitude changes sign at $\alpha = \pi/3$.

$$X_0 = \int_1^\infty dx \, [x^3 - 1 + (x-1)X_0^{-4}\Delta_{\mathrm{Cas}}^{(\alpha)}]^{-1/2} \tag{2.39a}$$

and

$$\alpha = \sqrt{1 + X_0^{-4}\Delta_{\mathrm{Cas}}^{(\alpha)}} \int_1^\infty dx \, x^{-1}[x^3 - 1 + (x-1)X_0^{-4}\Delta_{\mathrm{Cas}}^{(\alpha)}]^{-1/2}. \tag{2.39b}$$

2.4 Numerical Solution of the Model

Here, we will briefly describe the numerical methods used in order to obtain the Casimir scaling functions in each of the lattice and continuum models.

2.4.1 Numerical Solution of the Lattice Model

We proceed from the results of section 2.2. The numerical problem is that of solving Eqns. (2.8), which we reproduce here:

$$\mathbf{m}_i = m \cdot \frac{2(d-1)\mathbf{m}_i + \mathbf{m}_{i-1} + \mathbf{m}_{i+1}}{|2(d-1)\mathbf{m}_i + \mathbf{m}_{i-1} + \mathbf{m}_{i+1}|} \cdot R\left(\beta m J \left| 2(d-1)\mathbf{m}_i + \mathbf{m}_{i-1} + \mathbf{m}_{i+1} \right| \right). \tag{2.8}$$

35

The mean-field magnetic moments $\mathbf{m}_i$ are each two-component vectors of length m and i runs from 1 to N, with $\mathbf{m}_0$ and $\mathbf{m}_{N+1}$ fixed according to twisted boundary conditions. The spatial dimensionality d will be taken to be three, $\beta = 1/(k_B T)$ is inverse temperature and J is the strength of the ferromagnetic interaction. $R(u) = I_1(u)/I_0(u)$ with modified Bessel functions I_0 and I_1.

For each i, we have two equations. Let $\mathbf{m}_i = m \cdot (x_i, y_i)$ with $x_i^2 + y_i^2 = 1$. Introduce the shorthand

$$\rho_i = |4\mathbf{m}_i + \mathbf{m}_{i-1} + \mathbf{m}_{i+1}| = m\sqrt{(4x_i + x_{i-1} + x_{i+1})^2 + (4y_i + y_{i-1} + y_{i+1})^2}, \qquad (2.40)$$

and the combination of variables

$$K = \beta J. \qquad (2.41)$$

Then at each layer the two equations to be solved are

$$f_i = \rho_i x_i - (4x_i + x_{i-1} + x_{i+1}) R(Km\rho_i) = 0, \qquad (2.42a)$$

$$g_i = \rho_i y_i - (4y_i + y_{i-1} + y_{i+1}) R(Km\rho_i) = 0. \qquad (2.42b)$$

There are a total of $2N$ equations in $2N$ variables. The boundary conditions are that $\mathbf{m}_0 = m \cdot (1, 0)$ and $\mathbf{m}_{N+1} = m \cdot (\cos\alpha, \sin\alpha)$. We will employ Newton's method to find solutions, which will involve constructing and inverting a $2N \times 2N$ matrix (see appendix C).

Concatenate the function components as $\mathbf{h} = (f_1, \ldots, f_N, g_1, \ldots, g_N)$, and the variables as $\mathbf{z} = (x_1, \ldots, x_N, y_1, \ldots, y_N)$. We populate the Jacobian matrix

$$[Dh]_{ij} = \frac{\partial h_i}{\partial z_j} = \left(\begin{array}{c|c} \nabla_{\mathbf{x}}\mathbf{f} & \nabla_{\mathbf{y}}\mathbf{f} \\ \hline \nabla_{\mathbf{x}}\mathbf{g} & \nabla_{\mathbf{y}}\mathbf{g} \end{array} \right)_{ij}, \qquad (2.43)$$

by computing partial derivatives. For instance, with $1 \le i = j \le N$ we have

$$[Dh]_{ii} = \frac{\partial f_i}{\partial x_i} = \rho_i + \frac{4x_i(4x_i + x_{i-1} + x_{i+1})}{\rho_i} - 4R(Km\rho_i)$$
$$- \frac{4Km(4x_i + x_{i-1} + x_{i+1})^2 R'(Km\rho_i)}{\rho_i}. \qquad (2.44)$$

Most entries in the matrix $[Dh]$ are zero. Each row of the matrix has either four or six non-zero entries, all of which look similar to the above. At a boundary, we insert the fixed values of $\mathbf{m}_0$ or $\mathbf{m}_{N+1}$.

We give an initial value to the vector $\mathbf{z}$ which we expect to be somewhat close to the solution, namely a uniform twist from $\mathbf{m}_0$ to $\mathbf{m}_{N+1}$. Therefore, we seed Newton's method with

$$x_i = \cos\left(\alpha i/(N+1)\right) \quad \text{and} \quad y_i = \sin\left(\alpha i/(N+1)\right), \tag{2.45}$$

where $i = 1, \ldots, N$. At each iteration, we compute $|\mathbf{h}|$ and stop the algorithm when it is sufficiently small (10^{-10} in our computations). We implemented the routine in Mathematica, and it performs reasonably quickly. Inversion of the matrix $[Dh]$ is sufficiently fast with Mathematica's built-in `Inverse` command.

After obtaining the solution $\mathbf{z} = (\mathbf{x}, \mathbf{y})$ to Eqns. (2.8), it remains to compute the free energy via Eqn. (2.9) and then the Casimir force. The discrete approximation to the derivative, Eqn. (2.11), has us compare the free energies of a system of length N and of length $N+1$. The boundary conditions remain the same, so this measures the free energy change associated with inserting a layer into the center of the system. Finally, we subtract off the bulk free energy density. This is given by Eqn. (2.10) where $m_{i,\text{bulk}}$ is determined by the transcendental equation

$$m_{i,\text{bulk}} = mR(6mKm_{i,\text{bulk}}), \tag{2.46}$$

as detailed in section 2.2. Given values of m and K, the solution is easily found using Mathematica's `FindRoot` command.

2.4.2 Numerical Solution of the Continuum Model

This problem amounts to solving the simultaneous equations

$$X_0 = \int_1^\infty dx \, \frac{1}{\sqrt{(x-1)\left(x^2 + \left(1 + \frac{x_t}{X_0^2}\right)x + \frac{X_\varphi^2}{X_0^6}\right)}} \tag{2.47}$$

$$\alpha = \frac{X_\varphi}{X_0^3} \int_1^\infty dx \, \frac{1}{x\sqrt{(x-1)\left(x^2 + \left(1 + \frac{x_t}{X_0^2}\right)x + \frac{X_\varphi^2}{X_0^6}\right)}} \tag{2.48}$$

which are the same as Eqns. (2.24) and (2.25) under a change to the scaling variables defined in Eqn. (2.30). For the moment, we do not employ the variables τ and p, defined in Eqn. (2.34), in order to explicitly show the non-trivial dependence on the unknowns X_0 and X_φ. We wish to solve for those variables, supposing that the twist α and the scaled temperature x_t are given.

In appendix D, we derive two separate closed form results for the above integrals, depending on the nature of the roots of the quadratic in the radical. There is good reason to believe that the two results should be in some way connected via analytic continuation. In fact, we find that we can take the result for complex roots and use it to correctly solve the system in Mathematica, even when the roots are not complex. Therefore, we will limit our attention to the closed forms (cf. Eqns. (D.15) and (D.18) in appendix D):

$$X_0 = \frac{2}{\sqrt{r}} K(w) \tag{2.49}$$

and

$$\alpha = \frac{p}{1-r}\left(X_0 - \frac{r+1}{\sqrt{r}} \cdot \Pi\left[-\frac{(r-1)^2}{4r}, w\right]\right), \tag{2.50}$$

where r and w are simple functions of p and τ:

$$r = \sqrt{2 + \tau + p^2} \quad \text{and} \quad w^2 = \frac{1}{2}\left(1 - \frac{3 + \tau}{2\sqrt{2 + \tau + p^2}}\right), \tag{2.51}$$

and we connect with the original problem through the relations $p = X_\varphi/X_0^3$ and $\tau = x_t/X_0^2$.

The virtue of this convoluted change of variables is that, in this set of variables, Eqns. (2.47) and (2.48) reduce to a single equation in the variable p. Indeed, plugging the X_0

equation into the α equation, we find

$$\alpha = \frac{2p}{(1-r)\sqrt{r}} \left(K(w) - \frac{r+1}{2} \cdot \Pi \left[-\frac{(r-1)^2}{4r}, w \right] \right) \equiv f(p), \qquad (2.52)$$

losing all explicit reference to X_0. Now, if we fix α and τ, the expression on the right hand side only depends on p and may be studied graphically, numerically, and, to some extent, analytically. In particular, in order for $f(p)$ to be real, we must have that $r > 0$ and $w^2 < 1$. The first condition yields $p^2 > -2 - \tau$ which is only a restriction on p when $\tau \leq -2$. The second condition gives $2\sqrt{2 + \tau + p^2} > -(3 + \tau)$, which again only restricts p when $\tau \leq -3$. There is also an apparent non-analyticity at $r = 1$, but we actually find $f(p) \approx pK(w) + O((r-1))$ in that vicinity, so everything is well-behaved.

Plotting the function for $\tau > -2$, we see that it is perfectly well-behaved, monotonically increasing from $f(0) = 0$ to $f(\infty) = \pi$. Therefore for $\tau > -2$ and $\alpha < \pi$, there will be always be a unique solution p. In the case $\tau \leq -2$, the function is only real-valued at sufficiently large p, namely $p > p_{\mathrm{asympt}} = \max\left(\sqrt{-2 - \tau}, \frac{1}{2}|\tau + 1|\right)$, the two options given by the conditions $r > 0$ and $w^2 < 1$, respectively. There is a vertical asymptote at the cutoff, with $f(p)$ dropping down from a value of $+\infty$ at that point, reaching a minimum value f_{min} at some larger value of p, and then approaching the value π from below as $p \to \infty$, as in the $\tau > -2$ case.

As τ is taken further negative, the value f_{min} increases. For $\alpha < \pi$, there exists a value $\tau_{\mathrm{min}}(\alpha)$ with $f_{\mathrm{min}} = \alpha$. If $\tau < \tau_{\mathrm{min}}$, then there is no physical solution to our problem. The case $\alpha = 0$ has $\tau_{\mathrm{min}} = -2$ as pointed out in appendix D, while $\tau_{\mathrm{min}} \to -\infty$ for $\alpha \to \pi$. When $\tau > \tau_{\mathrm{min}}$, though, there are two solutions, one at small p and one at large p. The various cases are illustrated in fig. 2.7. When the solutions come as a pair, they both have the same τ value, but they do not correspond to the same *temperature*, because the scaled temperature is $x_t = \tau X_0^2$, and X_0 is a function of p given by Eqn. (2.49). After computing the values of p, we have the full solution of the system.

Given $\alpha < \pi$, we now outline the computation of the Casimir profile in Mathematica. The first thing that must be done is to find τ_{min}, the lowest physically meaningful value of
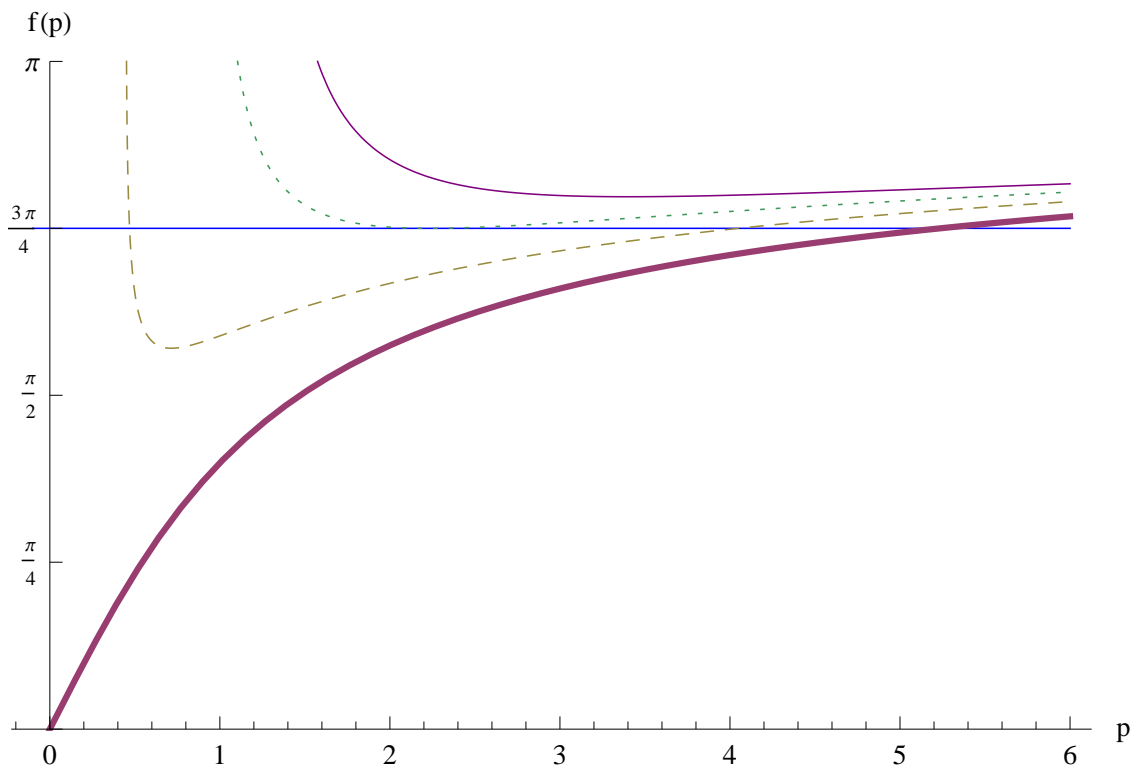
Figure 2.7: Graphical solution of Eqn. (2.52) with $\alpha = 3\pi/4$ and several values of τ. As τ is decreased, the number of solutions changes. Thick curve ($\tau = -1$): $\tau > -2$ always has one solution. Dashed curve ($\tau = -2.2$): $\tau_{\min} < \tau < -2$ has two solutions, one at $p \approx 0.5$ and the other at $p \approx 4$. Dotted curve ($\tau \approx -2.915$): $\tau = \tau_{\min}$ has only one solution. Thin, solid curve ($\tau = -3.5$): $\tau < \tau_{\min}$ has no solutions.

τ. $\tau_{\min}$ is determined by the simultaneous conditions $df/dp = 0$ and $f_{\min} = \alpha$. `FindRoot` can easily solve these two equations, given adequate initial values of τ and p. It was found that $\{$p, `Tan[`α`/2]^2`$\}$ and $\{\tau, -2.01\}$ worked over a wide range of α.

In the range $[\tau_{\min}, -2]$, each value of τ yields two data points. Because `FindRoot` only finds one solution at a time, we must tell it to look on each side of the minimum of $f(p)$. We find the location $p_{\min}$ of the minimum using `FindMinimum` and then ask `FindRoot` for a solution starting at $\frac{p_{\min} + p_{\mathrm{asympt}}}{2}$ and then again starting at $2p_{\min}$, where $p_{\mathrm{asympt}} = \max\left(\sqrt{-2 - \tau}, \frac{1}{2}|\tau + 1|\right)$ as discussed earlier. The range $(-2, \infty)$ is more straight-

forward, and a single call to `FindRoot` determines p without issue.

Once p is determined for a given τ, X_0 is given by Eqn. (2.49). Then $x_t = \tau X_0^2$ and the Casimir force is given by Eqn. (2.32), so the work is complete. It should be noted, however, that the case $\alpha = \pi$ is exceptional, and will be discussed separately in section 2.5 and appendix F. Indeed, there is no solution p to $f(p) = \pi$ when $\tau > -2$. This is because $\tau > -2$ corresponds to $x_t > x_{t,\text{kink}}$ and $X_0 = 0$ identically there[2]. Then $p = X_\varphi/X_0^3 = \infty$ is clearly the wrong variable to consider. The more useful combination, $M = X_\varphi/X_0$, remains non-zero and finite for all x_t. However, we cannot collapse the two equations into one equation if we use M in the place of p.

2.5 The Transition at $\alpha = \pi$

The case $\alpha = \pi$ warrants special investigation because it features behavior reminiscent of a phase transition. As mentioned in section 2.3, the high temperature behavior of the system at $\alpha \approx \pi$ tracks that of the Ising model with $(+, -)$ boundary conditions. However, we find that a kink develops in all quantities in the system at a temperature T_{kink} below the bulk critical temperature of the system, and the system changes its character at this temperature. The lattice model also features such a kink. In section 2.2, we illustrated how the lattice system switches from a "rotational" state below the kink temperature to a "planar" state above it. We note that this phase transition-like behavior is peculiar to the finite system with the given boundary conditions and is not present in the bulk. Below the kink temperature, there are two states of equal free energy: the rotational states with rotation plus or minus π. There is spontaneous symmetry breaking where the system orders in one of them. Above the kink temperature, there is a single state – the "planar" one.

The system incurs free energy penalties when adjacent moments vary in length or direction. We can see how the two types of states, rotational or planar, could extremize the energy.

---

[2]We can obtain solutions in the region $\tau \leq -2$, or equivalently $x_t < x_{t,\text{kink}}$, using the above method, though.
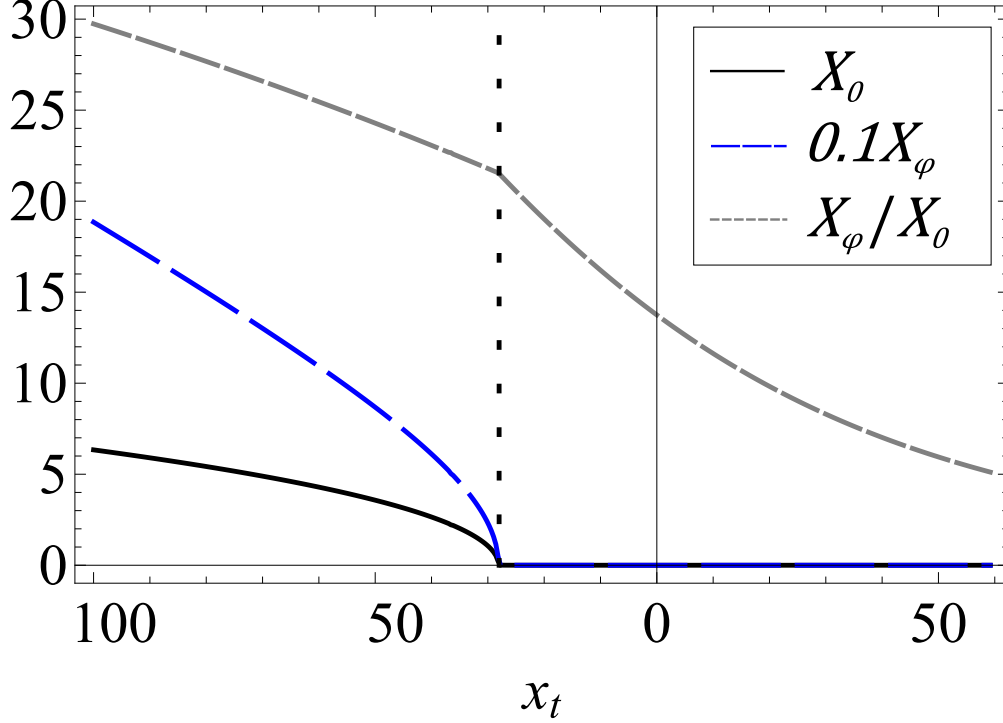
Figure 2.8: The dimensionless quantities X_0 (solid), $X_\varphi/10$ (long dashing; scale reduced for ease of plotting) and X_φ/X_0 (short dashing) as functions of x_t when $\alpha \approx \pi$. The vertical dotted line indicates $x_t = x_{t,\text{kink}}$.

The moments in the planar state minimize rotation: they reside in a plane and shorten to a length of zero at the center of the interval, where an abrupt reversal of direction occurs. The moments in the rotational state minimize length variation while gradually rotating from one end of the interval to the other. The temperature at which the kink occurs is the point at which the two energy penalties trade off in dominance. According to this description, the planar state is characterized by $X_0 = X_\varphi = 0$. Indeed, this is what comes out of the Ginzburg-Landau model above the kink temperature (see fig. 2.8). While these quantities vanish at high temperature, their ratio X_φ/X_0 remains non-zero at all temperatures.

In order to determine the kink temperature, we solve Eqns. (2.24) and (2.25) simultaneously in the vicinity of that transition point, i.e. with $X_0 = 0$ and X_φ/X_0 finite but

unknown. We find numerically (see appendix F)

$$x_{t,\text{kink}} \approx -28.1099. \tag{2.53}$$

Additionally, series expanding the conditions (2.24) and (2.25), we can find a first approximation to $X_0(x_t)$ in the vicinity of the kink. The result is that

$$X_0(x_t) \propto (x_{t,\text{kink}} - x_t)^{1/2}. \tag{2.54}$$

Recalling that X_0 is related to the magnitude of the order parameter and x_t proportional to reduced temperature, we have determined that the critical exponent $\beta = 1/2$ for this phase transition. This agrees with standard mean field results for, e.g. the magnetization of a ferromagnet.

We now present another, more transparent, analysis of this transition. We claim that, at high temperatures, the system's only energy extremum is the planar state, while, at low temperatures, the system has access to the planar state, as well as two energetically equivalent rotational states with a gradual turn of either π or $-\pi$. As previously described, the system favors the rotational state at low temperatures and ignores the planar state. Such a situation is commonly found in Ginzburg-Landau models, where the free energy has terms quartic and quadratic in a variable or field of interest. Depending on the coefficient of the quadratic term, there will be one fourth-order minimum at the origin or else a maximum at the origin and minima elsewhere. The planar state can be either an energy minimum or an energy maximum, while the rotational states are the symmetry-breaking minima that appear at sufficiently low temperature. By employing an approximation, we will show that this description fits the present system.

It is useful to turn to the scaling variables (2.30), in which the free energy functional, Eqn. (2.14), becomes

$$\mathcal{F} = \frac{b}{\hat{g}} \frac{1}{L^3} \int_{-1/2}^{1/2} d\zeta \left[\left(\frac{dX_\Phi}{d\zeta} \right)^2 + \frac{X_\varphi^2}{X_\Phi^2} + x_t X_\Phi^2 + X_\Phi^4 \right] \tag{2.55}$$

while the amplitude equation (2.18) reads

$$\frac{d^2 X_\Phi}{d\zeta^2} = \frac{X_\varphi^2}{X_\Phi^3} + x_t X_\Phi + 2X_\Phi^3. \tag{2.56}$$

Due to the boundary conditions (2.19) the amplitude profile near the edges, $X_\Phi(\zeta \approx \pm 1/2)$, is largely temperature independent, i.e. it is almost the same above and below the transition temperature. The behavior near $\zeta = 0$ must therefore account for the physics of the transition. Near the transition temperature, we have $X_0 \approx 0$ and thus $X_\Phi(\zeta) \ll 1$ for $\zeta \approx 0$. Then Eqn. (2.56) reduces to

$$\frac{d^2 X_\Phi}{d\zeta^2} = \frac{X_\varphi^2}{X_\Phi^3} \tag{2.57}$$

with solution

$$X_\Phi(\zeta) = \sqrt{X_0^2 + \left(\frac{X_\varphi}{X_0}\right)^2 \zeta^2} \equiv \sqrt{X_0^2 + M^2\zeta^2}, \tag{2.58}$$

defining $M \equiv X_\varphi/X_0$.

The free energy integral can now be computed in closed form using the asymptotic expression (2.58). The expression for $X_\Phi(\zeta)$ is only valid up to some cutoff $\zeta = Y < 1/2$, but the free energy from the edges of the interval ($|\zeta| > Y$) will not contribute to the behavior of the system, provided that Y is large enough. The result of the integral is

$$\mathcal{F} \approx \frac{2bY}{\hat{g}L^3}\left[X_0^4 + \left(x_t + \frac{2}{3}Y^2M^2\right)X_0^2 + \left(\frac{1}{5}Y^4M^4 + \frac{1}{3}x_tY^2M^2 + M^2\right)\right] \tag{2.59}$$

which is quartic in X_0, the (scaled) amplitude of the order parameter at the center of the interval. In the planar state, $X_0 = 0$, while rotational states have $X_0 > 0$. Therefore we expect to always see an extremum at $X_0 = 0$, corresponding to the planar state, which will be a free energy minimum at high temperature and a maximum at low temperature. When the planar state is a maximum, two minima (rotational states) with $|X_0| > 0$ should emerge. Indeed, this behavior is clear from the form of (2.59). The position of the non-zero minimum is found to be

$$X_0 = \pm\sqrt{-\frac{1}{2}\left(x_t + \frac{2}{3}Y^2M^2\right)}, \tag{2.60}$$

which is only real for sufficiently low temperature: $x_t \leq -2Y^2M^2/3 < 0$. The transition occurs when equality holds. This does not fully determine the temperature of the transition because both Y and M are functions of x_t. The additional constraints are afforded by matching the hyperbolic expression (2.58) for $X_\Phi(\zeta)$ with another expression correct near the edge of the interval.

44

When $\zeta \approx \pm 1/2$, $X_\Phi \to \infty$ and, according to (2.56) the amplitude profile is determined by

$$\frac{d^2 X_\Phi}{d\zeta^2} = x_t X_\Phi + 2X_\Phi^3 \tag{2.61}$$

which, with $x_t < 0$, is solved by

$$X_\Phi(\zeta) = \sqrt{|x_t|} \csc\left[\sqrt{|x_t|}\left(\frac{1}{2} - |\zeta|\right)\right]. \tag{2.62}$$

Now imposing the continuity of $X_\Phi(\zeta)$ and $X_\Phi'(\zeta)$ from (2.58) and (2.62) at $\zeta = Y$ allows us to solve for the parameters at the transition point. Proceeding numerically, we find:

$$x_{t,\mathrm{kink}} \approx -22.4587, \qquad M_{\mathrm{kink}} \approx 19.4498,$$

$$X_{0,\mathrm{kink}} = 0, \qquad Y_{\mathrm{kink}} \approx 0.2984. \tag{2.63}$$

Compared to the exact numerical results obtained in appendix F, these values are consistent as a first approximation, as are the behaviors of $X_0(x_t)$ and $M(x_t)$. In particular, the leading order contribution to $X_0(x_t)$ goes as $(x_{t,\mathrm{kink}} - x_t)^{1/2}$, in agreement with the power law previously found. Finally, it is easy to show that at the kink temperature the rate of change of the phase in the middle of the system diverges. Indeed, from Eqn. (2.16) and using the definitions (2.30) one obtains

$$\left[\frac{X_\Phi(\zeta)}{X_0}\right]^2 \frac{d\varphi(\zeta)}{d\zeta} = \frac{X_\varphi}{X_0^2} = \frac{M}{X_0}. \tag{2.64}$$

Thus, in the limit $\zeta \to 0$ one derives at $x_t = x_{t,\mathrm{kink}}$ that $(d\varphi(\zeta)/d\zeta)|_{\zeta=0} = M/X_0 \to \infty$, since $X_{0,\mathrm{kink}} = 0$. Therefore, at the kink temperature all the change in the phase of the moments happens at the middle of the system, where their length becomes zero. The phase of the moments jumps there from 0 to π.

2.6 Discussion and Concluding Remarks

We have studied the $O(2)$ model in a three-dimensional film geometry, and find identical predictions from lattice and continuum mean-field theories. Consistent with systems of

similar type, the Casimir force with symmetric boundary conditions ($\alpha = 0$) is attractive, while the Casimir force with anti-symmetric boundary conditions ($\alpha = \pi$) is repulsive. In particular, the critical Casimir force, i.e. F_{Cas} at the bulk transition temperature, changes from repulsive to attractive. This is a standard result, but we also find intermediate scenarios when $0 < \alpha < \pi$ which feature critical Casimir forces, and scaling functions for the Casimir force (illustrated in fig. 2.2), different from those of the symmetric and anti-symmetric cases. The Casimir force may therefore be continuously adjusted at constant temperature by varying the twist α, or at constant twist by varying the temperature.

Additionally we find that, when the boundary conditions are perfectly anti-symmetric ($\alpha = \pi$), the system undergoes a phase transition at a temperature below the bulk critical temperature. We are able to understand this transition as a symmetry-breaking effect: at high temperatures the moments of the system are confined to a plane, while at low temperatures they rotate about the z-axis by either π or $-\pi$ to satisfy the boundary conditions. The high temperature behavior tracks that of an Ising model whose order parameter is always simply up or down, but our system departs from that behavior at the transition point, once moments find it energetically favorable to rotate out of a plane.

CHAPTER 3

The Casimir Force in the $O(n)$ Model with $n \to \infty$

3.1 Introduction

On the heels of Onsager's 1944 solution of the two-dimensional Ising model[69], it was hoped that some clever approach could dispatch the Ising model in three dimensions as Onsager had shown it possible in two. In 1947, looking for a simpler system that might shed light on the Ising problem, Kac[1] came up with the "Gaussian" model where each spin variable is a Gaussian random variable of width 1, rather than being restricted to the values ± 1. The Ising model has a partition function

$$Z_{\text{Ising}} = \sum_{s_1 = \pm 1} \cdots \sum_{s_N = \pm 1} \exp \left[\beta J \sum_{\langle s_i, s_j \rangle} s_i s_j \right], \tag{3.1}$$

with $J > 0$ the ferromagnetic coupling, β the inverse temperature and $\sum_{\langle x, y \rangle}$ indicating a sum over nearest neighbors. In contrast, the Gaussian model has

$$Z_{\text{Gaussian}} = \int_{-\infty}^{\infty} ds_1 \cdots ds_N \, \exp \left[-\frac{1}{2} \sum_i s_i^2 \right] \exp \left[\beta J \sum_{\langle s_i, s_j \rangle} s_i s_j \right], \tag{3.2}$$

which can be integrated in closed form after taking a Fourier transform. In section 3.2, a similar calculation will be performed.

There is a striking similarity between the functional form of the results from the Gaussian and Ising models. For example, the thermodynamic limit of the Gaussian model in two

---

[1]Kac gives a first-hand description of the events leading up to his invention of the spherical model as part of an interesting article in memoriam of T. Berlin[70].

dimensions has a free energy per site

$$\frac{1}{2\beta} \cdot \frac{1}{(2\pi)^2} \int_0^{2\pi} d\omega_1 \, d\omega_2 \, \ln\left[1 - 2\beta J \left(\cos\omega_1 + \cos\omega_2\right)\right], \tag{3.3}$$

while the Ising model has

$$-\frac{1}{2\beta} \cdot \frac{1}{(2\pi)^2} \int_0^{2\pi} d\omega_1 \, d\omega_2 \, \ln\left[\cosh^2(2\beta J) - \sinh(2\beta J)\left(\cos\omega_1 + \cos\omega_2\right)\right], \tag{3.4}$$

and the two agree very well at high temperatures except for the negative sign[23]. However, we see that the Gaussian model is unphysical because, when $2\beta J > \frac{1}{2}$, the free energy becomes complex. Thus, there is a positive temperature below which the model is entirely broken. This may be traced back to the quadratic form in the partition function developing a negative eigenvalue, and it happens in any spatial dimension.

After some time, Kac hit upon the "spherical" constraint, which avoids the low-temperature breakdown while retaining some of the simplicity of the Gaussian model's mathematics. The Ising model with N spins has 2^N possible configurations $\{\pm 1, \ldots, \pm 1\}$, and these configurations may be visualized as the vertices of a cube in N dimensions. The spherical constraint puts the spins on a sphere in N dimensions, instead:

$$s_1^2 + \ldots + s_N^2 = N. \tag{3.5}$$

The partition function for the spherical model is therefore

$$Z_{\text{SM}} = \int_{-\infty}^{\infty} ds_1 \cdots ds_N \, \exp\left[\beta J \sum_{\langle s_i, s_j \rangle} s_i s_j\right] \delta\left(\sum_{i=1}^{N} s_i^2 - N\right). \tag{3.6}$$

Kac solved the model in one, two and three dimensions with help from T. Berlin[23]. Montroll also arrived at the same results independently[71]. They found that the spherical model undergoes a phase transition in three dimensions (and, it turns out, in higher dimensions[37]) but not in one or two. The Ising model, of course, exhibits phase transitions in dimensions two and higher. Nonetheless, as an exactly solvable model in three dimensions with a phase transition, the spherical model was a sensational discovery.

About two decades later, Stanley showed that there is a formal correspondence between the spherical model and the $O(n)$ model in the $n \to \infty$ limit[22] if translational invariance

is assumed (i.e. an infinite lattice or periodic boundary conditions). So, while the spherical model was invented as an approximation to the $O(1)$ model, it was eventually understood to be, in some sense, the $O(n \to \infty)$ model. It is worthwhile to note that the spherical model also maps onto the ideal Bose gas in the neighborhood of their transitions[72].

Shortly after Kac and Berlin published their initial paper on the spherical model, Lewis and Wannier showed that the same thermodynamic results followed if the spherical constraint is simply enforced in the mean[73, 74],

$$\left\langle \sum_{i=1}^{N} s_i^2 \right\rangle = N, \tag{3.7}$$

while the partition function is modified to

$$Z_{\text{MSM}} = \int_{-\infty}^{\infty} ds_1 \cdots ds_N \, \exp\left[\beta J \sum_{\langle s_i, s_j \rangle} s_i s_j - \beta\Lambda \sum_{i=1}^{N} s_i^2\right]. \tag{3.8}$$

The condition (3.7), given by $-\partial \ln Z_{\text{MSM}}/\partial\Lambda = N$, replaces the computationally challenging constraint on the integration domain, and we call the resulting model the "mean" spherical model.

The relationship between the spherical model and the mean spherical model is analogous to that between a canonical ensemble and its grand canonical ensemble. In that case, a restricted sum over states with fixed particle count N is replaced by an unrestricted sum over states but the Boltzmann factor is multiplied by $\exp(-\beta\mu N)$ which makes it a sharply peaked function of N if the chemical potential μ is chosen appropriately[66]. In the analogy to the spherical model, the particle count corresponds to $\sum_i s_i^2$ and the chemical potential to the Lagrange multiplier Λ which we call the "spherical field". Thus, the spherical and mean spherical models describe the same system in two different ensembles. Because the ensembles are equivalent in the thermodynamic limit[66], it is not surprising that the two models give the same results[73, 75].

As in earlier chapters, we are interested in finite-size effects, and the natural geometry to consider is that of a thin film. Such a geometry is not translationally invariant along its finite dimension, and therefore the Stanley correspondence (between $O(n \to \infty)$ and

spherical models) breaks down. The appropriate generalization was shown to be one in which each transverse layer of the film satisfies its own independent spherical (or mean spherical) constraint[76]. In other words, if we are interested in the film-geometry behavior of the $O(n)$ model with $n \to \infty$, then we may equally well study this per-layer spherical model. One may also study the film-geometry behavior of the standard spherical model, with only one sum constraint for the entire system. However, these two systems are in general *not* equivalent.

The latter problem, a spherical model in film geometry with one system-wide constraint, has been worked out. In three dimensions, with periodic boundary conditions, closed form results for the scaling functions of the excess free energy and Casimir force were obtained by Danchev[77]. More recently, Kastening and Dohm studied the system under several other types of boundary conditions (which, unlike periodic boundary conditions, break translational invariance). Their results indicated violations of finite-size scaling[78] which may point to this system being unphysical.

We will now study the Casimir force in a three-dimensional $O(n \to \infty)$ model with film geometry. We will model it using the per-layer mean spherical constraints mentioned above. An equivalent system was independently analyzed, very recently, by Diehl et al.[41] using different methods than will be presented here. The results of that analysis appear to be restricted to a limited range of temperatures, and the model they employ must be regularized, with a free parameter fixed in an arbitrary manner.

The present work features a solution of the model at *all* temperatures, including closed form asymptotic results for the Casimir force in the neighborhood of $T = 0$ (appendix I). In section 3.2, we will define our lattice model, which has no free parameters, and formulate the spherical constraints. In section 3.3, we will consider the three-dimensional bulk system before describing the finite-size system in section 3.4. The numerical methods used to solve the system and generate our Casimir scaling curves are explained in section 3.5. Finally, we conclude with a summary and discussion of our findings in section 3.6.

3.2 The Model

We are interested in the $O(n)$ model, with $n \to \infty$, in a film geometry and with free boundary conditions. Consider a d-dimensional square lattice, each of whose lattice sites is occupied by an n-component vector spin interacting with its nearest neighbors in the usual way. We will single out one dimension (called z) to be finite, L lattice spacings long. At each of the L sites along the finite dimension, there is a $(d-1)$-dimensional transverse layer containing a total of A spins (A is large and will later be taken to infinity). We will eventually specialize to $d = 3$, but for the time being we can describe this more general setup. Free boundary conditions mean, in this system, that there is a layer of all zero spins on the top and on the bottom of the film (i.e. $z = 0$ and $z = L + 1$).

The model, as described, is not especially amenable to analysis. However, owing to the work of Stanley[22] and Knops[76], we know that this model is equivalent to a form of the spherical model, wherein the vector spins are replaced by real-valued scalar spins and each $(d-1)$-dimensional layer satisfies a spherical constraint $\sum s^2 = A$. We simplify matters even further by using the mean spherical model which gives the same results as the spherical model in the thermodynamic limit, i.e. when A is large.

Our Hamiltonian is

$$H = -J \sum_{\langle s, s' \rangle} ss' + J \sum_i \Lambda_i \left(\sum_j s_{i,j}^2 - A \right) \tag{3.9}$$

where the first summation is taken over nearest neighbor spins s and s', which may each lie in the same layer or in adjacent layers. J is the positive ferromagnetic coupling and Λ_i is the spherical field for layer i which will be used to enforce the mean spherical constraints. The notation $s_{i,j}$ refers to spin j in layer i, with $i = 1, \ldots, L$ and $j = 1, \ldots, A$. The partition function is

$$Z = \sum_{\{s\}} e^{-\beta H} = \int \left(\prod_{i,j} ds_{i,j} \right) e^{-\beta H}, \tag{3.10}$$

51

summing over all possible configurations of the spins. The per-layer spherical constraints are

$$0 = \left\langle \sum_j s_{i,j}^2 \right\rangle - A = -\frac{1}{\beta J} \frac{\partial \ln Z}{\partial \Lambda_i}, \tag{3.11}$$

for each $i = 1, \ldots, L$. Satisfying the constraints determines the Lagrange multipliers Λ_i.

Now we use some tricks, standard for the Gaussian and spherical models, which enable us to find a closed form for the partition function. Once we have done that, it will be possible to concisely write down the mathematical problem facing us. First, we Fourier expand our spin variables in lattice modes. Let

$$s_{i,j} = A^{-1/2} \sum_{\mathbf{q}} s_i(\mathbf{q}) e^{i\mathbf{r}_j \cdot \mathbf{q}}, \tag{3.12}$$

where $\mathbf{q}$ ranges over the first Brillouin zone of the ith layer's $(d-1)$-dimensional lattice and $\mathbf{r}_j$ is the position of spin $s_{i,j}$ within that lattice.

To understand the nearest neighbor terms, first fix i and j and consider spin $s_{i,j}$. It has $2(d-1)$ nearest neighbors in layer i, and one nearest neighbor in each of layer $i-1$ and layer $i+1$. At the boundaries, $i=1$ and $i=L$, this is still valid; our free boundary conditions put $s_{0,j} = s_{N+1,j} = 0$ for all j. For neighbors within the layer, the Fourier-expanded interaction has terms like

$$\sum s_{i,j} s_{i,j'} = \frac{1}{A} \sum_{j',\mathbf{q},\mathbf{q}'} s_i(\mathbf{q}) s_i(\mathbf{q}') e^{i\mathbf{r}_j \cdot \mathbf{q}} e^{i\mathbf{r}_{j'} \cdot \mathbf{q}'},$$

and $\mathbf{r}_{j'}$ is simply related $\mathbf{r}_j$ because they are neighbors on a square lattice. Specifically, $\mathbf{r}_{j'} = \mathbf{r}_j \pm a\mathbf{e}_i$, $i = 1, \ldots, (d-1)$, with lattice spacing a and standard basis vectors $\mathbf{e}_i$ in the layer (this will lead to cosine terms). On the other hand, the neighbors in adjacent layers have the same $\mathbf{r}_j$ but $s_{i\pm 1}$ rather than s_i. Summing over i and j will count every nearest-neighbor link in the system twice, so we divide everything by two to correct the double-counting. Taking the lattice spacing a to be one, we therefore have

$$-J \sum_{\langle s,s' \rangle} ss' = -\frac{J}{2A} \sum_{i,j} \sum_{\mathbf{q},\mathbf{q}'} \left\{ \sum_{k=1}^{d-1} s_i(\mathbf{q}) s_i(\mathbf{q}') e^{i\mathbf{r}_j \cdot (\mathbf{q}+\mathbf{q}')} 2\cos(q_k') \right.$$

$$\left. + \left[s_i(\mathbf{q}) s_{i-1}(\mathbf{q}') + s_i(\mathbf{q}) s_{i+1}(\mathbf{q}') \right] e^{i\mathbf{r}_j \cdot (\mathbf{q}+\mathbf{q}')} \right\}. \tag{3.13}$$

An orthogonality relation on this lattice is

$$\sum_j \exp\left(i\mathbf{r}_j \cdot \mathbf{q}\right) = A\delta_{\mathbf{q}0} \tag{3.14}$$

which allows us to perform the sums over j and $\mathbf{q}'$ in Eqn. (3.13). We find

$$-J\sum_{\langle s,s'\rangle} ss' = -\frac{J}{2}\sum_{i,\mathbf{q}}\left[s_i(\mathbf{q})s_{i-1}(-\mathbf{q}) + s_i(\mathbf{q})s_{i+1}(-\mathbf{q}) + \sum_{k=1}^{d-1} 2\cos(q_k)s_i(\mathbf{q})s_i(-\mathbf{q})\right]. \tag{3.15}$$

The Lagrange multiplier terms give

$$J\sum_i \Lambda_i\left(\sum_j s_{i,j}^2 - A\right) = J\sum_i \Lambda_i \sum_{\mathbf{q}} s_i(\mathbf{q})s_i(-\mathbf{q}) - JA\sum_i \Lambda_i, \tag{3.16}$$

and so the entire Hamiltonian is

$$H = \frac{J}{2}\sum_{i,j,\mathbf{q}} s_i(\mathbf{q})\left[\left(2\Lambda_i - 2\sum_{k=1}^{d-1}\cos(q_k)\right)\delta_{ij} - \left(\delta_{i,j+1} + \delta_{i,j-1}\right)\right]s_j(-\mathbf{q})$$

$$- JA\sum_i \Lambda_i. \tag{3.17}$$

If the system was translationally invariant along the z direction, then the Hamiltonian would have been diagonalized by this method. As it stands, it is tri-diagonal instead. Nevertheless, we may use this result to evaluate the partition function integral. First, we compactify our notation by defining

$$\mathcal{H}_{ij} = \begin{pmatrix} 2\Lambda_1 & -1 & 0 & \cdots \\ -1 & 2\Lambda_2 & -1 & \\ 0 & -1 & 2\Lambda_3 & \\ \vdots & & & \ddots \end{pmatrix}_{ij} = \begin{cases} 2\Lambda_i, & i = j \\ -1, & |i-j| = 1 \\ 0, & \text{otherwise} \end{cases} \tag{3.18}$$

and the corresponding

$$\mathcal{H}(\mathbf{q}) = \mathcal{H} - \left[2\sum_{k=1}^{d-1}\cos q_k\right]I_L, \tag{3.19}$$

with I_L the $L \times L$ identity matrix. Finally, taking the complex conjugate of Eqn. (3.12) shows that $s_i(-\mathbf{q}) = s_i(\mathbf{q})^\dagger$. This enables us to express the Hamiltonian as the quadratic form

$$H = -JA\sum_i \Lambda_i + \frac{J}{2}\sum_{\mathbf{q}}\sum_{i,j} s_i(\mathbf{q})^\dagger\left[\mathcal{H}(\mathbf{q})\right]_{ij} s_j(\mathbf{q}). \tag{3.20}$$

Now the partition function may be evaluated:

$$Z = \int \left(\prod_{i,j} ds_{i,j} \right) e^{-\beta H}$$

$$= e^{\beta JA \sum_i \Lambda_i} \int \prod_{\mathbf{q}} \left(\prod_i ds_i(\mathbf{q}) \, \exp\left[-\frac{\beta J}{2} \mathbf{s}(\mathbf{q})^\dagger \mathcal{H}(\mathbf{q}) \mathbf{s}(\mathbf{q}) \right] \right) \quad (3.21)$$

where we have changed variables $s_{i,j} \to s_i(\mathbf{q})$, as defined in Eqn. (3.12). The Jacobian of the transformation can be shown to be unitary and thus have determinant of magnitude 1. For each value of $\mathbf{q}$, the Gaussian integral is evaluated according to

$$\int dx_1 \cdots dx_L \, \exp\left(-\mathbf{x}^\dagger \mathcal{M} \mathbf{x} \right) = \sqrt{\frac{\pi^L}{\det \mathcal{M}}}. \quad (3.22)$$

Therefore the partition function is

$$Z = e^{\beta JA \sum_i \Lambda_i} \prod_{\mathbf{q}} \sqrt{\frac{\pi^L}{\det(\beta J \mathcal{H}(\mathbf{q})/2)}} = e^{\beta JA \sum_i \Lambda_i} \prod_{\mathbf{q}} \sqrt{\frac{(2\pi)^L}{(\beta J)^L \det(\mathcal{H}(\mathbf{q}))}}. \quad (3.23)$$

Again, we remark at this point that, in a translationally invariant system, the matrix $\mathcal{H}(\mathbf{q})$ is diagonal and its determinant is simply the product of its diagonal elements. Thus, that system has a truly closed form expression for its partition function. On the other hand, we have a tri-diagonal matrix in our problem, and its eigenvalues are not known in closed form (though they can easily be determined numerically if all other parameters are specified).

Continuing, the free energy in this system is

$$\mathcal{F} = -\frac{1}{\beta} \ln Z = -JA \sum_i \Lambda_i + \frac{1}{2\beta} \sum_{\mathbf{q}} \ln[\det(\mathcal{H}(\mathbf{q}))] - \frac{1}{2\beta} AL \ln\left(\frac{2\pi}{\beta J} \right) \quad (3.24)$$

where we have made use of the fact that there are A points in the first Brillouin zone of the lattice of the $(d-1)$-dimensional layer. The mean spherical constraint, equivalent to minimizing the free energy with respect to the Λ_i, is

$$0 = \frac{\partial \mathcal{F}}{\partial \Lambda_i} = \frac{1}{2\beta} \sum_{\mathbf{q}} \frac{\partial \ln[\det(\mathcal{H}(\mathbf{q}))]}{\partial \Lambda_i} - JA \quad (3.25)$$

for each $i = 1, \ldots, L$. We can write the constraints more explicitly by using the matrix identity

$$\frac{\partial \ln[\det(\mathcal{M})]}{\partial \Lambda_i} = \mathrm{tr}\left(\mathcal{M}^{-1} \frac{\partial \mathcal{M}}{\partial \Lambda_i} \right) = \sum_{j,k} \mathcal{M}_{kj}^{-1} \left(\frac{\partial \mathcal{M}}{\partial \Lambda_i} \right)_{jk}, \quad (3.26)$$

and computing $(\partial \mathcal{H}(\mathbf{q})/\partial \Lambda_i)_{jk} = 2\delta_{ij}\delta_{ik}$ for our particular matrix, Eqn. (3.19). Thus the constraints take the form

$$\beta J A = \sum_{\mathbf{q}} [\mathcal{H}(\mathbf{q})]_{ii}^{-1}. \tag{3.27}$$

Now the problem is that of determining the spherical fields Λ_i which satisfy Eqn. (3.27) for $i = 1, \ldots, L$. Before proceeding with that computation, we consider the simpler bulk model which is needed in computing the Casimir force.

3.3 The Bulk System

In considering the bulk version of the model from section 3.2, we retain the Hamiltonian, cf. Eqn. (3.9),

$$H = -J \sum_{\langle s,s' \rangle} s s' + J \sum_i \Lambda_i \left(\sum_j s_{i,j}^2 - A \right). \tag{3.28}$$

The difference is that we now let the system extend infinitely along the z-axis. This grants us two simplifications. First, translational invariance implies that all Λ_i will effectively be equal to some value Λ. Second, we can Fourier transform over the entire lattice rather than over individual layers independently. To draw a clear analogy with the previous computation, we will still say that the z-axis has L layers, but with the understanding that L is very large or infinite. The Hamiltonian then simplifies as

$$H = -J \sum_{\langle s,s' \rangle} s s' + J\Lambda \sum_i \left(\sum_j s_{i,j}^2 - A \right) = -J \sum_{\langle s,s' \rangle} s s' - J\Lambda A L + J\Lambda \sum_s s^2. \tag{3.29}$$

Next, we Fourier transform our spins according to

$$s_i = (AL)^{-1/2} \sum_{\mathbf{q}} s(\mathbf{q}) e^{i \mathbf{r}_i \cdot \mathbf{q}} \tag{3.30}$$

where $\mathbf{q}$ ranges over the first Brillouin zone of the entire d-dimensional lattice. The Hamiltonian then takes the form

$$H = J \sum_{\mathbf{q}} \left(\Lambda - \sum_{k=1}^{d} \cos(q_k) \right) s(\mathbf{q}) s(-\mathbf{q}) - J\Lambda A L \tag{3.31}$$

and the partition function is computed to be

$$Z = \exp(\beta J \Lambda A L) \prod_{\mathbf{q}} \left[\frac{\beta J}{\pi} \left(\Lambda - \sum_{k=1}^{d} \cos(q_k) \right) \right]^{-1/2}. \tag{3.32}$$

The free energy per transverse length per unit area is

$$\frac{\mathcal{F}_{\text{bulk}}}{AL} = -J\Lambda + \frac{1}{2\beta AL} \sum_{\mathbf{q}} \ln \left(\Lambda - \sum_{k=1}^{d} \cos(q_k) \right) + \frac{1}{2\beta} \ln \left(\frac{\beta J}{\pi} \right), \tag{3.33}$$

so that the spherical constraint is

$$0 = \frac{\beta}{AL} \frac{\partial \mathcal{F}_{\text{bulk}}}{\partial \Lambda} = -\beta J + \frac{1}{2AL} \sum_{\mathbf{q}} \frac{1}{\Lambda - \sum_{k=1}^{d} \cos(q_k)}. \tag{3.34}$$

For large system size AL, the sum over Brillouin zone is well-approximated by an integral

$$\sum_{\mathbf{q}} \approx (\mathbf{q} = 0 \text{ term}) + \frac{AL}{(2\pi)^d} \int_{-\pi}^{\pi} d^d q, \tag{3.35}$$

where the $\mathbf{q} = 0$ term must be singled out (as in the Bose-Einstein condensate) when the dimension is greater than two[2]. Specifically, in $d = 3$, the spherical constraint is (letting $R = \beta J$)

$$16\pi^3 R = \frac{8\pi^3}{AL} \cdot \frac{1}{\Lambda - 3} + \int_{-\pi}^{\pi} \frac{dq_x \, dq_y \, dq_z}{\Lambda - \cos q_x - \cos q_y - \cos q_z}, \tag{3.36}$$

determining the spherical field Λ for a given temperature. Note that, because $AL \gg 1$, the first term on the right hand side is entirely negligible unless Λ is extremely close to 3. Ignoring it, we have

$$16\pi^3 R = \int_{-\pi}^{\pi} \frac{dq_x \, dq_y \, dq_z}{\Lambda - \cos q_x - \cos q_y - \cos q_z}. \tag{3.37}$$

In order to avoid integrating across a singularity, we evidently must have $\Lambda \geq 3$. In fact, when $\Lambda = 3$, this integral is *finite* and was first computed by Watson[79]. As Λ increases from 3, the value of the integral decreases, and so there exists a maximum value of $R = \beta J$ for which we can find a solution. This value is given by

$$R_c = \frac{1}{16\pi^3} \int_{-\pi}^{\pi} \frac{dq_x \, dq_y \, dq_z}{3 - \cos q_x - \cos q_y - \cos q_z} \approx 0.25273, \tag{3.38}$$

---

[2] $\int d^d q / (d - \sum_k \cos(q_k)) \sim \int dq \, q^{d-3}$ in the vicinity of small $q = |\mathbf{q}|$, after switching to polar coordinates. This integral is convergent if $d > 2$ and needs the $\mathbf{q} = 0$ term in order for there to be a solution to the spherical constraint for $T < T_c$.

and the corresponding temperature $T_c \approx J/(0.25273 k_B)$. When $T > T_c$, Λ is determined numerically from Eqn. (3.37), while for $T < T_c$, we must appeal to Eqn. (3.36) and find that $\Lambda = 3 + O\left(\frac{1}{AL}\right) \approx 3$. Berlin and Kac discuss this result in more detail in their appendix C, and show that T_c is in fact a critical point[23].

We observe that the unitless free energy density, $\beta \mathcal{F}_{\text{bulk}}/AL$, is approximately constant with respect to Λ for $T < T_c$. Specifically, in that regime, we keep the $\mathbf{q} = 0$ term of the sum in Eqn. (3.33) but find it to be vanishingly small:

$$\frac{1}{2AL} \ln(\Lambda - 3) \sim \frac{1}{2AL} \ln(AL) \to 0. \tag{3.39}$$

Therefore, in the bulk system, we may take $\Lambda = 3$ when $T < T_c$.

Once the spherical field Λ has been determined, the free energy density in units of $k_B T$ is, from Eqn. (3.33),

$$\beta f_{\text{bulk}} = \frac{\beta \mathcal{F}_{\text{bulk}}}{AL} = -R\Lambda + \frac{1}{2} \ln\left(\frac{R}{\pi}\right)$$
$$+ \frac{1}{16\pi^3} \int_{-\pi}^{\pi} dq_x \, dq_y \, dq_z \, \ln\left(\Lambda - \cos q_x - \cos q_y - \cos q_z\right). \tag{3.40}$$

Recall that $R = \beta J$ contains the explicit temperature dependence in the above expression (though Λ also depends on temperature). This free energy density is the bulk model's quantity of interest, to which we will need to refer when we subsequently compute the Casimir force. The numerical evaluation of the integral will be discussed in section 3.5.

3.4 The Finite-Size System

We now return to the model as defined in section 3.2, with a finite number of layers, L. It was previously shown that the spherical fields Λ_l, with $l = 1, \ldots, L$, satisfy the constraint equations, cf. Eqn. (3.27),

$$RA = \sum_{\mathbf{q}} [\mathcal{H}(\mathbf{q})]_{ii}^{-1} \tag{3.41}$$

for each $i = 1, \ldots, L$. Our present aim is to rewrite this equation in a nicer form.

Given values for the Λ_l, the spectrum of the matrix $\mathcal{H}$ is determined. Let $\{a_l\}$ and $\{|\psi^{(l)}\rangle\}$ be the sets of eigenvalues and normalized eigenvectors, respectively, of $\mathcal{H}$. As $\mathcal{H}(\mathbf{q})$ is simply related to $\mathcal{H}$ via Eqn. (3.19), we see that its eigenvectors are the same while its eigenvalues are slightly modified. We can thus perform an outer product expansion for $\mathcal{H}(\mathbf{q})^{-1}$:

$$\mathcal{H}(\mathbf{q})^{-1} = \sum_{l=1}^{L} |\psi^{(l)}\rangle \frac{1}{a_l - 2\sum_{k=1}^{d-1} \cos q_k} \langle \psi^{(l)}|. \tag{3.42}$$

The constraint equations involve diagonal entries of this matrix, so the constraint now reads

$$R = \frac{1}{A} \sum_{l=1}^{L} \psi_i^{(l)\,2} \sum_{\mathbf{q}} \frac{1}{a_l - 2\sum_{k=1}^{d-1} \cos q_k}, \tag{3.43}$$

for each $i = 1, \ldots, L$, and the sum over Brillouin zone can once again be approximated by an integral,

$$\sum_{\mathbf{q}} \approx (\mathbf{q} = 0 \text{ term}) + \frac{A}{(2\pi)^{d-1}} \int_{-\pi}^{\pi} d^{d-1}q, \tag{3.44}$$

if we take the transverse system size A to be large.

We now limit our focus to the three dimensional system. The $\mathbf{q} = 0$ term may safely be ignored, per the comments and footnote in section 3.3. In higher dimensions, it would have to be retained. With $d = 3$, the constraint is therefore

$$R = \frac{1}{(2\pi)^2} \sum_{l=1}^{L} \psi_i^{(l)\,2} \int_{-\pi}^{\pi} \frac{dq_x\, dq_y}{a_l - 2\cos q_x - 2\cos q_y} \tag{3.45}$$

for each i. The integral can be evaluated in closed form (see appendix G), giving the concise result

$$R = \frac{2}{\pi} \sum_{l=1}^{L} \psi_i^{(l)\,2} \frac{1}{a_l} K\left(\frac{4}{a_l}\right), \qquad i = 1, \ldots, L, \tag{3.46}$$

with $K(k)$ the complete elliptic integral of the first kind with modulus k.

The problem is therefore, given an inverse temperature $R = \beta J$, to determine the values $\{\Lambda_l\}$ such that the spectrum of the matrix $\mathcal{H}$ satisfies the L simultaneous equations, Eqn. (3.46). Once the $\{\Lambda_l\}$ are in hand, we must compute the free energy according to Eqn. (3.24). In the case $d = 3$, that expression for the free energy specializes to

$$\frac{\beta \mathcal{F}}{A} = \frac{1}{2} L \ln\left(\frac{R}{2\pi}\right) - R \sum_{l=1}^{L} \Lambda_l + \frac{1}{8\pi^2} \sum_{l=1}^{L} \int_{-\pi}^{\pi} dq_x\, dq_y\, \ln\left(a_l - 2\cos q_x - 2\cos q_y\right). \tag{3.47}$$

This integral may also be evaluated in terms of special functions (see appendix G), yielding

$$\frac{\beta\mathcal{F}}{A} = \frac{1}{2}L\ln\left(\frac{R}{2\pi}\right) + \frac{1}{2}\sum_{l=1}^{L}\left(\ln a_l - 2R\Lambda_l - \frac{2}{a_l^2}\cdot {}_4F_3\left(1,1,\frac{3}{2},\frac{3}{2};\ 2,2,2;\ \frac{16}{a_l^2}\right)\right) \tag{3.48}$$

as our final expression for the free energy density, with ${}_4F_3$ a generalized hypergeometric function. In what follows, we analyze the system numerically and compute its Casimir force.

3.5 Numerical Solution of the Model

We will use Newton's method to solve for the $\{\Lambda_l\}$ which satisfy the simultaneous equations, Eqn. (3.46), for any particular temperature. In order to implement the method, we must first compute derivatives of the constraint equations with respect to the spherical fields $\{\Lambda_l\}$. To begin, define

$$f_i(\Lambda) = -R + \frac{2}{\pi}\sum_{l=1}^{L}\psi_i^{(l)\,2}\frac{1}{a_l}K\left(\frac{4}{a_l}\right) \tag{3.49}$$

for each $i = 1,\ldots,L$. We will require that $f_i(\Lambda) = 0$ for each i. The dependence on Λ is implicit in the eigenvalues a_l and eigenvectors $|\psi^{(l)}\rangle$ of the matrix $\mathcal{H}$. Derivatives of these with respect to parameters are computed in appendix H. The results, familiar from first order perturbation theory, are that

$$\frac{\partial a_l}{\partial \Lambda_j} = 2\,\psi_j^{(l)\,2} \tag{3.50}$$

and

$$\frac{\partial \psi_i^{(l)}}{\partial \Lambda_j} = 2\sum_{m\neq l}\frac{\psi_j^{(m)}\psi_j^{(l)}}{a_l - a_m}\psi_i^{(m)}. \tag{3.51}$$

Therefore, we compute the Jacobian for Newton's method to be

$$D_{ij} = \frac{\partial f_i}{\partial \Lambda_j} = \frac{4}{\pi}\sum_{l=1}^{L}\sum_{m=1}^{L}\psi_i^{(l)}\psi_i^{(m)}\psi_j^{(l)}\psi_j^{(m)}\begin{cases}\frac{E(4/a_l)}{16-a_l^2}, & m = l \\[2mm] \frac{2K(4/a_l)}{a_l(a_l-a_m)}, & m \neq l\end{cases}, \tag{3.52}$$

where $E(k)$ is the complete elliptic integral of the second kind with modulus k.

Newton's method works very well at high temperatures, where the eigenvalues a_l are comfortably larger than 4. We see empirically that one eigenvalue, call it a_1, gets arbitrarily

close to 4 as we approach low temperatures. The condition $a_l > 4$ is physically necessary, because $\mathcal{H}(\mathbf{q})$ must be positive definite for the partition function, Eqn. (3.21), to not diverge. It is not *a priori* obvious that the system will be attracted to an eigenvalue of 4, but that is nevertheless how the system behaves.

Mathematically, we see why this might happen. $K(x) \sim -\ln(1-x)$ for x just below 1. When T gets small and R gets large, the constraint equations, Eqn. (3.49), begin to rely on the divergence of $K(x)$, forcing an eigenvalue to approach 4 from above. In fact, a back of the envelope computation shows that

$$R \sim -\ln\left(1 - \frac{4}{a_1}\right) \tag{3.53}$$

leads to $(a_1 - 4) \sim e^{-R}$, i.e. a_1 gets exponentially close to 4. Newton's method is, unsurprisingly, unstable in this region because the guesses computed often send the system into unphysical regions with eigenvalues below 4.

Once a_1 is close enough to 4 that Newton's method begins to have issues, the problem can be solved to an excellent approximation by implementing the following changes:

- Replace $K(a_1/4)$ in the constraint equation with a new free coefficient, C.

- Enforce the condition that $a_1 = 4$ exactly.

Specifically, the new constraints are

$$0 = f_i(\Lambda, C) = -R + C\,\psi_i^{(1)\,2} + \frac{2}{\pi}\sum_{l=2}^{L} \psi_i^{(l)\,2}\,\frac{1}{a_l}K\left(\frac{4}{a_l}\right) \tag{3.54}$$

for $i = 1, \ldots, L$, and an additional constraint

$$0 = g(\Lambda, C) = a_1 - 4. \tag{3.55}$$

These $(L+1)$ equations are to be solved for the $(L+1)$ variables $\{\Lambda_l\}$ and C. The $(L+1) \times (L+1)$ Jacobian is computed in the same way as before, but with the $(L+1)$-st column given by $\partial f_i/\partial C$. and the $(L+1)$-st row given by $\partial g/\partial \Lambda_j$.

Once we have the means to compute the $\{\Lambda_l\}$ for a given system size and temperature, we would like to construct the Casimir force. This involves taking a (discrete) derivative of free energy with respect to system size, and subtracting off the corresponding bulk free energy in order to capture the purely finite-size contribution. Therefore, we write

$$\frac{F_{\text{Cas}}(L)}{A} = -\frac{\partial}{\partial L}\left(\frac{\mathcal{F}}{A} - Lf_{\text{bulk}}\right) = f_{\text{bulk}} - \frac{\mathcal{F}(L+1)/A - \mathcal{F}(L-1)/A}{2}, \tag{3.56}$$

where we have symmetrized the discrete derivative, and we refer to the quantities defined in Eqns. (3.40) and (3.48).

A final note, pertaining to the numerical evaluation of the bulk free energy, is in order. The integral appearing in Eqn. (3.40),

$$I = \frac{1}{16\pi^3}\int_{-\pi}^{\pi} dq_x\, dq_y\, dq_z\, \ln\left(\Lambda - \cos q_x - \cos q_y - \cos q_z\right), \tag{3.57}$$

is tricky to compute numerically unless Λ is considerably larger than 3. The case of $\Lambda = 3$ was studied by Joyce and Zucker[80], and they succeeded in computing it to 51 digits,

$$I(\Lambda = 3) \approx 0.4901210612051\ldots \quad . \tag{3.58}$$

We note that

$$\frac{dI}{d\Lambda} = \frac{1}{16\pi^3}\int_{-\pi}^{\pi} dq_x\, dq_y\, dq_z\, \frac{1}{\Lambda - \cos q_x - \cos q_y - \cos q_z}, \tag{3.59}$$

is the relatively well-studied "generalized Watson integral". Fisher and Barber developed a series expansion of this integral[37] for $\Lambda \approx 3$, showing that

$$\frac{dI}{d\Lambda} = R_c - \frac{1}{4\pi}\sqrt{2(\Lambda - 3)} + O(\Lambda - 3), \tag{3.60}$$

where we recall from Eqn. (3.38) that $R_c = \frac{dI}{d\Lambda}(\Lambda = 3)$. Integrating with respect to Λ, we find the series expansion for $I(\Lambda)$,

$$I(\Lambda) \approx I(\Lambda = 3) + R_c(\Lambda - 3) - \frac{\sqrt{2}}{6\pi}(\Lambda - 3)^{3/2} + O\left((\Lambda - 3)^2\right), \tag{3.61}$$

valid when $\Lambda \approx 3$. This series can be used in the region where numerical evaluation of the integral $I(\Lambda)$ is slow and inaccurate.

3.6   Discussion and Concluding Remarks

After implementing the numerical methods of section 3.5, we study the system for a wide range of system sizes L. The appropriate scaling variable in this model is

$$x = Lt = LR_c \left(\frac{1}{R} - \frac{1}{R_c} \right), \tag{3.62}$$

because $\nu = 1$ for the bulk three-dimensional spherical model[15]. The scaled Casimir pressure, $L^3 \beta F_{\mathrm{Cas}}/A$, is plotted versus x in fig. 3.1 around the critical region. By the definition of x, each curve extends to $x = -L$ which corresponds to $T = 0$. However, fig. 3.1 highlights the most interesting part of the curve, which is the dramatic dip near T_c. A similar dip is seen in the data from Garcia and Chan's experiment on ^{4}He near the lambda
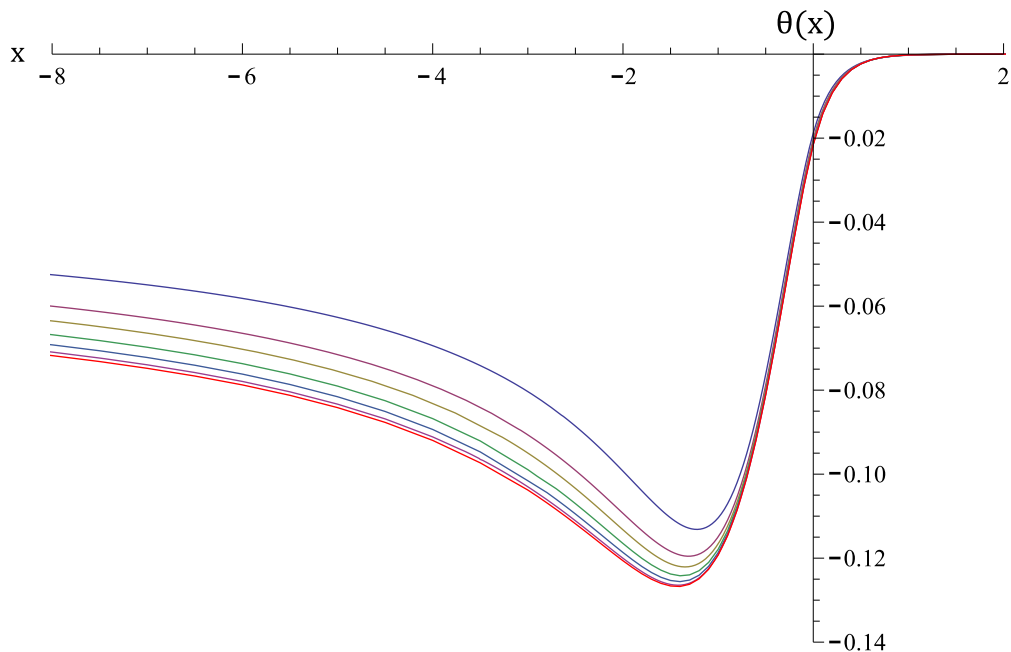
Figure 3.1: The Casimir force in the $O(n \to \infty)$ model with free boundary conditions in a three-dimensional film geometry, focusing on the critical region $x \approx 0$. The curves, from top to bottom, are for system sizes $L = 10$, $L = 20$, $L = 30$, $L = 50$, $L = 100$, $L = 200$, and $L = 500$. The scaled Casimir pressure, in units of $k_B T/L^3$, is plotted against the scaling variable $x = Lt$.

point. That system is the $O(2)$ model under free boundary conditions, whereas ours is the $O(n \to \infty)$ model. The plots are qualitatively similar, but should not be expected to be precisely the same.

As L becomes very large, the curves converge to the finite-size scaling function $\vartheta(x)$ for the Casimir force in this system. We find a value for the Casimir amplitude,

$$\Delta = \frac{1}{2}\vartheta(0) \approx -0.0107712, \tag{3.63}$$

which agrees with the value reported by Diehl[41] to within 0.02%. The extremum of the Casimir force is located at $x \approx -1.43438$ and has a value of

$$\vartheta_{\min} \approx -0.1269001, \tag{3.64}$$

which again agrees with the previously reported value to within 0.03%.

A lot may be said about this system in the asymptotic low temperature regime. In appendix I, we perform a full calculation to derive the fact that, for $T \approx 0$,

$$
\begin{aligned}
F_{\text{Cas}}(x) \sim & -\frac{\zeta(3)}{8\pi L^3}\left[1 + \frac{2.755}{L^2} + \frac{7.890}{L^4}\right] \\
& + \frac{1}{4L^4}\frac{x+L}{xR_c}\left[0.02246 + 0.04567\ln L + \frac{0.01973 + 0.2672\ln L}{L^2}\right], \quad (3.65)
\end{aligned}
$$

where the numerical constants are specified in closed form in sections I.3 and I.4. The agreement with the numerical data is excellent even as the temperature gets moderately large. A comparative plot is given in fig. 3.2 for $L = 10$. Of particular note in the asymptotic result is the asymptotic value of the Casimir force, $F_{\text{Cas}}(T = 0)$, being non-zero. This was seen by Garcia and Chan experimentally for the $O(2)$ model, and it is a famous result[12] for systems with spontaneously broken symmetries at $T = 0$.

The $\ln L$ terms in the asymptotic regime are an unexpected result, as they do not appear to fit into a scaling form. That is, we would expect only a scaling combination Lt to show up, which would imply the existence of a $\ln|T - T_c|$. However, the calculation perfomed explicitly in appendix I leaves little room to question that this $\ln|T - T_c|$ is not there.
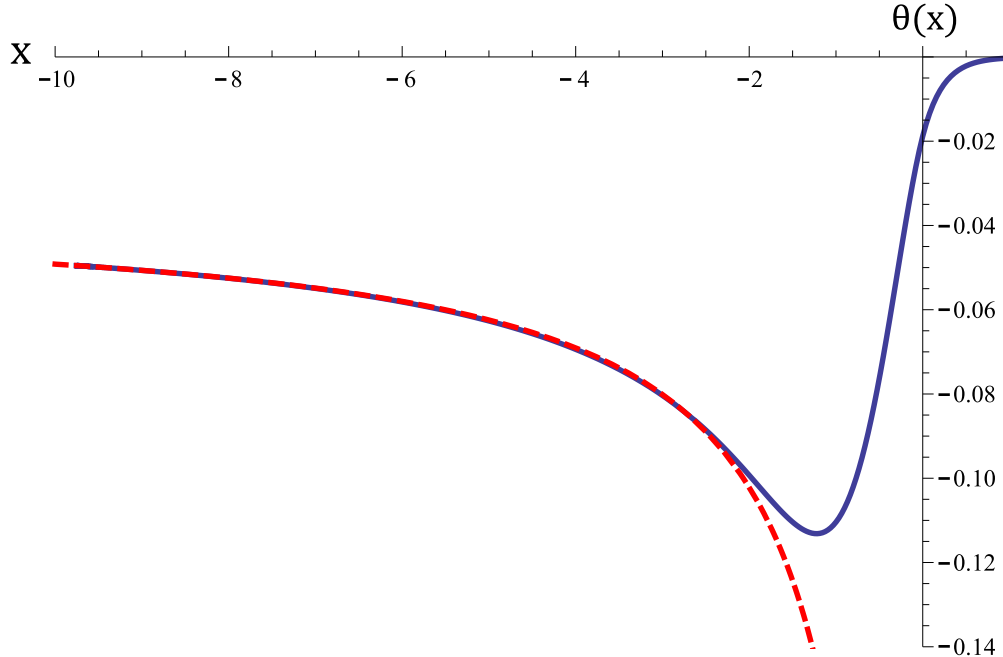
Figure 3.2: The Casimir force for $L = 10$: numeric results (solid, blue) compared to the asymptotic expression (red, dashed) given by Eqn. (3.65). The asymptotic result is valid in the vicinity of $x = -L$. With $L = 10$, it offers stunning agreement with the numerics even into the critical region just below $x = 0$.

Finite-size scaling theory only makes predictions about the neighborhood around the bulk critical point, so this does not contradict scaling.

In the vicinity of T_c, we have still not determined what scaling corrections exist, accounting for the lack of data collapse in fig. 3.1 at small values of L. Privman argues that there exists a $\ln|t|$ correction near criticality for a system with $d = 3$ and free boundary conditions, but does not predict $\ln L$ dependence away from the critical region[19]. Diehl contends that degeneracy of critical exponents shows that the Casimir amplitude (i.e. at $T = T_c$) will have a correction[41] $\sim \ln L/L$. Brankov and Danchev find logarithmic corrections below T_c, but not at T_c, for the spherical model under free boundary conditions[81]. We intend to determine the nature of the scaling corrections in our results in a subsequent publication, but the issue remains open for the present.

The results thus presented on the $O(n \to \infty)$ model with free boundary conditions are interesting and encouraging. While reaffirming the numerical results of Diehl in the critical region, they also extend to low temperatures, both numerically and with explicit closed form expressions. Furthermore, the model as defined in this chapter has no free parameters, requires no regularization, and does not find need to employ any effective L, which may all be seen as advantages over the model of Diehl. Being related to the Bose gas and with a Casimir scaling function bearing a strong resemblance to the experimental results of Garcia and Chan, the model may yet find practical applications.

APPENDIX A

Free Energy in the Lattice XY Mean-Field Model

We claim that

$$f(\{\mathbf{m}_i\}, N) = \sum_{i=0}^{N+1} \left[\frac{1}{2} \mathbf{m}_i \cdot \mathbf{H}_i - \frac{1}{\beta} \ln\left(I_0\left(\beta m H_i\right)\right) \right] \tag{A.1}$$

is the free energy functional of the lattice model considered in section 2.2. Indeed, here we will demonstrate that minimizing it with respect to the $\mathbf{m}_i$ leads to the mean-field consistency equations

$$\mathbf{m}_i = m \frac{\mathbf{H}_i}{H_i} \frac{I_1(\beta m H_i)}{I_0(\beta m H_i)}. \tag{A.2}$$

Recall that $\mathbf{H}_i = J(2(d-1)\mathbf{m}_i + \mathbf{m}_{i-1} + \mathbf{m}_{i+1})$, and take $\mathbf{m}_{-1} = \mathbf{m}_{N+2} = 0$ for notational convenience. Differentiating,

$$0 = \nabla_{\mathbf{m}_i} f = 2J(d-1)\left[\mathbf{m}_i - m \frac{\mathbf{H}_i}{H_i}\frac{I_1(\beta m H_i)}{I_0(\beta m H_i)}\right] + J\left[\mathbf{m}_{i-1} - m \frac{\mathbf{H}_{i-1}}{H_{i-1}}\frac{I_1(\beta m H_{i-1})}{I_0(\beta m H_{i-1})}\right]$$
$$+ J\left[\mathbf{m}_{i+1} - m \frac{\mathbf{H}_{i+1}}{H_{i+1}}\frac{I_1(\beta m H_{i+1})}{I_0(\beta m H_{i+1})}\right] \tag{A.3}$$

for $i = 1, \ldots, N$. If $i = 0$ ($i = N+1$), we find the same condition with the second (third) term omitted. Defining

$$\mathbf{g}_i = \mathbf{m}_i - m \frac{\mathbf{H}_i}{H_i}\frac{I_1(\beta m H_i)}{I_0(\beta m H_i)}, \qquad \mathbf{g}_{-1} = \mathbf{g}_{N+2} = 0, \tag{A.4}$$

we may write Eqn. (A.3) as

$$0 = \nabla_{\mathbf{m}_i} f = 2J(d-1)\mathbf{g}_i + J\mathbf{g}_{i-1} + J\mathbf{g}_{i+1} \tag{A.5}$$

for each $i = 0, \ldots, N+1$. In order to show that (2.8) holds, we must show that (A.5) is only solved when $\mathbf{g}_i = 0$ for all i. This is seen by writing the linear equations (A.5) in matrix

form, i.e. $A\mathbf{g} = 0$ with tridiagonal $(N + 2) \times (N + 2)$ matrix

$$A = J \begin{pmatrix} 2(d-1) & 1 & 0 & \cdots & & 0 \\ 1 & 2(d-1) & 1 & & & \vdots \\ 0 & 1 & \ddots & & & \\ \vdots & & & & & \\ & & & & & 1 \\ 0 & & \cdots & & 1 & 2(d-1) \end{pmatrix}. \tag{A.6}$$

whose determinant is computed by recursion as

$$\det A = \frac{J^{N+2}}{2\sqrt{(d-1)^2 - 1}} \left[\left(d - 1 + \sqrt{(d-1)^2 - 1} \right)^{N+3} \right.$$
$$\left. - \left(d - 1 - \sqrt{(d-1)^2 - 1} \right)^{N+3} \right]. \tag{A.7}$$

Simplifying the difference of powers, we have

$$\det A = J^{N+2} \sum_{k=0}^{N+2} \left(d - 1 + \sqrt{(d-1)^2 - 1} \right)^{k} \left(d - 1 - \sqrt{(d-1)^2 - 1} \right)^{N+2-k}, \tag{A.8}$$

which is patently positive for $d \geq 2$ and integer $N \geq 0$, so that the only solution is $\mathbf{g}_i = 0$, as desired.

APPENDIX B

Derivatives of the Ginzburg-Landau Free Energy Functional

We take the free energy functional

$$\mathcal{F}[\Phi(z), \varphi(z)] = \int_{-L/2}^{L/2} dz \left[\frac{b}{2} \left(\frac{d\Phi}{dz} \right)^2 + \frac{b}{2} \Phi^2 \left(\frac{d\varphi}{dz} \right)^2 + \frac{1}{2} at\Phi^2 + \frac{1}{4} g\Phi^4 \right] \quad \text{(B.1)}$$

and wish to extremize it with respect to the amplitude and phase profiles, $\Phi(z)$ and $\varphi(z)$. First consider a variation $\varphi \to \varphi + \delta\varphi$ with the increment $\delta\varphi$ small throughout and vanishing at the boundaries $z = \pm L/2$. We have

$$\mathcal{F}[\Phi, \varphi + \delta\varphi] = \int_{-L/2}^{L/2} dz \left[\frac{b}{2} \left(\frac{d\Phi}{dz} \right)^2 + \frac{b}{2} \Phi^2 \left(\frac{d\varphi}{dz} + \frac{d}{dz} \delta\varphi \right)^2 + \frac{1}{2} at\Phi^2 + \frac{1}{4} g\Phi^4 \right]$$

$$= \mathcal{F}[\Phi, \varphi] + b \int_{-L/2}^{L/2} dz \, \Phi^2 \frac{d\varphi}{dz} \cdot \frac{d}{dz} \delta\varphi + O((\delta\varphi)^2), \quad \text{(B.2)}$$

where we neglect terms of higher order. We integrate by parts, finding

$$\mathcal{F}[\Phi, \varphi + \delta\varphi] - \mathcal{F}[\Phi, \varphi] = b\Phi^2 \frac{d\varphi}{dz} \delta\varphi \Big|_{-L/2}^{L/2} - b \int_{-L/2}^{L/2} dz \, \frac{d}{dz} \left(\Phi^2 \frac{d\varphi}{dz} \right) \delta\varphi. \quad \text{(B.3)}$$

The surface terms vanish because the variation $\delta\varphi$ vanishes there. In order to be at a free energy extremum, the difference on the left hand side of the above equation must vanish (to first order in $\delta\varphi$) for arbitrary $\delta\varphi$. This can only happen if the rest of the integrand vanishes identically, i.e. if

$$\frac{d}{dz} \left(\Phi^2 \frac{d\varphi}{dz} \right) = 0. \quad \text{(B.4)}$$

This is Eqn. (2.15), which may also be understood in terms of functional derivatives as the condition that $\delta\mathcal{F}/\delta\varphi = 0$.

Now we turn our attention to extremizing with respect to Φ. The same approach yields

$$\mathcal{F}[\Phi + \delta\Phi, \varphi] = \mathcal{F}[\Phi, \varphi] + \int_{-L/2}^{L/2} dz \left(b\frac{d\Phi}{dz} \cdot \frac{d}{dz}\delta\Phi + \left[b\Phi \left(\frac{d\varphi}{dz}\right)^2 + at\Phi + g\Phi^3 \right] \delta\Phi \right), \quad \text{(B.5)}$$

and we again integrate by parts which gives

$$\mathcal{F}[\Phi + \delta\Phi, \varphi] - \mathcal{F}[\Phi, \varphi] = b\frac{d\Phi}{dz}\delta\Phi \bigg|_{-L/2}^{L/2}$$
$$+ \int_{-L/2}^{L/2} dz \left[-b\frac{d^2\Phi}{dz^2} + b\Phi \left(\frac{d\varphi}{dz}\right)^2 + at\Phi + g\Phi^3 \right] \delta\Phi. \quad \text{(B.6)}$$

As before, we notice that the surface terms vanish and we argue that this integral should be zero for arbitrary $\delta\Phi$ and therefore

$$b\frac{d^2\Phi}{dz^2} = b\Phi \left(\frac{d\varphi}{dz}\right)^2 + at\Phi + g\Phi^3, \quad \text{(B.7)}$$

which agrees with Eqn. (2.17).

In order to compute the Casimir force, we take a functional derivative of $\mathcal{F}$ with respect to L. This is non-trivial because Φ and φ implicitly depend on L. Again we consider a difference

$$\mathcal{F}[\Phi + \delta\Phi, \varphi + \delta\varphi, L + \delta L] - \mathcal{F}[\Phi, \varphi, L], \quad \text{(B.8)}$$

but the variations $\delta\Phi$ and $\delta\varphi$ are no longer arbitrary. Instead, they are reactions to the interval being stretched.

Break up $\mathcal{F}$ into an integral over the old interval $[-L/2, L/2]$ and an integral over the tiny extensions $[\pm L/2, \pm(L + \delta L)/2]$. For the integration over $[-L/2, L/2]$, we have already computed the result of perturbing Φ and φ. However, the variations $\delta\Phi$ and $\delta\varphi$ now vanish at $\pm(L + \delta L)/2$ rather than at $\pm L/2$, so the surface terms from integration by parts give non-zero contributions. We will handle those terms carefully in a moment. On the other hand, the integrals over the extension regions are trivially given by approximating them as rectangles of width $\delta L/2$ and height equal to the value of the integrand at $z = \pm L/2$.

Therefore, since the integrand is an even function of z, we have

$$\mathcal{F}[\Phi + \delta\Phi, \varphi + \delta\varphi, L + \delta L] - \mathcal{F}[\Phi, \varphi, L] \approx b\frac{d\Phi}{dz}\delta\Phi\bigg|_{-L/2}^{L/2} + b\Phi^2\frac{d\varphi}{dz}\delta\varphi\bigg|_{-L/2}^{L/2}$$
$$+ 2 \cdot \frac{\delta L}{2}\left(\frac{b}{2}\left(\frac{d\Phi}{dz}\right)^2 + \frac{b}{2}\Phi^2\left(\frac{d\varphi}{dz}\right)^2 + \frac{1}{2}at\Phi^2 + \frac{1}{4}g\Phi^4\right)\bigg|_{L/2}. \quad \text{(B.9)}$$

Now, we reiterate that the quantities $\delta\Phi(\pm L/2)$ and $\delta\varphi(\pm L/2)$ are not arbitrary, but reflect the changes that the profiles Φ and φ suffered as a result of varying L (this is illustrated in fig. B.1). Taylor expanding φ, we find

$$\varphi\left(\frac{L}{2}\right) = \varphi\left(\frac{L+\delta L}{2} - \frac{\delta L}{2}\right) = \varphi\left(\frac{L+\delta L}{2}\right) - \frac{\delta L}{2}\frac{d\varphi}{dz}\bigg|_{\frac{L+\delta L}{2}}$$
$$= \varphi_{\text{old}}\left(\frac{L}{2}\right) + \delta\varphi\left(\frac{L}{2}\right), \quad \text{(B.10)}$$

where we retain our old boundary condition which means that $\varphi((L + \delta L)/2) = \varphi_{\text{old}}(L/2)$. Continuing,

$$\delta\varphi\left(\frac{L}{2}\right) = -\frac{\delta L}{2}\frac{d\varphi}{dz}\bigg|_{\frac{L+\delta L}{2}} \approx -\frac{\delta L}{2}\frac{d\varphi}{dz}\bigg|_{L/2}, \quad \text{(B.11)}$$

where we have Taylor expanded again and kept only leading order terms in δL. The other three perturbations are expressed in similar fashion in terms of δL, and we find the result

$$\frac{\mathcal{F}[\Phi + \delta\Phi, \varphi + \delta\varphi, L + \delta L] - \mathcal{F}[\Phi, \varphi, L]}{\delta L} \approx -b\left(\frac{d\Phi}{dz}\right)^2\bigg|_{L/2} - b\Phi^2\left(\frac{d\varphi}{dz}\right)^2\bigg|_{L/2}$$
$$+ \left(\frac{b}{2}\left(\frac{d\Phi}{dz}\right)^2 + \frac{b}{2}\Phi^2\left(\frac{d\varphi}{dz}\right)^2 + \frac{1}{2}at\Phi^2 + \frac{1}{4}g\Phi^4\right)_{L/2}. \quad \text{(B.12)}$$

Combining terms and using Eqns. (2.16) and (2.22) to remove the derivatives, we end up with

$$\frac{\delta\mathcal{F}}{\delta L} = -\frac{1}{2}b\frac{P_\varphi^2}{\Phi_0^2} + \frac{1}{2}at\Phi_0^2 + \frac{1}{4}g\Phi_0^4, \quad \text{(B.13)}$$

so that the Casimir force reported in Eqn. (2.29) follows immediately.
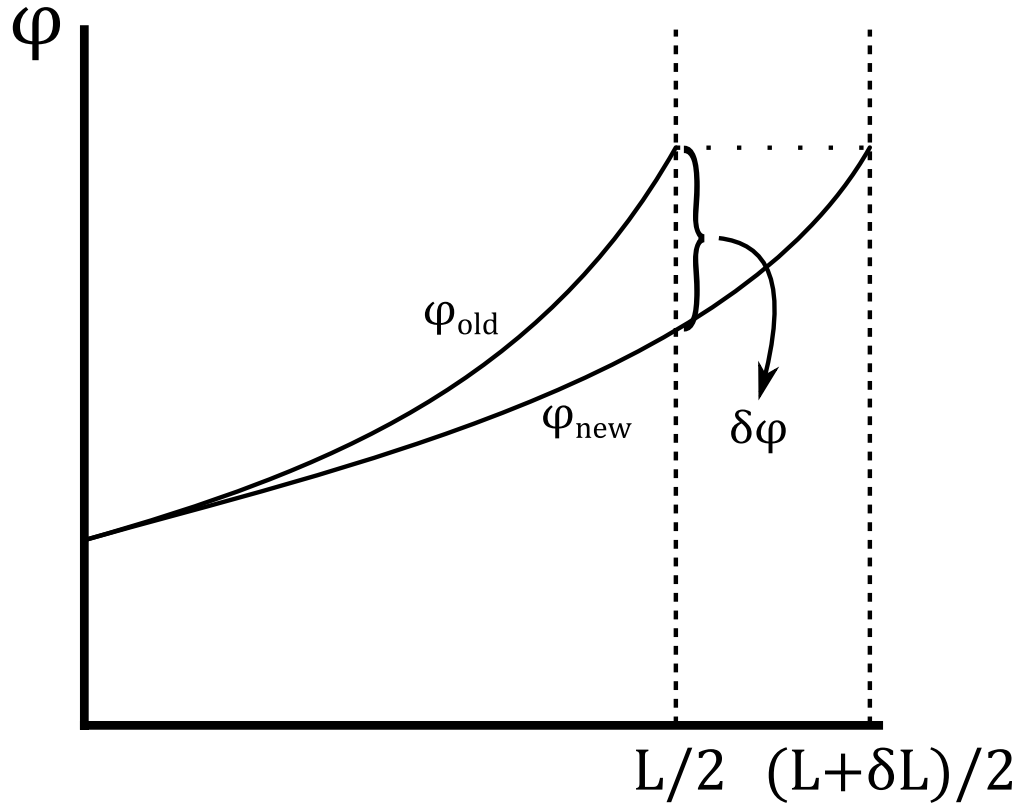
Figure B.1: A schematic illustration of the change suffered by the angle profile $\varphi(z)$ when L is increased by δL. The old and new profiles share the same boundary condition, but the boundary moves. We are interested in the quantity $\delta\varphi(L/2)$, indicated by $\delta\varphi$ in the figure, which is the change in $\varphi(L/2)$.

APPENDIX C

Newton's Method

For a function $f : \mathbb{R} \to \mathbb{R}$, Newton's method is an algorithm for finding a root, i.e. a point r such that $f(r) = 0$. Starting at some chosen r_1, one computes the tangent to the graph of f at $(r_1, f(r_1))$ and follows it to its intersection with the x-axis. That intersection point is taken to be r_2 and the procedure is repeated. There are instances in which Newton's method can fail (certain functions or bad starting points, etc.), but we will forgo their discussion here. In non-pathological cases, Newton's method usually converges and does so very quickly[6]. In what follows, we assume the absence of any pathology.

The tangent line at $(r_i, f(r_i))$ is $y = f(r_i) + (x - r_i)f'(r_i)$. The next iteration, r_{i+1}, is that x value which gives an intersection with the x-axis, i.e.

$$r_{i+1} = r_i - [f'(r_i)]^{-1} f(r_i). \tag{C.1}$$

Of course, the multiplicative inverse of $f'(r_i)$ is simply $1/f'(r_i)$. However, writing it as in Eqn. (C.1) suggests a general form.

Suppose we now have a function $\mathbf{f} : \mathbb{R}^n \to \mathbb{R}^n$. Instead of following a tangent line to zero, we imagine following the tangent *plane* to zero in each coordinate. The tangent plane at $\mathbf{r}^{(i)}$ is given by

$$\mathbf{y}_j = f_j \left(\mathbf{r}^{(i)} \right) + \left[Df \left(\mathbf{r}^{(i)} \right) \right]_{jk} \left(\mathbf{r} - \mathbf{r}^{(i)} \right)_k \tag{C.2}$$

where the upper index $\mathbf{r}^{(i)}$ now refers to the iteration counter, while lower indices are reserved for spatial components of the vectors. In particular, we split $\mathbf{f}$ into components $\mathbf{f}(\mathbf{r}) = (f_1(\mathbf{r}), \ldots, f_n(\mathbf{r}))$. A summation is implied over $k = 1, \ldots, n$ and we define the Jacobian

$$\left[Df \left(\mathbf{r}^{(i)} \right) \right]_{jk} = \left. \frac{\partial f_j}{\partial r_k} \right|_{\mathbf{r}^{(i)}}. \tag{C.3}$$

Now we solve for the next iteration $\mathbf{r}^{(i+1)}$ by multiplying through by $[Df]_{lj}^{-1}$, finding

$$\mathbf{r}_l^{(i+1)} = \mathbf{r}_l^{(i)} - [Df\left(\mathbf{r}^{(i)}\right)]_{lj}^{-1} f_j(\mathbf{r}^{(i)}), \qquad \text{(C.4)}$$

in perfect analogy with Eqn. (C.1) but now involving matrix inversion.

APPENDIX D

Analytical Results for the XY Ginzburg-Landau Model Under Twisted Boundary Conditions

In this Appendix, we derive some analytical expressions needed for the numerical evaluation of Eqn. (2.32) for the scaling function of the Casimir force.

We start by determining the behavior of the amplitude profile $X_\Phi(\zeta)$ per Eqn. (2.38). In addition, we will also determine the phase angle profile $\varphi(\zeta)$. Note that, in terms of the scaling variables (2.30) and (2.34), we obtain the phase angle $\varphi(\zeta)$ as

$$\varphi(\zeta) = pX_0^3 \int_0^\zeta \frac{d\zeta}{X_\Phi^2(\zeta)}. \tag{D.1}$$

via Eqn. (2.16). For convenience, we repeat Eqn. (2.38):

$$\frac{1}{2} - \zeta = \frac{1}{2X_0} \int_{[X_\Phi(\zeta)/X_0]^2}^\infty \frac{dx}{\sqrt{(x-1)[x^2 + x(1+\tau) + p^2]}}, \tag{D.2}$$

which will enable us to solve for $X_\Phi(\zeta)$. Let

$$x_\pm = \frac{1}{2} \left[-(\tau+1) \pm \sqrt{(\tau+1)^2 - 4p^2} \right] \tag{D.3}$$

be the roots of the quadratic term in the square brackets in the denominator of (D.2).

In order to perform the integration in Eqn. (D.2), where the integrand is a positive function for all points from the integration interval, one needs to know if these roots are real or complex (see Fig. 8). Thus, there are two cases: A) the roots are real, and B) the roots are complex conjugates of each other.

First consider the case

A) The roots $x_\pm$ are real.
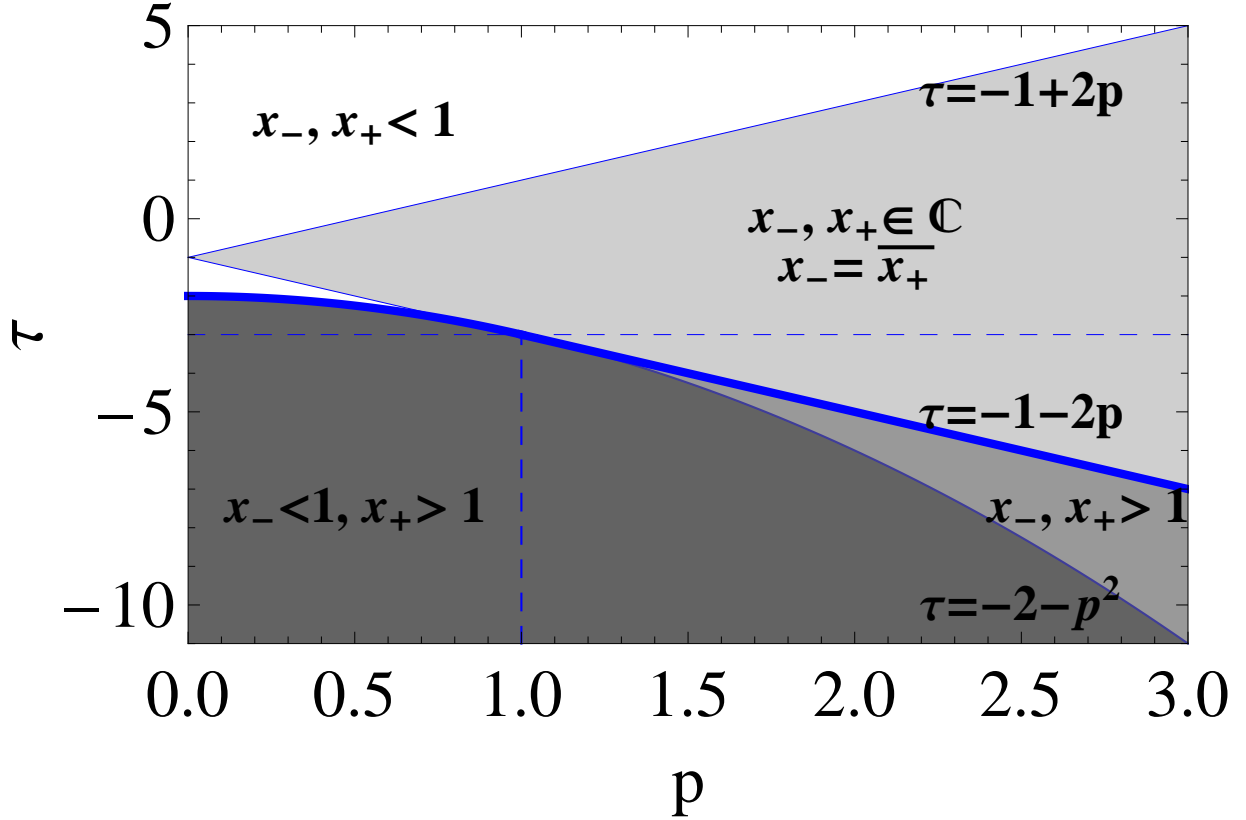
Figure D.1: The loci of points in the (p, τ)-plane for which the roots $x_\pm$ possess the properties discussed in the text. When any of the roots approaches the thick blue line, $X_0 \to \infty$. This is only possible for $\tau < 0$, i.e. when $\tau X_0^2 = x_t \to -\infty$.

In order to get a real-valued result, we must have the singularities to the left of $x = 1$, forcing $x_- < x_+ < 1$. Then the value may be found in a table of integrals[82]:

$$\int_y^\infty \frac{dx}{\sqrt{(x-1)(x-x_+)(x-x_-)}} = \frac{2}{\sqrt{1-x_-}} F\left(\arcsin\sqrt{\frac{1-x_-}{y-x_-}}, \sqrt{\frac{x_+-x_-}{1-x_-}}\right), \quad \text{(D.4)}$$

provided $y \geq 1 > x_+ > x_-$. In fact, Eqn. (2.36) fixes $y = 1$, so we rewrite it as

$$X_0 = \frac{2}{\sqrt{1-x_-}} K(k), \quad \text{(D.5)}$$

where $k = \sqrt{\frac{x_+-x_-}{1-x_-}}$, F is the incomplete elliptic integral of the first kind and $K(k) = F(\frac{\pi}{2}, k)$ is the complete elliptic integral of the first kind with modulus k. From Eqn. (D.2), we

similarly obtain the more general relation

$$\frac{1}{2} - \zeta = \frac{1}{X_0\sqrt{1 - x_-}} F\left(\arcsin\sqrt{\frac{1 - x_-}{(X_\Phi(\zeta)/X_0)^2 - x_-}}, k\right),\tag{D.6}$$

of which Eqn. (D.5) is the special case $\zeta = 0$. Solving (D.6) for $X_\Phi(\zeta)$ we find

$$X_\Phi(\zeta)^2 = X_0^2\left[x_- + \frac{1 - x_-}{\operatorname{sn}^2\left[X_0\sqrt{1 - x_-}\left(\frac{1}{2} - \zeta\right), k\right]}\right],\tag{D.7}$$

where sn denotes the sine-amplitude Jacobi elliptic function.

Finally, inserting (D.7) into (D.1) and (2.37) and performing the integration, we arrive at

$$\varphi\left(\zeta\right) = \frac{pX_0}{x_-}\left\{\frac{1}{X_0\sqrt{1 - x_-}}\Pi\left[\frac{x_-}{x_- - 1}, \operatorname{am}\left(X_0\sqrt{1 - x_-}\left(\frac{1}{2} - \zeta\right), k\right), k\right]\right.$$
$$\left.+\zeta - \frac{1}{X_0\sqrt{1 - x_-}}\Pi\left[\frac{x_-}{x_- - 1}, k\right]\right\},\tag{D.8}$$

and the special case $\alpha/2 = \varphi(1/2)$ gives

$$\alpha = \frac{pX_0}{x_-}\left\{1 - \frac{2}{X_0\sqrt{1 - x_-}}\Pi\left[\frac{x_-}{x_- - 1}, k\right]\right\},\tag{D.9}$$

where $\Pi(n, \phi, k)$ and $\Pi(n, k)$ are the incomplete and complete, respectively, elliptic integrals of the third kind with modulus k[1], and $\operatorname{am}(u, k)$ is the amplitude for Jacobi elliptic functions with modulus k.

We also note here that the relationship between $x_\pm$, τ and p is straightforward. From (D.3) we have

$$\tau = -1 - x_- - x_+, \qquad p^2 = x_-x_+.\tag{D.10}$$

With these relations and Eqn. (D.5), we can compute everything. Fixing α and τ, we can solve (D.9) numerically for p. Then, knowing X_0, the scaling function for the Casimir force is found from Eqn. (2.35). These scaling functions are plotted in fig. 2.3.

---

[1]Note that Mathematica's definition of the elliptic functions F, K, Π, am, etc. all use the "parameter" $m = k^2$, rather than the "modulus" k as the final argument. There is no discrepancy in the other arguments. Therefore, to correctly input these functions into Mathematica, one has to square the final argument relative to how it is written here.

We now consider the case

B) The roots $x_\pm$ are complex.

In this case, the roots are complex conjugates of each other, i.e. $x_- = \overline{x_+}$. Taking this into account and using the corresponding expression from a table of integrals[83], we obtain

$$\int_y^\infty \frac{dx}{\sqrt{(x-1)(x-x_+)(x-x_-)}} = \frac{1}{\sqrt{r}}F\left[\arccos\left(\frac{y-1-r}{y-1+r}\right),w\right], \tag{D.11}$$

where

$$r = \sqrt{(1-x_-)(1-x_+)} = \sqrt{2+\tau+p^2}, \tag{D.12}$$

and

$$w^2 = \frac{1}{2} + \frac{x_- + x_+ - 2}{4r} = \frac{1}{2}\left(1 - \frac{3+\tau}{2\sqrt{2+\tau+p^2}}\right). \tag{D.13}$$

According to Eqn. (D.2), the above implies that

$$\zeta = \frac{1}{2} - \frac{1}{2X_0\sqrt{r}}F\left[\arccos\left(\frac{(X_\Phi/X_0)^2-1-r}{(X_\Phi/X_0)^2-1+r}\right),w\right], \tag{D.14}$$

and, for $\zeta = 0$ with $X_\Phi(\zeta = 0) = X_0$, it follows that

$$X_0 = \frac{2}{\sqrt{r}}K(w). \tag{D.15}$$

Solving (D.14) for X_Φ gives

$$X_\Phi(\zeta)^2 = X_0^2\left[1 - r + \frac{2r}{1 - \mathrm{cn}\left(2X_0\sqrt{r}\left(\frac{1}{2}-\zeta\right),w\right)}\right], \tag{D.16}$$

where cn denotes the cosine-amplitude Jacobi elliptic function. Finally, inserting (D.16) in (D.1) and (2.37) and performing the integration, cf. Eqn. (361.60) in Byrd and Friedman[83], we find

$$\varphi(\zeta) = \frac{pX_0}{1-r}\zeta + \frac{p(r+1)}{4\sqrt{r}(r-1)}\left\{2\Pi\left[-\frac{(r-1)^2}{4r},w\right]\right.$$
$$-\Pi\left[-\frac{(r-1)^2}{4r},\mathrm{am}\left(2X_0\sqrt{r}\left(\frac{1}{2}-\zeta\right),w\right),w\right]\right\}$$
$$+\frac{1}{2}\cot^{-1}\left(\frac{2\sqrt{r}}{p}\cdot\frac{\mathrm{dn}\left(2X_0\sqrt{r}\left(\frac{1}{2}-\zeta\right),w\right)}{\mathrm{sn}\left(2X_0\sqrt{r}\left(\frac{1}{2}-\zeta\right),w\right)}\right). \tag{D.17}$$

Now, setting $\zeta = 1/2$ in the above equation, we have

$$\alpha = \frac{pX_0}{1-r} + \frac{p(r+1)}{\sqrt{r}(r-1)} \Pi \left[-\frac{(r-1)^2}{4r}, w \right],$$

(D.18)

where we have used Eqn. (D.15) and the identities $\mathrm{dn}(2K(w), w) = 1$ and $\mathrm{sn}(2K(w), w) = 0$. The amplitude profile $X_\Phi(\zeta)$ and the angle profile $\varphi(\zeta)$ are plotted in Fig. 9. Recall that the relationships between x_-, x_+, τ and p are given by Eqn. (D.10). As in the previous case, X_0, x_- and x_+ are known functions of τ and p, and this equation is solved numerically to produce the scaling function for the Casimir force.

From the expressions derived above, it is easy to reproduce the results previously known for $\alpha = 0$. As we will see, this provides a new representation of the older results which is quite convenient for numerical evaluation. First, we note that, from Eqns. (2.16) and (2.34), $\alpha = 0$ implies that $p = 0$. Thus, from Eqn. (D.3), it follows that we are in the case A) of real roots. Indeed, if $\tau \geq -1$ then $x_+ = 0$ and $x_- = -(\tau+1)$, while for $\tau < -1$, $x_+ = |\tau+1|$ and $x_- = 0$. Note that, because the problem is non-physical when $x_+ \geq 1$, the case $\tau < -1$ actually only extends down[2] to $\tau = -2$. With that in mind, we find, from Eqn. (D.5),

$$X_0(\tau) = \begin{cases} 2K\left(\sqrt{|\tau+1|}\right), & -2 < \tau \leq -1 \\ \frac{2}{\sqrt{\tau+2}}K\left(\sqrt{\frac{\tau+1}{\tau+2}}\right), & \tau \geq -1 \end{cases}$$

(D.19)

For the scaling function of the Casimir force, Eqn. (2.35) gives

$$X_{\mathrm{Cas}}^{(+,+)}(\tau) = \begin{cases} -4(\tau+2)^2 K\left(\sqrt{|\tau+1|}\right)^4, & \tau \leq -1 \\ -4K\left(\sqrt{\frac{\tau+1}{\tau+2}}\right)^4, & -1 \leq \tau \leq 0 \\ -16\frac{\tau+1}{(\tau+2)^2}K\left(\sqrt{\frac{\tau+1}{\tau+2}}\right)^4, & \tau \geq 0 \end{cases}$$

(D.20)

where we have denoted the $\alpha = 0$ boundary conditions as $(+,+)$. Denoting the argument of the elliptic K function in a standard way with k and recalling that $x_t = \tau X_0^2$, the above expressions can be rewritten in the parametric form

$$X_{\mathrm{Cas}}^{(+,+)}(x_t) = \begin{cases} -4(1-k^2)^2 K(k)^4, & x_t = -4(k^2+1)K(k)^2, & x_t \leq -\pi^2 \\ -4K(k)^4, & x_t = 4(2k^2-1)K(k)^2, & -\pi^2 \leq x_t \leq 0 \\ -16k^2(1-k^2)K(k)^4, & x_t = 4(2k^2-1)K(k)^2, & x_t \geq 0 \end{cases}.$$

(D.21)

---

[2]See also: fig. D.1.

78

The parameter k ranges over $[0, 1)$ for the segment corresponding to $x_t \leq -\pi^2$, over $[0, \frac{1}{\sqrt{2}}]$ for $-\pi^2 \leq x_t \leq 0$ and over $[\frac{1}{\sqrt{2}}, 1)$ for $x_t \geq 0$. The result (D.21) was originally due to Krech[24]. The behavior of $X_{\text{Cas}}^{(+,+)}(x_t)$ is shown[3] as a thick black line in fig. 2.3.

The scaling function of the Casimir force under $(+, -)$ boundary condition in the Ising mean-field model is[24]

$$
X_{\text{Cas}}^{(+,-)}(x_t) = \begin{cases} 64k^2(1-k^2)K(k)^4, & x_t = -8(2k^2-1)K(k)^2, \quad x_t \leq 0 \\ 16K(k)^4, & x_t = -8(2k^2-1)K(k)^2, \quad 0 \leq x_t \leq 2\pi^2 \\ 16(1-k^2)^2K(k)^4, & x_t = 8(k^2+1)K(k)^2, \quad x_t \geq 2\pi^2 \end{cases} . \quad (\text{D}.22)
$$

In this case, k runs over $[0, 1)$ for $x_t \geq 2\pi^2$, over $[0, \frac{1}{\sqrt{2}}]$ for $0 \leq x_t \leq 2\pi^2$ and over $[\frac{1}{\sqrt{2}}, 1)$ for $x_t \leq 0$. This scaling function is shown in fig. 2.3 as a dashed line; it coincides with the scaling function for $\alpha \approx \pi$ until they split apart at large, negative temperatures.

Finally, note that the scaling functions $X_{\text{Cas}}^{(+,+)}(x)$ and $X_{\text{Cas}}^{(+,-)}(x)$, just derived, are related through[84]

$$
X_{\text{Cas}}^{(+,+)}(x) = -\frac{1}{4}X_{\text{Cas}}^{(+,-)}(-x/2), \quad (\text{D}.23)
$$

which is easily checked. For instance, the $x_t \geq 2\pi^2$ branch of $X_{\text{Cas}}^{(+,-)}$ gets mapped to $x_t \leq -\pi^2$. The relationship between x_t and k acquires a factor of $-1/2$ and the value of the function picks up a factor of $-1/4$. This then corresponds identically to the correct branch of $X_{\text{Cas}}^{(+,+)}$. Furthermore, for the corresponding mean-field Casimir amplitudes, we have

$$
\frac{\Delta_{\text{Cas}}^{(+,+)}}{\Delta_{\text{Cas}}^{(+,-)}} = \frac{-4K\left(1/\sqrt{2}\right)^4/3}{16K\left(1/\sqrt{2}\right)^4/3} = -\frac{1}{4}. \quad (\text{D}.24)
$$

---

[3] Again one must be careful of the notation in order to handle this in a CAS. For instance, to plot this in Mathematica, it is necessary to input $K(k)$ as `EllipticK[k^2]`.
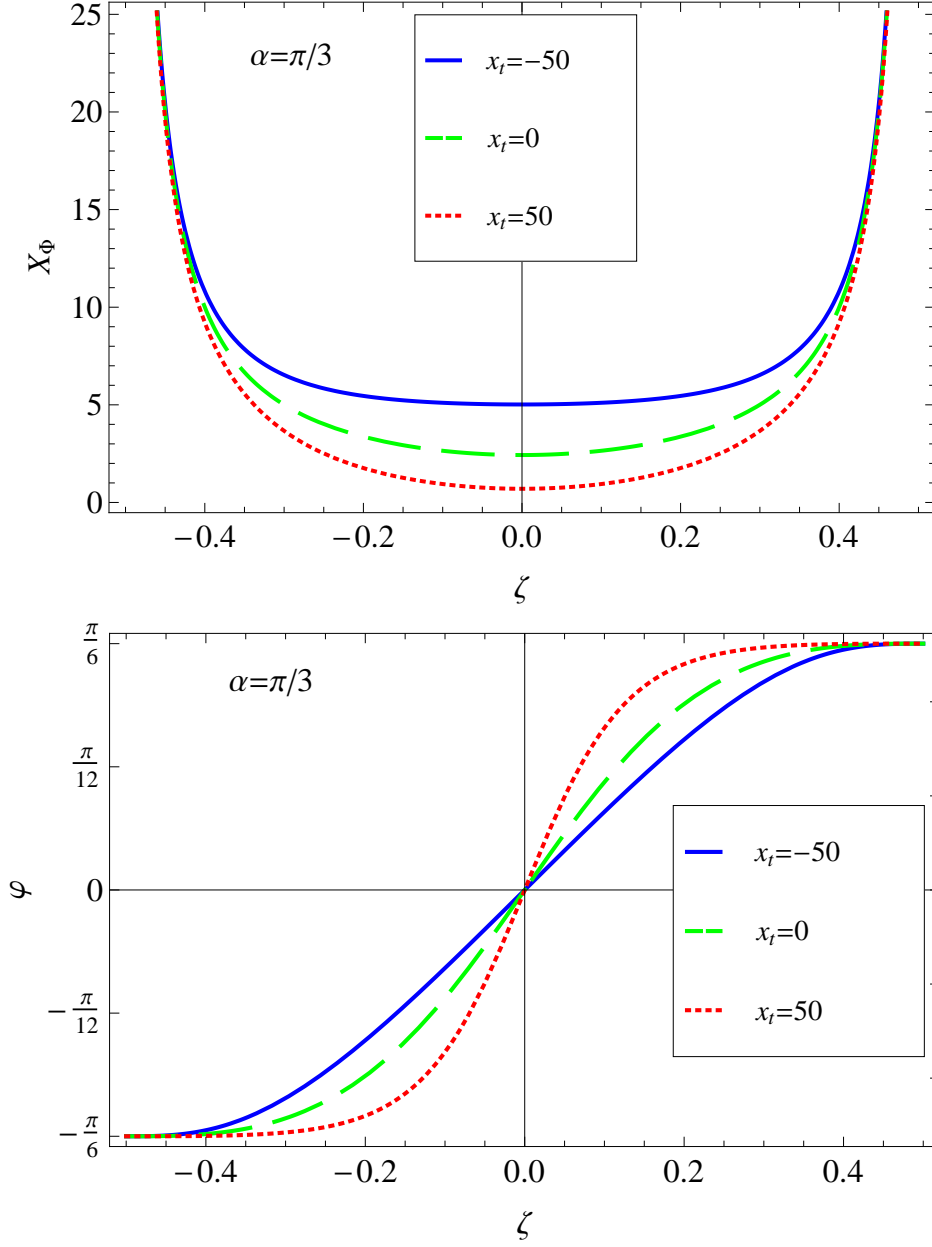
Figure D.2: Plots of the amplitude profile and the angle of the order parameter for $\alpha = \pi/3$ and some choices of x_t. We observe that, when the temperature increases, the value of the amplitude in the middle of the system decreases. The twist of the local variables through the system spans over the total system almost uniformly for low temperatures, while for higher ones it concentrates more and more in the middle of the system where the amplitude is at its smallest values.

APPENDIX E

Low-Temperature Asymptotics of the XY Ginzburg-Landau Model Under Twisted Boundary Conditions

According to Eqn. (2.35), when $x_t < 0$,

$$X_{\text{Cas}}^{(\alpha)}(\tau) = X_0^4[p^2 - (1 + \tau/2)^2], \tag{E.1}$$

where τ and p are defined in Eqn.(2.34). We now endeavor to find the behavior of $X_{\text{Cas}}^{(\alpha)}(\tau)$ for $x_t \to -\infty$.

Let us first clarify what is meant by the asymptotic behavior of τ and p in the regime $x_t \to -\infty$. For low temperatures, one expects $\Phi(z) \approx \Phi(z = 0) \equiv \Phi_0$ and $d\varphi/dz \approx \alpha/L$, which correspond to a simple, smooth rotation from 0 to α with minimal amplitude variation. From Eqn. (2.16) and the definition given in Eqn. (2.30), one then obtains $X_\varphi \approx \alpha X_0^2$ and, thus, from Eqn. (2.34), $p \approx \alpha/X_0$. In terms of x_t, the equation for the order parameter amplitude is given in (2.56). Under the assumptions already made, the above equation becomes $0 \approx \alpha^2 X_0 + x_t X_0 + 2X_0^3$. One concludes that $X_0 \gg 1$ with

$$X_0^2 \approx -(x_t + \alpha^2)/2 \tag{E.2}$$

when $x_t \to -\infty$, and that $2 + \tau + p^2 \approx 0$, i.e., that $\tau \to -2 - p^2$ when $x_t \to -\infty$. Thus, the regime which we need to consider in (E.1) is $\tau \to -2 - p^2$ with $p \approx \alpha/X_0 \ll 1$. For the Casimir force from Eqn. (E.1) we then obtain

$$X_{\text{Cas}}^{(\alpha)}(x_t \to -\infty) \approx X_0^4[p^2 - p^4/4]. \tag{E.3}$$

In the asymptotic regime of interest, the roots $x_\pm$ of the previous section are real because $p \ll 1$ and $\sqrt{(\tau+1)^2 - 4p^2} = \sqrt{1 - 2p^2 + p^4} \approx \sqrt{1 - 2p^2}$. Thus, we need to study the asymptotic behavior of X_0 given by Eqn. (D.5), taking into account the right-hand side of Eqn. (D.9) which relates X_0 to α.

Setting

$$\tau = -2 - p^2 + \epsilon, \tag{E.4}$$

where $p \ll 1$ and $\epsilon \to 0$, Eqn. (D.5) becomes

$$X_0 \approx \frac{2}{\sqrt{1-x_-}} K\left(1 - \frac{1}{2}\epsilon\right) \approx \ln\left(\frac{16}{\epsilon}\right), \tag{E.5}$$

while Eqn. (D.9) simplifies as

$$\alpha \approx \frac{pX_0}{x_-}\left[1 - \frac{2}{X_0}\Pi\left(-p^2, 1 - \frac{a}{2}\right)\right] \approx \frac{pX_0}{x_-}\left[1 - \frac{2}{X_0} \cdot \frac{X_0}{2}\left(1 + \frac{p^2}{X_0}(2 - X_0)\right)\right] \tag{E.6}$$

leading to the result

$$\alpha = p(X_0 - 2), \tag{E.7}$$

where we have used Eqn. (E.5) when series expanding the elliptic Π. Note that Eqns. (E.5) and (E.2) imply that ϵ is exponentially small in $\sqrt{|x_t|}$ and, thus, in the remainder we will omit ϵ in Eqn. (E.4) and in any expansion that involves τ. Expressing p from Eqn. (E.7) in terms of X_0 and α and inserting the result in Eqn. (E.3), we obtain an expression for the Casimir force in terms of X_0 and α:

$$X_{\text{Cas}}^{(\alpha)}(x_t \to -\infty) \approx \alpha^2 \left(X_0^2 + 4X_0 + 12\right) - \frac{\alpha^4}{4}. \tag{E.8}$$

Then, making use of Eqn. (E.2), it follows that

$$X_{\text{Cas}}^{(\alpha)}(x_t) \approx \frac{1}{2}\alpha^2 \left[|x_t| + 4\sqrt{2|x_t|} + \frac{1}{2}\left(48 - 3\alpha^2\right)\right], \tag{E.9}$$

where $x_t \to -\infty$. This is the result reported in Eqn. (2.33).

APPENDIX F

Determining the Kink Temperature

In this Appendix, we employ the scaled variables defined by Eqn. (2.30). When the boundary conditions are fully anti-symmetric, $\alpha = \pi$, we find a kink in the Casimir force at a temperature $x_{t,\text{kink}}$ below the bulk critical temperature, i.e. $x_{t,\text{kink}} < 0$. At that point, the two integration constants X_0 and X_φ both switch from being identically zero $(x_t > x_{t,\text{kink}})$ to being positive $(x_t < x_{t,\text{kink}})$. Note, however, that the quotient $M = X_\varphi/X_0$ remains non-zero for all temperatures. We determine the kink temperature by enforcing the boundary conditions, Eqns. (2.24) and (2.25).

At the transition point, things are simplified because $X_0, X_\varphi \to 0$. The length condition (2.24) takes the form

$$\frac{1}{2} = \int_0^\infty \frac{dX_\Phi}{\left(M_{\text{kink}}^2 + x_{t,\text{kink}}X_\Phi^2 + X_\Phi^4\right)^{1/2}}. \tag{F.1}$$

The twist condition must be treated with more care because the integrand appears to be singular when $X_0 = 0$. Without taking X_0 to zero, (2.25) may be re-expressed as

$$\frac{\pi}{2} = MX_0 \int_{X_0}^\infty \frac{dX_\Phi}{X_\Phi \sqrt{X_\Phi^2 - X_0^2}} \cdot \frac{1}{\left(M^2 + x_t X_\Phi^2 + X_\Phi^2 \left(X_\Phi^2 + X_0^2\right)\right)^{1/2}}$$

$$\equiv f(M, X_0), \quad \text{(F.2)}$$

which holds at all temperatures. In particular, just below the kink temperature, X_0 is small but non-zero, and (abbreviating $M_k = M_{\text{kink}}$ and $x_{t,k} = x_{t,\text{kink}}$)

$$\frac{\pi}{2} = f(M_k, 0) + \frac{\partial f}{\partial X_0}(M_k, 0) X_0 + O(X_0^2) \tag{F.3}$$

at that point. If we make the substitution $X_\Phi = X_0 y$, we see that $f(M_k, 0)$ is actually

non-singular:

$$f(M_k, 0) = M_k \int_1^\infty \frac{dy}{y\sqrt{y^2 - 1}} \cdot \frac{1}{\left(M_k^2 + x_{t,k}y^2 X_0^2 + y^2\left(y^2 + 1\right)X_0^4\right)^{1/2}}\Bigg|_{X_0=0}$$

$$= \int_1^\infty \frac{dy}{y\sqrt{y^2 - 1}} = \frac{\pi}{2}. \quad (\text{F.4})$$

This means that $(\partial f/\partial X_0)(M_k, 0)$ must vanish due to Eqn. (F.3). The derivative is taken most easily from the expression in (F.4), giving

$$\frac{\partial f}{\partial X_0}(M_k, 0) = -M_k X_0 \int_1^\infty \frac{y\,dy}{\sqrt{y^2 - 1}} \cdot \frac{x_{t,k} + 2y^2 X_0^2 + 2X_0^2}{\left(M_k^2 + x_{t,k}y^2 X_0^2 + y^2\left(y^2 + 1\right)X_0^4\right)^{3/2}}\Bigg|_{X_0=0}. \quad (\text{F.5})$$

Despite its appearance, this does not trivially vanish when $X_0 \to 0$. Instead, restore the original variable $X_\Phi = X_0 y$ to find

$$\frac{\partial f}{\partial \Phi_0}(M_k, 0) = -M_k \int_{X_0}^\infty \frac{X_\Phi\,dX_\Phi}{\sqrt{X_\Phi^2 - X_0^2}} \cdot \frac{x_{t,k} + 2X_\Phi^2 + 2X_0^2}{\left(M_k^2 + x_{t,k}X_\Phi^2 + X_\Phi^2\left(X_\Phi^2 + X_0^2\right)\right)^{3/2}}\Bigg|_{X_0=0} \quad (\text{F.6})$$

which suffers no singularity when X_0 is replaced by zero. Thus the second condition on $x_{t,k}$ and M_k is

$$0 = \int_0^\infty dX_\Phi \frac{x_{t,k} + 2X_\Phi^2}{\left(M_k^2 + x_{t,k}X_\Phi^2 + X_\Phi^4\right)^{3/2}}. \quad (\text{F.7})$$

Eqns. (F.1) and (F.7) may be recast, with the aid of Eqns. (D.15) and (D.18), into

$$\sqrt{M_k} = 2K\left(\sqrt{\frac{1}{2} - \frac{x_{t,k}}{4M_k}}\right) \quad (\text{F.8})$$

and

$$\frac{1}{2}M_k\sqrt{x_{t,k} + 2M_k} =$$

$$4M_k K\left(\sqrt{\frac{x_{t,k} - 2M_k}{x_{t,k} + 2M_k}}\right) - (x_{t,k} + 2M_k)E\left(\sqrt{\frac{x_{t,k} - 2M_k}{x_{t,k} + 2M_k}}\right), \quad (\text{F.9})$$

which are easily solved numerically to give

$$x_{t,\text{kink}} \approx -28.1099 \quad \text{and} \quad M_{\text{kink}} \approx 21.5491. \quad (\text{F.10})$$

In Eqn. (F.9), $E(x)$ is the complete elliptic integral of the second kind.

84

It is worth noting that the kink develops at the same temperature as where the mean-field Ising model's scaling function $X_{\mathrm{Cas}}^{(+,-)}$ achieves its maximum. Indeed, we can independently arrive at the temperature in Eqn. (F.10) by considering Eqn. (D.22). We are squarely in the region $x_t < 0$, so the relationships are

$$X_{\mathrm{Cas}}^{(+,-)} = 64k^2(1-k^2)K(k)^4 \qquad \text{and} \qquad x_t = -8(2k^2-1)K(k)^2 \qquad \text{(F.11)}$$

and the slope of the scaling function is given by

$$\frac{dX_{\mathrm{Cas}}^{(+,-)}}{dx_t} = \frac{dX_{\mathrm{Cas}}^{(+,-)}/dk}{dx_t/dk}. \qquad \text{(F.12)}$$

Setting this expression to zero and solving for k in the region $[\frac{1}{\sqrt{2}}, 1)$ yields $k \approx 0.909$. Plugging that value in to Eqn. (F.11), we find $x_{t,\mathrm{max}} \approx -28.1099$.

APPENDIX G

Some Integrals of Interest

We are interested in finding a closed form for the integral

$$I(s) = \int_{-\pi}^{\pi} dx\, dy \, \ln\left(s - 2\cos x - 2\cos y\right), \tag{G.1}$$

appearing in Eqn. (3.47). We proceed by looking at its derivative,

$$\frac{dI}{ds} = \int_{-\pi}^{\pi} \frac{dx\, dy}{s - 2\cos x - 2\cos y}, \tag{G.2}$$

which also appears in Eqn. (3.45). We note that it resembles the following complex analysis exercise:

$$J(a,b) = \int_{-\pi}^{\pi} \frac{dx}{a + b\cos x}, \tag{G.3}$$

where $a, b \in \mathbb{R}$ and $a > |b|$. Therefore, we will attempt the calculation of $J(a,b)$, first writing $z = e^{ix}$ so that

$$J(a,b) = \int_{-\pi}^{\pi} \frac{dx}{a + \frac{b}{2}\left(e^{ix} + e^{-ix}\right)} = \frac{2}{ib} \int \frac{dz}{z^2 + \frac{2a}{b}z + 1} \tag{G.4}$$

and the integration proceeds on the unit circle in the complex plane, oriented counter-clockwise.

The integrand has poles at

$$z_{\pm} = \frac{-a \pm \sqrt{a^2 - b^2}}{b}, \tag{G.5}$$

and the root z_- is outside the unit disk, because

$$|z_-| = \frac{a + \sqrt{a^2 - b^2}}{|b|} > \frac{a}{|b|} > 1. \tag{G.6}$$

On the other hand, z_+ is inside:

$$|z_+| = \left|\frac{-a + \sqrt{a^2 - b^2}}{b} \cdot \frac{-a - \sqrt{a^2 - b^2}}{-a - \sqrt{a^2 - b^2}}\right| = \left|\frac{b}{a + \sqrt{a^2 - b^2}}\right| < \frac{|b|}{a} < 1. \tag{G.7}$$

Therefore the residue theorem gives

$$J(a,b) = \frac{2}{ib} \cdot 2\pi i \cdot \text{Res}\left(\frac{1}{(z-z_-)(z-z_+)}, z = z_+\right) = \frac{2\pi}{\sqrt{a^2-b^2}}. \qquad \text{(G.8)}$$

Returning to our original problem, we see that

$$\frac{dI}{ds} = \int_{-\pi}^{\pi} dx \frac{dy}{(s-2\cos x) - 2\cos y} = \int_{-\pi}^{\pi} dx\, J(s-2\cos x, -2)$$

$$= \int_{-\pi}^{\pi} dx \frac{2\pi}{\sqrt{(s-2\cos x)^2 - 4}}. \qquad \text{(G.9)}$$

Integrating instead over $[0, \pi]$ (thus gaining a factor of two), and making the change of variables

$$\tan\left(\frac{x}{2}\right) = \sqrt{\frac{s}{s+4}} \tan u, \qquad \text{(G.10)}$$

with $dx = 2\sqrt{s(s+4)}\frac{\sec^2 u\, du}{4+s\cdot\sec^2 u}$ and $\cos x = \frac{4+s(1-\tan^2 u)}{4+s\cdot\sec^2 u}$, we proceed carefully and end up with

$$\int_{-\pi}^{\pi} \frac{dx\, dy}{s - 2\cos x - 2\cos y} = \frac{dI}{ds} = \frac{8\pi}{s} \int_0^{\pi/2} \frac{du}{\sqrt{1 - \frac{16}{s^2}\cos^2 u}} = \frac{8\pi}{s} K\left(\frac{4}{s}\right). \qquad \text{(G.11)}$$

Now we refer to a table of integrals[1] in order to find an anti-derivative of dI/ds,

$$I(s) = \int ds \frac{8\pi}{s} K\left(\frac{4}{s}\right) = \text{const} + 4\pi^2 \ln s + 2\pi^2 \left(\gamma^2 + 1 + i\pi\right)$$

$$- \frac{8\pi^2}{s^2} \cdot {}_4F_3\left(1, 1, \frac{3}{2}, \frac{3}{2};\ 2, 2, 2;\ \frac{16}{s^2}\right). \qquad \text{(G.12)}$$

We determine the constant by considering $s = 4$, which gives[80]

$$I(s = 4) = 16\pi G - 4\pi^2 \ln 2 \qquad \text{(G.13)}$$

from Eqn. (G.1), with G being Catalan's constant. On the other hand,

$$\frac{8\pi^2}{s^2} \cdot {}_4F_3\left(1, 1, \frac{3}{2}, \frac{3}{2};\ 2, 2, 2;\ \frac{16}{s^2}\right)\bigg|_{s=4} = -16\pi G + 8\pi^2 \ln 2. \qquad \text{(G.14)}$$

Thus, we find

$$\text{const} = -2\pi^2 \left(\gamma^2 + 1 + i\pi\right), \qquad \text{(G.15)}$$

---

[1] `http://functions.wolfram.com/08.02.21.0007.01`, with $z = 16/s^2$.

with the final result

$$I(s) = 4\pi^2 \left[\ln s - \frac{2}{s^2} \cdot {}_4F_3\left(1, 1, \frac{3}{2}, \frac{3}{2};\ 2, 2, 2;\ \frac{16}{s^2}\right)\right].$$

(G.16)

APPENDIX H

Spectral Derivatives

Consider a real, symmetric $L \times L$ matrix $\mathcal{H}$ with a non-degenerate spectrum, whose entries depend on a parameter x. Let the eigenvalues and normalized eigenvectors be denoted $\{a_l\}$ and $\{|\psi^{(l)}\rangle\}$, respectively, with $l = 1, \ldots, L$. We would like to compute derivatives of the eigenvalues and normalized eigenvectors with respect to the parameter x. First note that the condition $\langle \psi^{(l)} | \psi^{(l)} \rangle = 1$ gives

$$0 = \frac{\partial}{\partial x} \langle \psi^{(l)} | \psi^{(l)} \rangle = \frac{\partial \langle \psi^{(l)} |}{\partial x} | \psi^{(l)} \rangle + \langle \psi^{(l)} | \frac{\partial | \psi^{(l)} \rangle}{\partial x}. \tag{H.1}$$

By virtue of $\mathcal{H}$ being real and symmetric, its eigenvalues are real[] as are its eigenvectors. Therefore the above condition leads us to conclude the orthogonality of $|\psi^{(l)}\rangle$ and its derivative with respect to x:

$$\langle \psi^{(l)} | \frac{\partial | \psi^{(l)} \rangle}{\partial x} = 0. \tag{H.2}$$

Now we refer to the defining property of the eigenvalues,

$$\mathcal{H} | \psi^{(l)} \rangle = a_l | \psi^{(l)} \rangle, \tag{H.3}$$

and differentiate it to find

$$\frac{\partial \mathcal{H}}{\partial x} | \psi^{(l)} \rangle + \mathcal{H} \frac{\partial | \psi^{(l)} \rangle}{\partial x} = \frac{\partial a_l}{\partial x} | \psi^{(l)} \rangle + a_l \frac{\partial | \psi^{(l)} \rangle}{\partial x}. \tag{H.4}$$

Rearranging,

$$(\mathcal{H} - a_l) \frac{\partial | \psi^{(l)} \rangle}{\partial x} = \frac{\partial a_l}{\partial x} | \psi^{(l)} \rangle - \frac{\partial \mathcal{H}}{\partial x} | \psi^{(l)} \rangle. \tag{H.5}$$

At this point, we appeal to inner products. Multiplying on the left by $\langle \psi^{(l)} |$ and making use of Eqn. (H.2) and the fact that $\langle \psi^{(l)} | \mathcal{H} = \langle \psi^{(l)} | a_l$ because $\mathcal{H}$ is real and symmetric (i.e.

Hermitian), we find[1]

$$\frac{\partial a_l}{\partial x} = \langle \psi^{(l)} | \frac{\partial \mathcal{H}}{\partial x} | \psi^{(l)} \rangle. \tag{H.6}$$

On the other hand, if we apply $\langle \psi^{(m)} |$ with $m \neq l$, we find the following:

$$(a_m - a_l) \langle \psi^{(m)} | \frac{\partial |\psi^{(l)}\rangle}{\partial x} = -\langle \psi^{(m)} | \frac{\partial \mathcal{H}}{\partial x} | \psi^{(l)} \rangle. \tag{H.7}$$

Of course, this is a statement about the component of $\partial |\psi^{(l)}\rangle / \partial x$ along the vector $|\psi^{(m)}\rangle$. Therefore, we can reconstruct the entire vector by summing over the components in each of the eigenvectors' directions (we already know from Eqn. (H.2) that there is no component along $|\psi^{(l)}\rangle$ itself)

$$\frac{\partial |\psi^{(l)}\rangle}{\partial x} = \sum_{m \neq l} \frac{\langle \psi^{(m)} | \frac{\partial \mathcal{H}}{\partial x} | \psi^{(l)} \rangle}{a_l - a_m} | \psi^{(m)} \rangle. \tag{H.8}$$

In the particular case of the matrix $\mathcal{H}$ from Eqn. (3.18), we see that

$$\left[\frac{\partial \mathcal{H}}{\partial \Lambda_l} \right]_{ij} = 2 \delta_{il} \delta_{jl}. \tag{H.9}$$

Therefore,

$$\frac{\partial a_l}{\partial \Lambda_j} = \sum_{m,n} \psi_m^{(l)} \left[\frac{\partial \mathcal{H}}{\partial \Lambda_j} \right]_{mn} \psi_n^{(l)} = 2 \sum_{m,n} \psi_m^{(l)} \delta_{mj} \delta_{nj} \psi_n^{(l)} = 2 \, \psi_j^{(l)\,2} \tag{H.10}$$

and

$$\frac{\partial \psi_i^{(l)}}{\partial \Lambda_j} = \sum_{m \neq l} \frac{2 \psi_j^{(m)} \psi_j^{(l)}}{a_l - a_m} \psi_i^{(m)}. \tag{H.11}$$

---

[1] Also note that non-degenerate Hermiticity implies orthogonality of eigenvectors: $a_m \langle \psi^{(m)} | \psi^{(l)} \rangle = \langle \psi^{(m)} | \mathcal{H} | \psi^{(l)} \rangle = a_l \langle \psi^{(m)} | \psi^{(l)} \rangle$, by acting alternately on the left or the right with $\mathcal{H}$, forces $\langle \psi^{(m)} | \psi^{(l)} \rangle = \delta_{lm}$.

APPENDIX I

Asymptotic Solution of the $O(n)$ Model with $n \to \infty$

In this Appendix, we resume the study of the model defined in section 3.2.

I.1 Setting Up the Asymptotic Approach

The problem may be studied at low temperature (equivalently, large values of $R = \beta J$) more or less analytically. Recalling Eqn. (3.46), we see that when R is very large, the saving grace is the one eigenvalue, a_1, which approaches 4. This effectively renders the constraint as

$$R \approx \frac{2}{\pi} \, \psi_i^{(1)\,2} \, \frac{1}{a_1} K\left(\frac{4}{a_1}\right). \tag{I.1}$$

This holds for each $i = 1, \ldots, L$, which implies that $\psi_i^{(1)\,2} \approx$ const. Furthermore, the numerics indicate that, as R gets large, $\psi^{(1)}$ approaches a constant vector (as opposed to one varying with respect to i). This can also be argued in analogy to quantum mechanics where the lowest eigenstate generally features the least spatial variation. In any case, if we require that the constant vector be an eigenvector of $\mathcal{H}$ with an eigenvalue of 4, we find that

$$\Lambda^* = (5, 6, 6, \ldots, 6, 6, 5)/2 \tag{I.2}$$

is the one and only solution for the $\{\Lambda_l\}$. Indeed, the numerics show that $\Lambda \to \Lambda^*$ as the temperature decreases.

The spectrum of the resulting matrix $\mathcal{H}_0 \equiv \mathcal{H}(\Lambda^*)$, defined by Eqn. (3.18), may be computed in closed form by trying an ansatz $\phi_i = \cos(ai + b)$ as an eigenvector. Using trigonometric identities, we find that the associated eigenvalue is $4 + 4\sin^2\left(\frac{a}{2}\right)$ and then use

that to determine[1] a and b, yielding the eigenvalues

$$\lambda_l = 4 + 4\sin^2\left(\frac{\pi(l-1)}{2L}\right), \qquad l = 1,\ldots,L \tag{I.3}$$

with corresponding eigenvectors

$$\phi_i^{(l)} = \cos\left(\frac{\pi(l-1)}{2L}(2i-1)\right)/\text{norm}, \qquad i, l = 1,\ldots,L \tag{I.4}$$

where the norm may be shown to be $\sqrt{L}$ for $l = 1$ and $\sqrt{L/2}$ for all other l.

Now we will perturb the Lagrange multlipliers, $\Lambda_l = \Lambda_l^* + \epsilon_l/2$, and see the effect on the eigensystem. The perturbed Hamiltonian that we are studying is then

$$\mathcal{H} = \mathcal{H}_0 + \mathcal{E} = \begin{pmatrix} 5 + \epsilon_1 & -1 & 0 & & & \\ -1 & 6 + \epsilon_2 & -1 & & & \\ 0 & -1 & 6 + \epsilon_3 & & & \\ & & & \ddots & & \\ & & & & 6 + \epsilon_{L-1} & -1 \\ & & & & -1 & 5 + \epsilon_L \end{pmatrix}, \tag{I.5}$$

where $\mathcal{E} \equiv \text{diag}(\epsilon)$ is the small perturbative matrix. We recall from perturbation theory that, to first order, the eigenvalues of $\mathcal{H}$ are

$$a_l = \lambda_l + \langle\phi^{(l)}|\mathcal{E}|\phi^{(l)}\rangle = \lambda_l + \sum_{i=1}^{L} \epsilon_i\,\phi_i^{(l)\,2}, \tag{I.6}$$

while the eigenvectors become

$$|\psi^{(l)}\rangle = |\phi^{(l)}\rangle + \sum_{m\neq l} \frac{\langle\phi^{(m)}|\mathcal{E}|\phi^{(l)}\rangle}{\lambda_l - \lambda_m}|\phi^{(m)}\rangle. \tag{I.7}$$

In terms of components, this last equation reads

$$\psi_i^{(l)} = \phi_i^{(l)} + \sum_{m\neq l} \frac{1}{\lambda_l - \lambda_m}\phi_i^{(m)}\sum_{j=1}^{L}\epsilon_j\phi_j^{(m)}\phi_j^{(l)}. \tag{I.8}$$

---

[1]The identity $\tan\frac{x}{2} = \frac{1-\cos x}{\sin x}$ is especially useful here.

Our goal is to find the values $\{\epsilon_l\}$ which solve the constraint equations when R is very large. The constraint is particularly sensitive to variations in the first mode, $\{a_1, |\psi^{(1)}\rangle\}$ so we rewrite Eqn. (3.46) as

$$R = \frac{2}{\pi}\,\psi_i^{(1)\,2}\,\frac{1}{4}K\left(\frac{4}{a_1}\right) + \frac{2}{\pi}\sum_{l=2}^{L}\phi_i^{(l)\,2}\,\frac{1}{\lambda_l}K\left(\frac{4}{\lambda_l}\right), \tag{I.9}$$

where it will be noted that the terms involving modes $l \geq 2$ refer to the unperturbed states and eigenvalues. Numerics will later confirm that this simplifying approximation is acceptable.

The perturbations to the first mode are especially simple:

$$a_1 = \lambda_1 + \sum_{i=1}^{L}\epsilon_i\,\phi_i^{(1)\,2} = 4 + \frac{1}{L}\sum_{i=1}^{L}\epsilon_i, \tag{I.10}$$

because $\lambda_1 = 4$ and $\phi_i^{(1)} = \frac{1}{\sqrt{L}}$ for all i. The perturbed eigenvector is

$$\psi_i^{(1)} = \frac{1}{\sqrt{L}} + \frac{1}{\sqrt{L}}\sum_{m=2}^{L}\frac{1}{4-\lambda_m}\phi_i^{(m)}\sum_{j=1}^{L}\epsilon_j\phi_j^{(m)}. \tag{I.11}$$

and its square, neglecting terms $O(\epsilon^2)$, is

$$\psi_i^{(1)\,2} \approx \frac{1}{L} + \frac{2}{L}\sum_{m=2}^{L}\frac{1}{4-\lambda_m}\phi_i^{(m)}\sum_{j=1}^{L}\epsilon_j\phi_j^{(m)}. \tag{I.12}$$

Now we define

$$C_i = \frac{2}{\pi}\sum_{l=2}^{L}\phi_i^{(l)\,2}\,\frac{1}{\lambda_l}K\left(\frac{4}{\lambda_l}\right), \tag{I.13}$$

which is an easily computed function of only L, and the constraint equation reads

$$R = \frac{2}{\pi}\left(\frac{1}{L} + \frac{2}{L}\sum_{m=2}^{L}\frac{1}{4-\lambda_m}\phi_i^{(m)}\sum_{j=1}^{L}\epsilon_j\phi_j^{(m)}\right)\frac{1}{4}K\left(\frac{4}{a_1}\right) + C_i \tag{I.14}$$

We recall two useful properties of the eigenvectors $\{|\phi^{(l)}\rangle\}$,

orthonormality: $\qquad \langle\phi^{(l)}|\phi^{(m)}\rangle = \sum_{i=1}^{L}\phi_i^{(l)}\phi_i^{(m)} = \delta_{lm}$ (I.15)

completeness: $\qquad \left[\sum_{l=1}^{L}|\phi^{(l)}\rangle\langle\phi^{(l)}|\right]_{ij} = \sum_{l=1}^{L}\phi_i^{(l)}\phi_j^{(l)} = \delta_{ij}.$ (I.16)

Multiplying Eqn. (I.14) by $\phi_i^{(1)}$ and then summing over i kills the complicated term via orthogonality. After moving around constants, we find

$$2\pi L R = K\left(\frac{4}{a_1}\right) + 2\pi \sum_{i=1}^{L} C_i, \tag{I.17}$$

which can be immediately solved for $a_1 \approx 4$ by expanding the elliptic K function. This gives

$$a_1 \approx 4\left(1 + 8e^{-4\pi L\left(R - \frac{1}{L}\sum_{i=1}^{L} C_i\right)}\right) \sim 4 + 32e^{-4\pi L R}. \tag{I.18}$$

Thus the exponential decay of a_1 with R, postulated in section 3.5, is recovered. Note that the quantity $\rho_L = \frac{1}{L}\sum_i C_i$ tends to a finite, non-zero limit as $L \to \infty$:

$$\rho_L = \frac{1}{L}\sum_{i=1}^{L} C_i = \frac{1}{2\pi L}\sum_{l=2}^{L}\frac{1}{1 + \sin^2\left(\frac{\pi(l-1)}{2L}\right)} K\left(\frac{1}{1 + \sin^2\left(\frac{\pi(l-1)}{2L}\right)}\right)$$

$$\to \frac{1}{2\pi}\int_0^1 \frac{dx}{1 + \sin^2\left(\frac{\pi x}{2}\right)} K\left(\frac{1}{1 + \sin^2\left(\frac{\pi x}{2}\right)}\right) \approx 0.25273. \tag{I.19}$$

In fact, $\rho_L \to R_c$: taking the definition of R_c from Eqn. (3.38), and performing two of the integrations according to Eqn. (G.11), we see that

$$R_c = \frac{1}{2\pi}\int_0^1 \frac{dx}{1 + \sin^2\left(\frac{\pi x}{2}\right)} K\left(\frac{1}{1 + \sin^2\left(\frac{\pi x}{2}\right)}\right). \tag{I.20}$$

Returning to the constraint, Eqn. (I.14), we now take an inner product with $|\phi^{(l)}\rangle$ where $l > 1$. That is, multiply by $\phi_i^{(l)}$ and sum over i. This gives

$$\sum_{j=1}^{L} \epsilon_j \phi_j^{(l)} = 2\pi L \frac{\lambda_l - 4}{2K(4/a_1)}\sum_{i=1}^{L} C_i \phi_i^{(l)}. \tag{I.21}$$

Now multiply by $\phi_k^{(l)}$ and sum over l, using completeness:

$$\epsilon_k = \frac{1}{\pi(R - \rho_L)}\sum_{l=1}^{L}\sum_{i=1}^{L}\sum_{m=2}^{L}\frac{\lambda_l - 4}{\lambda_m} K\left(\frac{4}{\lambda_m}\right)\phi_k^{(l)}\phi_i^{(l)}\phi_i^{(m)\,2}. \tag{I.22}$$

This can be further simplified by computing

$$\sum_{i=1}^{L}\phi_i^{(l)}\phi_i^{(m)\,2} = \frac{1}{N_l N_m^2}\sum_{i=1}^{L}\cos\left(\frac{\pi(l-1)}{2L}(2i-1)\right)\cos^2\left(\frac{\pi(m-1)}{2L}(2i-1)\right), \tag{I.23}$$

94

where N_i denotes the norm of $|\phi^{(i)}\rangle$. The result is

$$\sum_{i=1}^{L} \phi_i^{(l)} \phi_i^{(m)\,2} = \frac{L}{4N_l N_m^2} \left(2\delta_{l1} + \delta_{l+2m-3,0} - \delta_{l+2m-3,2L} + \delta_{l-2m+1,0}\right). \tag{I.24}$$

Therefore,

$$\epsilon_k = \frac{\sqrt{2/L}}{2\pi(R-\rho_L)} \sum_{m=2}^{\lfloor (L+1)/2 \rfloor} (\lambda_{2m-1} - 4)\phi_k^{(2m-1)} \left[\frac{K(4/\lambda_m)}{\lambda_m} - \frac{K(4/\lambda_{L+2-m})}{\lambda_{L+2-m}}\right]. \tag{I.25}$$

Referring to Eqn. (I.6) and reusing the result Eqn. (I.24), being mindful that $2m-1$ may be larger than L, we find a milestone result: the perturbed eigenvalues, for $l \geq 2$, are

$$a_l = \lambda_l + \frac{1}{2\pi L(R-\rho_L)}(\lambda_{2l-1} - 4)\left[\frac{K(4/\lambda_l)}{\lambda_l} - \frac{K(4/\lambda_{L+2-l})}{\lambda_{L+2-l}}\right], \tag{I.26}$$

where λ_l is as written in Eqn. (I.3) even when $l \in \mathbb{Z}$ is not confined to the range $\{1, \ldots, L\}$. It is worth pointing out that, for $l \geq 2$, the perturbations to the eigenvalues go as $1/R$, whereas the anomalous a_1 is perturbed by e^{-R}.

For a given L and large R, these eigenvalues may be compared to the data found numerically. The agreement is excellent, even when R is only moderately large. For instance, with $L = 6$ and $R = 10$,

a_l (numeric)	4.00000	4.26893	5.00123	6.00001	6.99878	7.73107
λ_l (unperturbed)	4.00000	4.26795	5.00000	6.00000	7.00000	7.73205
a_l (perturbed)	4.00000	4.26893	5.00123	6.00000	6.99877	7.73107

(I.27)

where the numeric results come from the implementation of the procedures discussed in section 3.5.

I.2 Casimir Force Considerations

Our ultimate goal is to find a closed form expression for the Casimir force in the asymptotic regime $R \to \infty$. Towards that end, we must consider the finite-size free energy, Eqn. (3.47). The clear difficulty in the expression for the free energy is the term

$$B(L,R) = \frac{1}{8\pi^2} \int_{-\pi}^{\pi} dq_x\,dq_y \sum_{l=1}^{L} \ln(a_l - 2\cos q_x - 2\cos q_y). \tag{I.28}$$

It is natural to ask what dominates the perturbative behavior of $B(L, R)$: the almost-singular mode $l = 1$ or the other modes which are perturbed by $\frac{1}{R}$? If we define $\delta\lambda_l = a_l - \lambda_l$, then we can simply Taylor expand for $l > 1$,

$$\int_{-\pi}^{\pi} dq_x\, dq_y \ln(a_l - 2\cos q_x - 2\cos q_y)$$

$$\approx \int_{-\pi}^{\pi} dq_x\, dq_y \ln(\lambda_l - 2\cos q_x - 2\cos q_y) + \delta\lambda_l \int_{-\pi}^{\pi} \frac{dq_x\, dq_y}{\lambda_l - 2\cos q_x - 2\cos q_y}. \quad \text{(I.29)}$$

Therefore the $l > 1$ perturbations make contributions to $B(L, R)$ on the order of $\delta\lambda_l \sim \frac{1}{R}$.

On the other hand, the $l = 1$ term cannot be developed in a simple Taylor series. Instead, we have the expansion[37, 80]

$$\int_{-\pi}^{\pi} dq_x\, dq_y \ln(4 + \delta\lambda_1 - 2\cos q_x - 2\cos q_y)$$

$$= \frac{2G}{\pi} + \frac{1}{256\pi}\delta\lambda_1\Big(32\,(1 + 5\ln 2) - 32\ln\delta\lambda_1\Big) + O\left(\delta\lambda_1{}^2\right), \quad \text{(I.30)}$$

where G is Catalan's constant. The perturbative contribution for $l = 1$ is on the order of Re^{-R} which is dwarfed by the $1/R$ contributions for $l > 1$.

According to Eqn. (I.26), and setting $u = \sin^2\left(\frac{\pi(l-1)}{2L}\right)$,

$$\delta\lambda_l = \frac{1}{2\pi L(R - \rho_L)} 4u(1 - u)\left[\frac{1}{1 + u}K\left(\frac{1}{1 + u}\right) - \frac{1}{2 - u}K\left(\frac{1}{2 - u}\right)\right]. \quad \text{(I.31)}$$

for $l = 2, \ldots, L$. For $l = 1$, the above equation predicts zero, while the true perturbation is $\delta\lambda_1 \sim e^{-R}$. In light of the comments above, we can take Eqn. (I.31) as correct for all $l = 1, \ldots, L$ without erring in the perturbative analysis.

In that case, we may expand $B(L, R)$ as a series in $\delta\lambda_l \sim 1/R$,

$$B(L, R) = \frac{1}{8\pi^2} \int_{-\pi}^{\pi} dq_x\, dq_y \sum_{l=1}^{L} \ln(\lambda_l - 2\cos q_x - 2\cos q_y)$$

$$+ \frac{1}{8\pi^2} \int_{-\pi}^{\pi} dq_x\, dq_y \sum_{l=1}^{L} \frac{\delta\lambda_l}{\lambda_l - 2\cos q_x - 2\cos q_y} + O\left(\delta\lambda_l{}^2\right), \quad \text{(I.32)}$$

whose first and second terms we will call B_0 and B_1, respectively. The Casimir force is

$$\frac{\beta F_{\text{Cas}}(L)}{A} = \beta f_{\text{bulk}}$$
$$- \frac{1}{2}\left[\ln\left(\frac{R}{2\pi}\right) + B(L+1) - B(L-1) - \frac{1}{2}R\left(\sum_l{}^{+} a_l - \sum_l{}^{-} a_l\right)\right], \quad \text{(I.33)}$$

where $\sum^{\pm}$ refers to a sum over the system with size $L \pm 1$. We can evaluate each of the $\sum a_l$ by considering the trace of our matrix $\mathcal{H}$. We see that

$$\sum_l a_l = \operatorname{tr}\mathcal{H} = 2\sum_l \Lambda_l^* + \sum_l \epsilon_l = 6L - 2 + \sum_l \epsilon_l, \quad \text{(I.34)}$$

and our previous analysis showed that, to first order in perturbation theory, $\sum_l \epsilon_l \approx 0$. More precisely, $\sum_l \epsilon_l = O(1/R^2)$. Because these terms are multiplied by R, we will find that they give rise to a non-zero contribution of order $1/R$. This computation will be performed in detail later.

The Casimir force will further simplify when we insert the expression for βf_{bulk} in the next section. For now, we may write it as

$$\frac{\beta F_{\text{Cas}}(L)}{A} = \beta f_{\text{bulk}} - \frac{1}{2}\ln\left(\frac{R}{2\pi}\right)$$
$$- \frac{1}{2}\left(B(L+1) - B(L-1)\right) + \frac{1}{4}R\left(12 + \sum_l{}^{+} \epsilon_l - \sum_l{}^{-} \epsilon_l\right). \quad \text{(I.35)}$$

I.3 Zero-Temperature Casimir Force

We will now consider the first term of $B(L, R)$, which we call B_0. This is the temperature-independent zero-order term in the $1/R$ expansion. Define

$$S_L(x) = \sum_{l=1}^{L} \ln(\lambda_l + x), \quad \text{(I.36)}$$

so that

$$B_0 = \frac{1}{8\pi^2}\int_{-\pi}^{\pi} dq_x\, dq_y\, S_L\Big(x = -2\cos q_x - 2\cos q_y\Big). \quad \text{(I.37)}$$

The λ_l are $2L$-periodic. In light of that, it makes sense to consider a sum over the entire period:

$$T_L(x) = \sum_{l=1}^{2L} \ln(\lambda_l + x), \tag{I.38}$$

which is related to $S_L(x)$ through

$$S_L(x) = \frac{1}{2}\Big[T_L(x) - \ln(8+x) + \ln(4+x)\Big]. \tag{I.39}$$

The $\ln(8+x)$ and $\ln(4+x)$ are the $l = L+1$ and $l = 2L+1$ terms which T_L "mistakenly" includes and excludes, respectively. Let M be the (formally infinite) number of copies of $\{1, \ldots, 2L\}$ needed to cover all of $\mathbb{Z}$ when lay end-to-end. Then we have

$$T_L(x) = \frac{1}{M} \sum_{l=-\infty}^{\infty} \ln(\lambda_l + x). \tag{I.40}$$

The derivative dT_L/dx is more amenable to analysis:

$$\frac{dT_L}{dx} = \frac{1}{M} \sum_{l=-\infty}^{\infty} \frac{1}{\lambda_l + x} = -\frac{1}{M} \sum \operatorname{Res}\left(\frac{\pi \cot(\pi z)}{\lambda(z) + x}\right), \tag{I.41}$$

where we invoke the cotangent summation formula, and the sum runs over the residues of $1/(\lambda(z) + x)$. $\lambda(z)$ is the analytic continuation of our eigenvalues which were previously indexed by integer l. Specifically,

$$\lambda(z) = 4 + 4\sin^2\left(\frac{\pi(z-1)}{2L}\right). \tag{I.42}$$

The function $\lambda(z)$ is $2L$-periodic, so we can restrict our attention to $0 < \operatorname{Re}(z) \leq 2L$, a vertical strip in the complex plane, with the understanding that any residues found there will be duplicated M times. Therefore we will have

$$\frac{dT_L}{dx} = -\sum \operatorname{Res}\left(\frac{\pi \cot(\pi z)}{\lambda(z) + x}\right), \tag{I.43}$$

where we now only include the residues in the vertical strip described above. The locations of the residues are determined by the equation $\lambda(z) = -x$. We note that $-4 \leq x \leq 4$ because $x = -2\cos q_x - 2\cos q_y$, so we expect the solutions to be complex. Indeed, they are

$$z_{\pm} = 1 \pm i\,\frac{2L}{\pi}\sinh^{-1}\sqrt{\frac{x+4}{4}}, \tag{I.44}$$

and the residues there are

$$\text{Res}\left(\frac{\pi \cot(\pi z)}{\lambda(z) + x}; z = z_\pm\right) = -\frac{L}{\sqrt{4+x}\sqrt{8+x}} \coth\left[2L \sinh^{-1}\sqrt{\frac{x+4}{4}}\right] \tag{I.45}$$

so that

$$\frac{dT_L}{dx} = \frac{2L}{\sqrt{4+x}\sqrt{8+x}} \coth\left[2L \sinh^{-1}\sqrt{\frac{x+4}{4}}\right]. \tag{I.46}$$

This is immediately integrated[2] with respect to x, giving

$$T_L(x) = 2\ln\left[\sinh\left(2L \sinh^{-1}\sqrt{\frac{x+4}{4}}\right)\right] + \text{const.} \tag{I.47}$$

We can determine the constant by considering $T_L(x \to \infty)$. From the definition, Eqn. (I.38), a large value of x washes out the l dependence. Therefore, we have $T_L(x \to \infty) \sim 2L \ln x$. For large argument, $\sinh^{-1}\alpha$ looks like $\ln(2\alpha)$, while $\sinh\alpha$ looks like $\frac{1}{2}e^\alpha$. Then

$$2\ln\left[\sinh\left(2L \sinh^{-1}\sqrt{\frac{x+4}{4}}\right)\right] + \text{const} \sim 2L\ln x - 2\ln 2 + \text{const} \tag{I.48}$$

must agree with $2L\ln x$, which determines our constant as $2\ln 2$. The closed form result for $S_L(x)$ is

$$S_L(x) = \ln\left[2\sinh\left(2L \sinh^{-1}\sqrt{\frac{x+4}{4}}\right)\right] + \frac{1}{2}\ln\left(\frac{4+x}{8+x}\right), \tag{I.49}$$

which remains to be integrated on q_x and q_y to find B_0. In the interest of computing the Casimir force, we now construct the combination $\frac{1}{2}(B_0(L+1) - B_0(L-1))$, finding

$$\frac{1}{2}\left(B_0(L+1) - B_0(L-1)\right) = \frac{1}{8\pi^2}\int_{-\pi}^{\pi} dq_x\, dq_y\, \frac{1}{2}\ln\left(\frac{\sinh 2(L+1)v}{\sinh 2(L-1)v}\right), \tag{I.50}$$

where $v = \sinh^{-1}\sqrt{\frac{4-2\cos q_x - 2\cos q_y}{4}}$.

The bulk free energy density has a term

$$B_{0,\text{bulk}} = \frac{1}{16\pi^3}\int_{-\pi}^{\pi} dq_x\, dq_y\, dq_z\, \ln\left(3 - \cos q_x - \cos q_y - \cos q_z\right), \tag{I.51}$$

---

[2]It is not an accident that this is easy to integrate. The residues are $\pi \cot(\pi z_\pm)/\lambda'(z_\pm)$ while $\lambda(z_\pm) = -x$ forces $\lambda'(z_\pm)\frac{dz_\pm}{dx} = -1$. Therefore $dT_L = \sum_\pm \pi \cot(\pi z_\pm)\frac{dz_\pm}{dx}\, dx$.

which we would like to bring into a form similar to that just computed for B_0. Doing the q_z integration gives us

$$B_{0,\text{bulk}} = \frac{1}{8\pi^2} \int_{-\pi}^{\pi} dq_x \, dq_y \left(\cosh^{-1} (3 - \cos q_x - \cos q_y) - \ln 2 \right), \qquad \text{(I.52)}$$

which is equivalent to

$$B_{0,\text{bulk}} = -\frac{1}{2} \ln 2 + \frac{1}{8\pi^2} \int_{-\pi}^{\pi} dq_x \, dq_y \, 2v, \qquad \text{(I.53)}$$

by a hyperbolic double angle formula, with v as defined above.

Therefore the temperature-independent part of the Casimir force, i.e. the zeroth order in $1/R$, is given by (see Eqns. (3.40) and (I.35))

$$\frac{\beta F_{\text{Cas}}(L)}{A} = \left(-3R + \frac{1}{2} \ln \left(\frac{R}{\pi} \right) - \frac{1}{2} \ln 2 - \frac{1}{2} \ln \left(\frac{R}{2\pi} \right) + 3R \right)$$
$$+ \frac{1}{8\pi^2} \int_{-\pi}^{\pi} dq_x \, dq_y \left[2v - \frac{1}{2} \ln \left(\frac{\sinh{(2(L+1)v)}}{\sinh{(2(L-1)v)}} \right) \right] + O(1/R). \quad \text{(I.54)}$$

The cancellation of the terms outside the integral is perfect, which leaves us with

$$\frac{\beta F_{\text{Cas}}(L)}{A} = \frac{1}{8\pi^2} \int_{-\pi}^{\pi} dq_x \, dq_y \left[2v - \frac{1}{2} \ln \left(\frac{\sinh{(2(L+1)v)}}{\sinh{(2(L-1)v)}} \right) \right] + O(1/R), \qquad \text{(I.55)}$$

In fact,

$$\frac{1}{2} \ln \left(\frac{\sinh{(2(L+1)v)}}{\sinh{(2(L-1)v)}} \right) = 2v + \frac{1}{2} \ln \left(\frac{1 - e^{-4(L+1)v}}{1 - e^{-4(L-1)v}} \right), \qquad \text{(I.56)}$$

so the bulk contribution cancels in a very elegant way and we therefore have

$$\frac{\beta F_{\text{Cas}}(L)}{A} = -\frac{1}{16\pi^2} \int_{-\pi}^{\pi} dq_x \, dq_y \ln \left(\frac{1 - e^{-4(L+1)v}}{1 - e^{-4(L-1)v}} \right) + O(1/R). \qquad \text{(I.57)}$$

This is an exact expression for the value of the Casimir force at zero temperature, which serves as an asymptote for the scaling function. Previous results[12, 85] indicate that, for $L \to \infty$, this value should be $-\zeta(3)/8\pi L^3$ due to the presence of Goldstone modes in the three-dimensional bulk (the $L \to \infty$ limit).

We can give a more precise result by Taylor expanding Eqn. (I.57) about $L = \infty$. If we let $q_x = r_x/L$ and $q_y = r_y/L$, expand the integrand in powers of $1/L$ and utilize polar

coordinates $r_x^2 + r_y^2 = r^2$, the leading order is

$$\frac{\beta F_{\text{Cas}}(L)}{A}\bigg|_{L,R\to\infty} \approx -\frac{1}{8\pi L^2} \int_0^\infty r\, dr\, \ln\left(\frac{1 - e^{-2(1+\frac{1}{L})r}}{1 - e^{-2(1-\frac{1}{L})r}}\right)$$

$$\approx -\frac{1}{8\pi L^3} 4 \int_0^\infty dr\, \frac{r^2}{e^{2r} - 1} = -\frac{\zeta(3)}{8\pi L^3}. \quad \text{(I.58)}$$

We find the next two corrections in similar fashion, and report the result

$$\frac{\beta F_{\text{Cas}}(L)}{A} \approx -\frac{\zeta(3)}{8\pi L^3} - \frac{2\zeta(3) + \frac{7}{8}\zeta(5)}{8\pi L^5} - \frac{3\zeta(3) + \frac{35}{8}\zeta(5) + \frac{681}{512}\zeta(7)}{8\pi L^7} + O\left(\frac{1}{R}\right). \quad \text{(I.59)}$$

These corrections to the expected $-\zeta(3)/8\pi L^3$ result signify the fact that our finite-L model does not have spontaneous symmetry breaking in its two-dimensional layers, although the finite-size system approximates the three-dimensional bulk which does feature spontaneous magnetization.

I.4 $T > 0$ Correction to Casimir Force

Now we consider the first order temperature dependence of the Casimir force. The first quantity of interest is therefore

$$B_1 = \frac{1}{8\pi^2} \int_{-\pi}^\pi dq_x\, dq_y \sum_{l=1}^L \frac{\delta\lambda_l}{\lambda_l - 2\cos q_x - 2\cos q_y}, \quad \text{(I.60)}$$

which will enter the Casimir force, by Eqn. (I.35), as a term

$$-\frac{1}{2}\Big(B_1(L+1) - B_1(L-1)\Big) \quad \text{(I.61)}$$

being added on to the result, Eqn. (I.59). The second quantity of interest is the sum of the eigenvalues, which enters the Casimir force as

$$+\frac{1}{4}R\left(\sum_l^+ \epsilon_l - \sum_l^- \epsilon_l\right), \quad \text{(I.62)}$$

with notation as defined in Eqn. (I.35). This term requires going to second order in perturbation theory but will yield a simple result nonetheless.

I.4.1 The Quantity B_1

We will now do some manipulation of B_1, which is defined by Eqns. (I.60) and (I.31). Because $\delta\lambda_1 \approx 0$, we can sum over $l = 2, \ldots, L$, omitting $l = 1$. The integral over $\mathbf{q}$ is easily done by Eqn. (G.11), and we bring it into the form

$$B_1 = \frac{1}{(R - \rho_L)} \cdot \frac{1}{L} \sum_{m=1}^{L-1} f\left(\frac{m}{L}\right), \tag{I.63}$$

where

$$f(x) = \frac{1}{8\pi^2} \sin^2(\pi x) \frac{1}{1 + \sin^2(\pi x/2)} K\left(\frac{1}{1 + \sin^2(\pi x/2)}\right)$$
$$\times \left[\frac{1}{1 + \sin^2(\pi x/2)} K\left(\frac{1}{1 + \sin^2(\pi x/2)}\right) \right.$$
$$\left. - \frac{1}{1 + \cos^2(\pi x/2)} K\left(\frac{1}{1 + \cos^2(\pi x/2)}\right) \right]. \tag{I.64}$$

In this form, B_1 may be evaluated numerically with great ease. It is desirable to analytically extract the leading L dependence, though. We may find an expansion for B_1 about $L = \infty$ by using a generalized form of the Euler-Maclaurin summation formula, valid when the function of interest has logarithmic singularities at its endpoints, as our f does[86, 87].

We develop series expansions for $f(x)$ about $x = 0$ and $x = 1$, finding

$$f(x) = x^2 \left(a_2 \left(\ln x\right)^2 + b_2 \ln x + c_2\right) + x^4 \left(a_4 \left(\ln x\right)^2 + b_4 \ln x + c_4\right) + O(x^6), \tag{I.65}$$

and

$$f(1 - \delta) = \delta^2 \left(a_2' \ln \delta + b_2'\right) + \delta^4 \left(a_4' \ln \delta + b_4'\right) + O(\delta^6), \tag{I.66}$$

with the various a and b easily determined but not of sufficient import to record here. The Euler-Maclaurin formula tells us that

$$\frac{1}{L} \sum_{m=1}^{L-1} f\left(\frac{m}{L}\right) = \int_0^1 dx\, f(x) + \frac{1}{L^3} \left(a_2 \zeta''(-2) + (2a_2 \ln L - a_2' - b_2) \zeta'(-2)\right)$$
$$+ \frac{1}{L^5} \left(a_4 \zeta''(-4) + (2a_4 \ln L - a_4' - b_4) \zeta'(-4)\right) + O\left(\frac{1}{L^7}\right), \tag{I.67}$$

102

where $\zeta(s)$ is the Riemann ζ-function, as usual. Inserting all of the coefficients, we have

$$B_1 = \frac{1}{R - \rho_L} \left(B_{1,0} + B_{1,3} + B_{1,5} + O\left(\frac{1}{L^7}\right) \right) \tag{I.68}$$

with

$$B_{1,0} = \int_0^1 dx \, f(x) \approx 0.001794818, \tag{I.69}$$

$$B_{1,3} = \frac{1}{8L^3} \left(\zeta''(-2) + \left(2\ln L - K\left(\frac{1}{2}\right) + 7\ln 2 - 2\ln(2\pi) \right) \zeta'(-2) \right), \tag{I.70}$$

and

$$B_{1,5} = \frac{\pi^2}{192L^5} \left(-14\zeta''(-4) \right.$$
$$\left. + \left(5 - 4E\left(\frac{1}{2}\right) + 11K\left(\frac{1}{2}\right) - 98\ln 2 + 28\ln(2\pi) - 28\ln L \right) \zeta'(-4) \right). \tag{I.71}$$

Furthermore, we can compute

$$B_1(L+1) - B_1(L-1) \tag{I.72}$$

which appears in the Casimir force. Using the Euler-Maclaurin formula, we first expand the quantity ρ_L, appearing in the denominator of B_1, in powers of $1/L$. The result is that

$$\rho_L = R_c - \frac{1}{4\pi L} \left(\frac{K(1/2) + 7\ln 2}{2} + \ln L \right) + O\left(\frac{1}{L^2}\right). \tag{I.73}$$

Then, if we are only interested in terms of order $1/(R - R_c)$, we find

$$\frac{1}{R - \rho_L} = \frac{1}{R - R_c} + O\left(\frac{1}{(R - R_c)^2}\right), \tag{I.74}$$

and thus

$$B_1(L+1) - B_1(L-1)$$
$$\approx \frac{1}{R - R_c} \left[\frac{1}{L^4} (0.02246 + 0.04567\ln L) + \frac{1}{L^6} (0.01973 + 0.2672\ln L) \right], \tag{I.75}$$

where we have made numerical approximations to the zoo of constants listed above.

I.4.2 Sum of Eigenvalues to Second Order

We now take up the problem of computing

$$\sum_l \epsilon_l, \tag{I.76}$$

where ϵ_l are the diagonal elements of the perturbation matrix $\mathcal{E}$, cf. Eqn. (I.5), which solve the spherical constraint. To first order in perturbation theory, we find the result, Eqn. (I.10), that the perturbations, despite being non-zero, conspire to cancel out:

$$\sum_l \epsilon_l \sim e^{-R} \approx 0. \tag{I.77}$$

However, we must also consider the second order corrections to the eigenvalues, because the term entering the Casimir force has R multiplying the sum.

We revisit the spherical constraint,

$$R = \frac{2}{\pi} \, \psi_i^{(1)\,2} \, \frac{1}{4} K\left(\frac{4}{a_1}\right) + C_i, \tag{I.78}$$

still only being concerned with the perturbations of the almost-singular first mode. We will now develop expressions to $O(\epsilon^2)$ for the corrections to the unperturbed λ_1 and $\phi^{(1)}$. These are (ignoring terms $\propto e^{-R}$)

$$a_1 = 4 + \frac{1}{L} \sum_{m=2}^{L} \frac{1}{4 - \lambda_m} \sum_{i,j=1}^{L} \epsilon_i \epsilon_j \phi_i^{(m)} \phi_j^{(m)} + O(\epsilon^3), \tag{I.79}$$

and

$$\psi_i^{(1)\,2} = \frac{1}{L} + \frac{2}{L} \sum_{m=2}^{L} \frac{\phi_j^{(m)}}{4 - \lambda_m} \sum_{j=1}^{L} \epsilon_j \phi_j^{(m)} + \left[\frac{1}{L} \sum_{k,m=2}^{L} \frac{\phi_i^{(m)} \phi_i^{(k)}}{(4 - \lambda_m)(4 - \lambda_k)} \sum_{j,l=1}^{L} \epsilon_j \epsilon_l \phi_j^{(k)} \phi_l^{(m)} \right.$$

$$+ \frac{2}{L} \sum_{k,m=2}^{L} \frac{\phi_i^{(k)}}{(4 - \lambda_m)(4 - \lambda_k)} \sum_{j,l=1}^{L} \epsilon_j \epsilon_l \phi_j^{(m)} \phi_l^{(k)} \phi_l^{(m)}$$

$$\left. - \frac{1}{L^2} \sum_{k=2}^{L} \frac{1}{(4 - \lambda_k)^2} \sum_{j,l=1}^{L} \epsilon_j \epsilon_l \phi_j^{(k)} \phi_l^{(k)} \right] + O(\epsilon^3). \tag{I.80}$$

The constraint is now very cumbersome to write, but the analysis proceeds as it did before. Take the inner product of the constraint with $|\phi^{(l)}\rangle$, $l > 1$, to find

$$\sum_{i=1}^{L} C_i \phi_i^{(l)} = (R - \rho_L) \left[\frac{2}{\lambda_l - 4} \sum_{j=1}^{L} \epsilon_j \phi_j^{(l)} - \frac{2}{\lambda_l - 4} \sum_{m=2}^{L} \frac{1}{\lambda_m - 4} \sum_{j,k=1}^{L} \epsilon_j \epsilon_k \phi_j^{(m)} \phi_k^{(l)} \phi_k^{(m)} \right.$$

$$\left. - \sum_{k,m=2}^{L} \frac{1}{(\lambda_m - 4)(\lambda_k - 4)} \sum_{i=1}^{L} \phi_i^{(l)} \phi_i^{(m)} \phi_i^{(k)} \sum_{j,n=1}^{L} \epsilon_j \epsilon_n \phi_j^{(k)} \phi_n^{(m)} \right]. \quad \text{(I.81)}$$

We now Taylor expand our ϵ about the old solutions, Eqn. (I.22). Therefore, put

$$\epsilon_r = \frac{1}{2(R - \rho_L)} \sum_{i,l=1}^{L} C_i \phi_i^{(l)} \phi_r^{(l)} (\lambda_l - 4) + \eta_r, \quad \text{(I.82)}$$

where η_r is $O(1/R^2)$. Then, inserting this expansion into Eqn. (I.81) and keeping only terms of $O(1/R^2)$, we find

$$\eta_r = \frac{1}{4(R - \rho_L)^2} \sum_{m=2}^{L} \sum_{jklpq=1}^{L} \frac{(\lambda_k - 4)(\lambda_l - 4)}{\lambda_m - 4} C_p C_q \phi_j^{(m)} \phi_r^{(m)} \phi_p^{(k)} \phi_r^{(k)} \phi_q^{(l)} \phi_j^{(l)}$$

$$+ \frac{1}{8(R - \rho_L)^2} \sum_{ijnl=1}^{L} \sum_{k,m=2}^{L} \sum_{abpq=1}^{L} \frac{(\lambda_l - 4)(\lambda_a - 4)(\lambda_b - 4)}{(\lambda_m - 4)(\lambda_k - 4)}$$

$$\times C_p C_q \phi_r^{(l)} \phi_i^{(l)} \phi_i^{(m)} \phi_i^{(k)} \phi_j^{(k)} \phi_n^{(m)} \phi_p^{(a)} \phi_j^{(a)} \phi_q^{(b)} \phi_n^{(b)}. \quad \text{(I.83)}$$

As luck would have it, we don't need η_r but actually $\sum_r \eta_r$. In that case, the second term immediately gives zero (thank goodness) because

$$\sum_{r=1}^{L} (\lambda_l - 4) \phi_r^{(l)} = 0, \quad \text{(I.84)}$$

by orthogonality, $\langle \phi^{(1)} | \phi^{(l)} \rangle = 0$ if $l > 1$, or by vanishing of $(\lambda_l - 4)$ if $l = 1$. The first term also greatly simplifies upon summing over r:

$$\sum_{r=1}^{L} \eta_r = \frac{1}{4(R - \rho_L)^2} \sum_{m=2}^{L} \sum_{jlpq=1}^{L} (\lambda_l - 4) C_p C_q \phi_j^{(m)} \phi_p^{(m)} \phi_q^{(l)} \phi_j^{(l)}. \quad \text{(I.85)}$$

Performing the j sum gives

$$\sum_{r=1}^{L} \eta_r = \frac{1}{4(R - \rho_L)^2} \sum_{m=2}^{L} \sum_{p,q=1}^{L} (\lambda_m - 4) C_p C_q \phi_p^{(m)} \phi_q^{(m)}, \quad \text{(I.86)}$$

105

Referring to the explicit expressions, Eqns. (I.3) and (I.4), for the unperturbed eigenvalues and eigenstates, the m sum gives

$$2\delta_{pq}\left(1 - \frac{1}{2}\delta_{q1} - \frac{1}{2}\delta_{qL}\right) - \delta_{p,q+1} - \delta_{p,q-1}, \tag{I.87}$$

and therefore we find a simpler form

$$\sum_{r=1}^{L} \eta_r = \frac{1}{4(R-\rho_L)^2}\left(-C_1^2 - C_L^2 + 2\sum_{q=1}^{L}C_q^2 - \sum_{q=2}^{L}C_qC_{q-1} - \sum_{q=1}^{L-1}C_qC_{q+1}\right). \tag{I.88}$$

Noting the fact that the final two summations are identical and that $C_1^2 = C_L^2$, by the definition of the C_i in Eqn. (I.13), we have further

$$\sum_{r=1}^{L} \eta_r = \frac{1}{4(R-\rho_L)^2}2\sum_{q=1}^{L-1}C_q(C_q - C_{q+1}). \tag{I.89}$$

Inserting the definition of C_q and making use of the trigonometric identity

$$\sum_{q=1}^{L-1}\sin\left(\frac{2\pi(l-1)q}{L}\right)\cos^2\left(\frac{\pi(m-1)(2q-1)}{2L}\right)$$
$$= \frac{L}{4}\sin\left(\frac{\pi(m-1)}{L}\right)(\delta_{lm} - \delta_{l,L+2-m}), \tag{I.90}$$

we have

$$\sum_{r=1}^{L} \eta_r = \frac{1}{4(R-\rho_L)^2} \cdot \frac{1}{2\pi^2 L}\sum_{m=2}^{L}\frac{4}{\lambda_m}K\left(\frac{4}{\lambda_m}\right)\sin^2\left(\frac{\pi(m-1)}{L}\right)$$
$$\times\left[\frac{4}{\lambda_m}K\left(\frac{4}{\lambda_m}\right) - \frac{4}{\lambda_{L+2-m}}K\left(\frac{4}{\lambda_{L+2-m}}\right)\right], \tag{I.91}$$

which bears more than a passing resemblance to Eqn. (I.63) for B_1! In fact, we have

$$\sum_{l=1}^{L}\epsilon_l = \sum_{l=1}^{L}\eta_l = \frac{1}{4}\cdot\frac{4B_1(L)}{R-\rho_L} = \frac{B_1(L)}{R-\rho_L}. \tag{I.92}$$

I.4.3   Putting Together the $T > 0$ Correction

At this point, we can combine the two terms. The term in the Casimir force of order $1/R$ is

$$-\frac{1}{2}\Big(B_1(L+1) - B_1(L-1)\Big) + \frac{1}{4}R\left(\frac{B_1(L+1)}{R-\rho_{L+1}} - \frac{B_1(L-1)}{R-\rho_{L-1}}\right) \tag{I.93}$$

If we are to keep strictly to order $1/R$, we see that

$$\frac{R}{R - \rho_L} = 1 + O(1/R),$$
(I.94)

so the combination simplifies even further to

$$-\frac{1}{4}\Big(B_1(L+1) - B_1(L-1) \Big) + O\left(\frac{1}{R^2}\right).$$
(I.95)

This is a quantity we fully understand, having already studied it and produced a series expansion, Eqn. (I.75).

References

[1] H. Casimir and D. Polder. The Influence of Retardation on the London-van der Waals Forces. *Physical Review*, 73(4):360, 1948.

[2] H. Casimir. On the attraction between two perfectly conducting plates. *Proc. K. Ned. Akad. Wet.*, 51:793, 1948.

[3] H. Casimir. Introductory Remarks on Quantum Electrodynamics. *Physica*, 19:846, 1953.

[4] T. Boyer. Quantum Electromagnetic Zero-Point Energy of a Conducting Spherical Shell and the Casimir Model for a Charged Particle. *Phys. Rev.*, 174(5):1764, 1968.

[5] L. H. Ryder. *Quantum Field Theory*. Cambridge Univ. Press, 2nd edition, 1996.

[6] M. Abramowitz and I. Stegun. *Handbook of Mathematical Functions with Formulas, Graphs, and Mathematical Tables*. Dover Publications, 1965.

[7] H. Goldstein, C. Poole, and J. Safko. *Classical Mechanics*. Addison Wesley, 3rd edition, 2002.

[8] M. Fisher and P.-G. de Gennes. Phénomènes aux parois dans un mélange binaire critique. *C. R. Acad. Sci. Paris Ser. B*, 287:207, 1978.

[9] H. E. Stanley. *Introduction to Phase Transitions and Critical Phenomena*. Oxford Univ. Press, 1971.

[10] A. Gambassi. The Casimir effect: From quantum to critical fluctuations. *J. Phys: Conf. Ser.*, 161(1), 2009.

[11] M. Krech. *The Casimir Effect in Critical Systems*. World Scientific, 1994.

[12] M. Kardar and H. Li. Fluctuation-induced forces between manifolds immersed in correlated fluids. *Phys. Rev. A*, 46(10):6490, 1992.

[13] M. Fisher and A. Ferdinand. Interfacial, Boundary, and Size Effects at Critical Points. *Phys. Rev. Lett.*, 19(4):169, 1967.

[14] B. Widom. Equation of State in the Neighborhood of the Critical Point. *J. Chem. Phys.*, 43(11):3898, 1965.

[15] J. Brankov, D. Danchev, and N. Tonchev. *Theory of Critical Phenomena in Finite-Size Systems*. World Scientific, 2000.

[16] M. Fisher and M. Barber. Scaling Theory for Finite-Size Effects in the Critical Region. *Phys. Rev. Lett.*, 28(23):1516, 1972.

[17] M. Fisher. Critical Phenomena in Films and Surfaces. *J. Vac. Sci. Technol.*, 10(5):665, 1973.

[18] M. Krech and S. Dietrich. Finite-Size Scaling for Critical Films. *Phys. Rev. Lett.*, 66(3):345, 1991.

[19] V. Privman. Universal size dependence of the free energy of finite systems near criticality. *Phys. Rev. B*, 38(13):9261, 1988.

[20] A. Pelissetto and E. Vicari. Critical phenomena and renormalization-group theory. *Phys. Rep.*, 368:549, 2002.

[21] V. Vaks and A. Larkin. On Phase Transitions of Second Order. *J. Exptl. Theoret. Phys.*, 49:678, 1966.

[22] H. Stanley. Spherical Model as the Limit of Infinite Spin Dimensionality. *Phys. Rev.*, 176(2):718, 1968.

[23] T. Berlin and M. Kac. The Spherical Model of a Ferromagnet. *Phys. Rev.*, 86(6):821, 1952.

[24] M. Krech. Casimir forces in binary liquid mixtures. *Phys. Rev. E*, 56(2):1642, 1997.

[25] O. Vasilyev, A. Gambassi, A. Maciolek, and S. Dietrich. Monte Carlo simulation results for critical Casimir forces. *Europhys. Lett.*, 80(6), 2007.

[26] Z. Borjan and P. Upton. Off-Critical Casimir Effect in Ising Slabs with Symmetric Boundary Conditions in $d = 3$. *Phys. Rev. Lett.*, 101, 2008.

[27] H. Au-Yang and M. Fisher. Bounded and inhomogeneous Ising models. II. Specific-heat scaling function for a strip. *Phys. Rev. B*, 11(9):3469, 1975.

[28] R. Evans and J. Stecki. Solvation force in two-dimensional Ising strips. *Phys. Rev. B*, 49(13):8842, 1994.

[29] J. Rudnick, R. Zandi, A. Shackell, and D. Abraham. Boundary conditions and the critical Casimir force on an Ising model film: Exact results in one and two dimensions. *Phys. Rev. E*, 82(4), 2010.

[30] M. Krech and S. Dietrich. Free energy and specific heat of critical films and surfaces. *Phys. Rev. A*, 46(4):1886, 1992.

[31] R. Garcia and M. Chan. Critical Fluctuation-Induced Thinning of ^{4}He Films near the Superfluid Transition. *Phys. Rev. Lett.*, 83(6):1187, 1999.

[32] R. Zandi, J. Rudnick, and M. Kardar. Casimir Forces, Surface Fluctuations, and Thinning of Superfluid Film. *Phys. Rev. Lett.*, 93(15), 2004.

[33] J. Rudnick, R. Zandi, A. Shackell, M. Kardar, and L. Chayes. Thinning of superfluid films below the critical point. *Phys. Rev. E*, 76(3), 2007.

[34] A. Maciolek, A. Gambassi, and S. Dietrich. Critical Casimir effect in superfluid wetting films. *Phys. Rev. E*, 76(3), 2007.

[35] A. Hucht. Thermodynamic Casimir Effect in ^{4}He Films near T_λ: Monte Carlo Results. *Phys. Rev. Lett.*, 99(18), 2007.

[36] M. Hasenbusch. The thermodynamic Casimir effect in the neighbourhood of the λ-transition: a Monte Carlo study of an improved three-dimensional lattice model. *J. Stat. Mech.*, 2009(P07031), 2009.

[37] M. Fisher and M. Barber. Critical Phenomena in Systems of Finite Thickness; I. The Spherical Model. *Annals of Phys.*, 77, 1973.

[38] D. Dantchev, H. Diehl, and D. Gruneberg. Excess free energy and Casimir forces in systems with long-range interactions of van der Waals type: General considerations and exact spherical-model results.

[39] D. Danchev. Exact three-dimensional Casimir force amplitude, C function, and Binders cumulant ratio: Spherical model results.

[40] B. Kastening and V. Dohm. Finite-size effects in film geometry with nonperiodic boundary conditions: Gaussian model and renormalization-group theory at fixed dimension. *Phys. Rev. E*, 81(6), 2010.

[41] H. Diehl, D. Gruneberg, M. Hasenbusch, A. Hucht, S. Rutkevich, and F. Schmidt. Exact thermodynamic Casimir forces for an interacting three-dimensional model system in film geometry with free surfaces. arXiv pre-print, 2012.

[42] B. Derjaguin, I. Abrikosova, and E. Lifshitz. Direct Measurement of Molecular Attraction Between Solids Separated by a Narrow Gap. *Q. Rev. Chem. Soc*, 10:295, 1956.

[43] M. Sparnaay. Measurements of Attractive Forces Between Flat Plates. *Physica*, 24:751, 1958.

[44] W. Black, J. de Jongh, J. Overbeek, and M. Sparnaay. Measurements of Retarded van der Waals' Forces. *Trans. Faraday Soc.*, 56:1597, 1960.

[45] D. Tabor and R. Winterton. The Direct Measurement of Normal and Retarded van der Waals Forces. *Proc. R. Soc. Lond. A*, 312(1511):435, 1969.

[46] S. K. Lamoreaux. Demonstration of the Casimir Force in the 0.6 to 6 μm Range. *Phys. Rev. Lett.*, 78(1):5, 1997.

[47] U. Mohideen and A. Roy. Precision Measurement of the Casimir Force from 0.1 to 0.9 μm. *Phys. Rev. Lett.*, 81(21):4549, 1998.

[48] A. Hanke, F. Schlesener, E. Eisenriegler, and S. Dietrich. Critical Casimir Forces between Spherical Particles in Fluids. *Phys. Rev. Lett.*, 81(9):1885, 1998.

[49] A. Mukhopadhyay and B. Law. Critical Casimir Effect in Binary Liquid Wetting Films. *Phys. Rev. Lett.*, 83(4):772, 1999.

[50] M. Fukuto, Y. Yano, and P. Pershan. Critical Casimir Effect in Three-Dimensional Ising Systems: Measurements on Binary Wetting Films. *Phys. Rev. Lett.*, 94(13), 2005.

[51] S. Rafai, D. Bonn, and J. Meunier. Repulsive and attractive critical Casimir forces. *Physica A*, 386(1):31, 2007.

[52] C. Hertlein, L. Helden, A. Gambassi, S. Dietrich, and C. Bechinger. Direct measurement of critical Casimir forces. *Nature*, 451:172, 2008.

[53] R. Evans. *Liquids at Interfaces*. Elsevier, 1990.

[54] T. Burkhardt and E. Eisenriegler. Casimir Interaction of Spheres in a Fluid at the Critical Point. *Phys. Rev. Lett.*, 74(16):3189, 1995.

[55] O. Kenneth and I. Klich. Opposites Attract: A Theorem about the Casimir Force. *Phys. Rev. Lett.*, 97(16), 2006.

[56] T. Mohry, A. Maciolek, and S. Dietrich. Crossover of critical Casimir forces between different surface universality classes. *Phys. Rev. E*, 81(6), 2010.

[57] D. Abraham and A. Maciolek. Casimir Interactions in Ising Strips with Boundary Fields: Exact Results. *Phys. Rev. Lett.*, 105(5), 2010.

[58] M. Hasenbusch. Thermodynamic Casimir force: A Monte Carlo study of the crossover between the ordinary and the normal surface universality class. *Phys. Rev. B*, 83(13), 2011.

[59] A. Hucht, D. Gruneberg, and F. Schmidt. Aspect-ratio dependence of thermodynamic Casimir forces. *Phys. Rev. E*, 83, 2011.

[60] E. Lifshitz. The Theory of Molecular Attractive Forces between Solids. *Soviet Physics*, 2(1):73, 1956.

[61] O. Kenneth, I. Klich, A. Mann, and M. Revzen. Repulsive Casimir Forces. *Phys. Rev. Lett.*, 89(3), 2002.

[62] E. Buks and M. Roukes. Metastability and the Casimir effect in micromechanical systems. *Europhys. Lett.*, 54:220, 2001.

[63] S. Lamoreaux. The Casimir force: background, experiments, and applications. *Rep. Prog. Phys.*, 68:201, 2005.

[64] C. Genet, A. Lambrecht, and S. Reynaud. The Casimir effect in the nanoworld. *Eur. Phys. J. Special Topics*, 160:183, 2008.

[65] A. Rodriguez, F. Capasso, and S. Johnson. The Casimir effect in microstructured geometries. *Nature Photonics*, 5:211, 2011.

[66] K. Huang. *Statistical Mechanics*. John Wiley & Sons, 2nd edition, 1987.

[67] M. Fisher and H. Nakanishi. Scaling theory for the criticality of fluids between plates. *J. Chem. Phys.*, 75(12):5857, 1981.

[68] E. Eisenriegler and M. Stapper. Critical behavior near a symmetry-breaking surface and the stress tensor. *Phys. Rev. B*, 50(14):10009, 1994.

[69] L. Onsager. Crystal Statistics. I. A Two-Dimensional Model with an Order-Disorder Transition. *Phys. Rev.*, 65(3-4), 1944.

[70] M. Kac. The Work of T. H. Berlin in Statistical Mechanics... a Personal Reminiscence. *Physics Today*, 17(10), 1964.

[71] E. Montroll. Continuum models of cooperative phenomenon. *Il Nuovo Cimento*, 6, 1949.

[72] J. Gunton and M. Buckingham. Condensation of the Ideal Bose Gas as a Cooperative Transition. *Phys. Rev.*, 166(1), 1968.

[73] H. Lewis and G. Wannier. Spherical Model of a Ferromagnet. *Phys. Rev.*, 88:682.

[74] H. Lewis and G. Wannier. Spherical Model of a Ferromagnet (Erratum). *Phys. Rev.*, 90:1131.

[75] C. Yan and G. Wannier. Observations on the Spherical Model of a Ferromagnet. *J. Math. Phys.*, 6(11):1833, 1965.

[76] H. Knops. Infinite spin dimensionality limit for nontranslationally invariant interactions. *J. Math. Phys.*, 14(12):1918, 1973.

[77] D. Danchev. Finite-size scaling Casimir force function: Exact spherical-model results. *Phys. Rev. E*, 53(3):2104, 1996.

[78] B. Kastening and V. Dohm. Critical Casimir Force Scaling Functions of the Mean Spherical Model in $2 < d \leq 3$ Dimensions for Non-Periodic Boundary Conditions. In A. Pelster W. Janke, editor, *Path Integrals: New Trends and Perspectives*, page 283, 2008.

[79] G. Watson. Three Triple Integrals. *Q. J. Math.*, 10(1):266, 1939.

[80] G. Joyce and I. Zucker. Evaluation of the watson integral and associated logarithmic integral for the d-dimensional hypercubic lattice. *J. Phys. A: Math. Gen.*, 34:7349, 2001.

[81] J. Brankov and D. Danchev. Logarithmic Finite-Size Corrections in the Three-Dimensional Mean Spherical Model. *J. Stat. Phys.*, 71(3/4):775, 1993.

[82] I. Gradshteyn and I. Ryzhik. *Table of Integrals, Series, and Products.* Academic, New York, 2007.

[83] P. Byrd and M. Friedman. *Handbook of elliptic integrals for engineers and physicists.* Springer, Berlin, 1971.

[84] O. Vasilyev, A. Gambassi, A. Maciolek, and S. Dietrich. Universal scaling functions of critical Casimir forces obtained by Monte Carlo simulations. *Phys. Rev. E*, 79(4), 2009.

[85] A. Ajdari, L. Peliti, and J. Prost. Fluctuation-Induced Long-Range Forces in Liquid Crystals. *Phys. Rev. Lett.*, 66(11):1481, 1991.

[86] O. Costin and S. Garoufalidis. Resurgence of the Euler-Maclaurin summation formula. *Annales de l' Institut Fourier*, 58:893, 2008.

[87] A. Sidi. EulerMaclaurin Expansions for Integrals with Arbitrary Algebraic-Logarithmic Endpoint Singularities. *Constructive Approximation*, page 1, 2011.